Reentry Dynamics and Handling Qualities of a Generic Hypersonic Vehicle

by

John Jun Araki

Submitted to the Department of Aeronautics and Astronautics
in partial fulfillment of the requirements for the degree of

Master of Science in Aeronautics and Astronautics

at the

MASSACHUSETTS INSTITUTE OF TECHNOLOGY

February 1992

Author .....
Department of Aeronautics and Astronautics
January 24,1992

Certified by .....
Professor Rudrapatna V. Ramnath
Adjunct Professor of Aeronautics and Astronautics
Thesis Supervisor

Accepted by .....
Professor Harold Y. Wachman
Chairman, Departmental Committee on Graduate Students

Reentry Dynamics and Handling Qualities of a Generic Hypersonic Vehicle

by

John Jun Araki

Submitted to the Department of Aeronautics and Astronautics
on January 24,1992, in partial fulfillment of the
requirements for the degree of
Master of Science in Aeronautics and Astronautics

Abstract

The reentry dynamics and handling qualities of the Generic Hypersonic Aerodynamic Model Example(GHAME) vehicle were studied employing Generalized Multiple Scales theory. The reentry dynamics were examined for an optimal trajectory designed for the Space Shuttle Orbiter 049 vehicle. Both longitudinal and lateral directional motions were modeled as time-varying linear differential equations. Generalized Multiple Scales solutions to vehicle reentry dynamics compared accurately with numerical integration approximations. Second order angle-of-attack perturbations behaved as damped oscillations with increasing frequency. Lateral-directional reentry dynamics were found to be unstable due to instability in the spiral divergence mode. The existence of non-continuous 'turning' points in the phugoid mode, prevented attempts to apply asymptotic methods to the fourth order longitudinal model. Sensitivity analysis showed the angle-of-attack perturbations to be most affected by changes in C_{m_α} during reentry. Also, angle-of-attack perturbation motions were found to be, in general, most sensitive at approximately 50,000 to 60,000 vehicle lengths into the trajectory. The lateral-directional reentry dynamics were shown to be most affected by changes in the stability derivatives N_v and L_v. Of the lateral-directional modes, spiral divergence motions were most sensitive to variations in the stability derivatives. Finally, handling qualities of the GHAME vehicle along shuttle reentry trajectory were determined to be inadequate. Effects of simple variations in the behavior of characteristic roots on the handling qualities were determined for a generic second order system.

Thesis Supervisor: Rudrapatna V. Ramnath
Title: Adjunct Professor of Aeronautics and Astronautics

Dedication

Dedicated to my grandparents.

Yoshiaki and Koharu Araki.

Kazunobu and Naragiku Kanda.

Acknowledgments

I would like to express my deepest gratitude to my parents without whom none of this would have been possible. Their love and support goes beyond my ability to express through words.

Also my sincerest gratitude to Professor Rudrapatna V. Ramnath for his invaluable guidance and wisdom through the completion of this work.

Partial support is acknowledged from NASA Dryden Flight Research Facility through Vimanic Systems and Professor Rudrapatna V. Ramnath.

The gang at Baker these two years:
Nuc, Dinger, Lump, Psycho, Danks, Karl. Thanks for letting me play. It isn't that you win championships, it's with whom you win them.

Jina and Liz. Smile. You deserve it.

Sally. No, I will never get off your bed. You're still a dummy, but you're ok for a sister.

The W's. Redman, Rithcie, Ollie, Carvin, Mas, Econ, Bronco, JJ, T, Eileraas, and Edge. The spirit lives. Thanks for being there. Love, in a Weenie way, WOTY '87.

Jennifer L. Going on 10 years now. Do you realize what fraction of my life that is?! Kill G.F. SFDPH.

The gang at the Greenhouse. The blackened lake! Homeless! Ben and Andy; Thanks for everything. The bod will never forget your countless hours of instruction in the art of clam digging.

Finally, to the Poor Fella, Bungy, Gato, Asparagus etc...
You have brightened my life in ways I thought impossible. I will never forget you.

> Maybe there aren't any such things as good friends or bad friends - maybe there are just friends. People who stand by you when you're hurt and who help you feel not so lonely. Maybe they're always worth feeling scared for,

and hoping for, and living for. Maybe worth dying for too, if that's what has to be. No good friends. No bad friends. Only people who you want, need to be with; people who build their houses in your heart... -S. King

Contents

List of Figures

List of Tables

Nomenclature

ξ ..... Vehicle lengths along trajectory

V ..... Speed along trajectory

h ..... Altitude

R ..... Radial distance from center of the earth

g ..... Acceleration due to gravity

M_{no} ..... Mach number

ρ ..... Air mass density

m ..... Vehicle mass

S ..... Reference area

$I_{xx}, I_{yy}, I_{zz}, I_{xz}$ ..... Moments of inertia

k_x, k_y, k_z ..... Radii of curvature

b ..... Reference span

c ..... Reference chord

A ..... Aspect ratio

l ..... Vehicle length

σ ..... Inverse nondimensional pitching moment of inertia

ν ..... Ratio of moments of inertia

δ ..... nondimensional mass of atmosphere

e ..... Span efficiency

T ..... Thrust

D ..... Drag

W ..... Weight

M ..... Moment

L ..... Lift in longitudinal equations

L ..... Rolling moment in lateral-directional equations

Y ..... Side force

N ..... Yawing moment

C_D ..... Drag coefficient

C_L ..... Lift coefficient

C_m ..... Moment coefficient

C_y ..... Side force coefficient

C_l ..... Rolling moment coefficient

C_N ..... Yawing moment coefficient

α_0 ..... Initial angle-of-attack

α ..... Angle-of-attack

$\bar{\alpha} = \alpha - \alpha_0$ ..... Angle-of-attack perturbation

γ ..... Flight path angle

θ ..... Pitch angle

q ..... Pitch angle rate

w ..... Side velocity

ϕ ..... Roll angle

p ..... Roll angle rate

r ..... Yaw angle rate

D_V ..... Drag damping derivative

D_α ..... Drag angle-of attack derivative

T_V ..... Thrust velocity derivative

L_V ..... Lift velocity derivative

L_α ..... Vertical damping derivative

M_V ..... Speed stability derivative

M_α ..... Angle-of-attack static stability derivative

$M_{\dot{\alpha}}$ ..... Angle-of-attack damping derivative

$M_{\dot{\theta}}$ ..... Pitch damping derivative

Y_v ..... Side force due to sideslip derivative

L_v ..... Dihederal effect derivative

L_r ..... Rolling moment due to yaw rate derivative

L_p ..... Roll damping derivative

N_v ..... Directional stability derivative

N_r ..... Yaw damping derivative

N_p ..... Yawing moment due to roll rate derivative

τ_1, τ_0 ..... Independent variables after extension

ϵ ..... Slowness of variations in coefficients

y ..... Generic variable representing dynamics

P ..... Stability parameter

ω_n ..... Natural frequency

ζ ..... Damping ratio

T ..... Total characteristic root path time

Subscripts

$-\alpha$ ..... per angle-of-attack

$-q$ ..... per pitch angle rate

-0 ..... Initial term

$-T$ ..... Trim value

$-s$ ..... Slowly varying quantity

$-f$ ..... Rapidly varying quantity

$-f$ ..... Final value

$-\beta$ ..... per sideslip angle

$-r$ ..... per yaw angle rate

$-p$ ..... per roll angle rate

$-sh$ ..... of short period mode

$-rc$ ..... of roll convergence mode

$-sp$ ..... of spiral divergence mode

$-dr$ .... of dutch roll mode

Chapter 1

Introduction

1.1 Background

With the emergence of new technologies, there has been recent interest in the development of hypersonic reentry vehicles. Unlike the Space Shuttle, these hypersonic vehicles would perform a conventional horizontal take-off and achieve a low-Earth orbit powered by a multimode propulsion system. Several vehicles of this nature such as the X-30 National Aerospace Plane have been proposed for both commercial and military purposes. It is clear that this class of hypersonic vehicles represents the next generation of aeronautical development.

One of the many issues encountered in the development of such hypersonic vehicles is the problem of predicting the dynamics of the aircraft during its reentry into the Earth's atmosphere. The task of analyzing the reentry dynamics of space vehicles is one which has already generated considerable research interest. For example, much work has been done to predict the reentry behavior of ballistic missiles. The equations of motion describing the dynamics of space vehicles during reentry are in general, nonlinear. An exact analytical solution to these equations has not been discovered, and many approximate solutions have been proposed. In the past, such approximations to reentry dynamics have been developed by making restricting assumptions on the nature of the vehicle and reentry trajectory as well as the forces affecting the motion. For example, after neglecting gravity in favor of aerodynamic forces , Allen[5]

showed that reentry dynamics can be represented in the form of Bessel functions. Etkin[6] developed approximations to reentry dynamics after limiting the trajectory to those with small flight path angles. In one particular approach, a unified linear time-varying differential equation was developed by Vinh and Laitone[4] to describe longitudinal angle-of-attack perturbation for any reentry trajectory. However, due to the variable coefficients, solutions could only be obtained by limiting the trajectories to two special cases. A straight line reentry trajectory reduced the equation to Kummer's equation while angle-of-attack perturbations were shown to be in the form of Mathieu's functions for a trajectory with shallow flight path angles.[3]

Similar to Vinh and Laitone's equation for angle-of-attack perturbations, in general, it is possible to accurately represent both the longitudinal and lateral-directional reentry dynamics of a vehicle with time-varying linear differential equations. The Generalized Multiple Scales(GMS) theory[7, 8] developed by Ramnath offers asymptotic approximations to such equation as well as other complex problems. The longitudinal dynamics of the Space Shuttle were predicted by Ramnath employing GMS theory[3]. By separating the inherent dynamics of the solution into 'fast' and 'slow' parts, Ramnath developed approximations to linear time-varying differential equations while offering complete generality. Unlike the solutions of Vinh and Laitone, only mild restrictions upon the trajectory or the nature of the vehicle are necessary to predict the reentry dynamics with these asymptotic approximations. As shown by Ramnath, the only assumption made by the GMS theory is that the coefficients of the differential equation vary slowly when compared to the time constant of the reentry motion. During entry into the earth's atmosphere, the main variations in the coefficients are due to changes in air density, aerodynamic forces, and moments. Experience with ballistic missiles has shown that these parameters vary relatively slowly when compare to the time constants of the dynamic motions. Aside from generality, another advantage that the GMS theory presents is that the asymptotic approximations to the reentry dynamics come in the form of simple elementary functions. This allows these approximations to be employed for further analysis regarding the stability and sensitivity of reentry dynamics. Such analysis is not possible with the

approximations developed by Vinh, Loh, and Laitone which result in representations of the dynamics in the form of non-elementary functions such as those of Bessel and Mathieu. Ramnath's approach is followed in this work and his technique is briefly presented in Chapter 3.

1.2 Approach

In this work, the reentry dynamics and handling qualities of the Generic Hypersonic Aerodynamic Model Example(GHAME) vehicle along an optimal Space Shuttle trajectory are studied employing GMS theory. The GHAME is a computer simulation model designed to provide accurate aerodynamic data for generic vehicles in the hypersonic flight regime. The reentry trajectory along which the the dynamics and handling qualities of the GHAME vehicle are studied is one which was originally designed to minimize the weight of the thermal protection system of the Space Shuttle orbiter 049 vehicle. The GHAME vehicle and the optimal shuttle trajectory are detailed in Chapter 2.

GMS theory is employed to predict both the longitudinal and lateral-directional reentry motions of the GHAME vehicle. The conceptual foundations of the GMS method as well as the second and fourth order GMS approximations used to study the GHAME vehicle dynamics are detailed in Chapter 3. The longitudinal reentry behavior of the aircraft is explored in two different ways. First, the behavior of angle-of-attack perturbation dynamics is studied in Chapter 4 by applying Ramnath's solutions to the second order time-varying linear differential equation developed by Vinh and Laitone. Sensitivity of the angle-of-attack perturbations to several different aerodynamic coefficients is examined through partial differentiation of the GMS approximation which is justified by Ramnath and Radovsky[16]. Also, second order longitudinal stability is assessed through a stability criterion derived by Ramnath's GMS method. A possible manner in which this stability information can be displayed to a flight crew is considered. The full fourth order longitudinal dynamics of the GHAME vehicle as it travels along the optimal shuttle reentry trajectory are

studied in Chapter 5. A fourth order linear differential equation describing the longitudinal motions is derived, and the GMS approximations are employed once again in an attempt to predict reentry dynamics.

Similarly, the lateral-directional dynamics of the GHAME vehicle along the Shuttle reentry trajectory are studied in Chapter 6. Again, following Ramnath's theory on parameter sensitivity of variable systems, a sensitivity analysis is conducted in order to determine the effects of variations in the stability derivatives on the reentry dynamics. Finally, the handling qualities of the GHAME vehicle are investigated in Chapter 7 through comparison of reentry parameters with set of flying quality specifications. Also, GMS theory is employed to study the relative differences in the handling qualities of generic time-varying second order systems whose characteristic roots exhibit different behaviors in time.

Chapter 2

GHAME Vehicle and Trajectory

2.1 GHAME Vehicle

The recent interest in the development of hypersonic vehicles has led to a need for accurate aerodynamic data in this flight regime. Much of the existing data is not available to general users. The Generic Hypersonic Aerodynamic Model Example[1] was developed at the Dryden Flight Research Facility in order to satisfy this demand for realistic aerodynamic data in hypersonic flight. The data included in the GHAME provides a model with which it is possible to conduct simulations for the design of control and guidance systems as well as trajectory optimization. The generic nature of the GHAME data enables it to be a starting point for working designs of both commercial and military aircraft.

The aerodynamic data contained in the GHAME model are for a particular generic vehicle geometry and were developed as a combination of existing aircraft and theories. Actual data from vehicles such as the Space Shuttle Orbiter, lifting body type aircraft, as well as theories such as the modified Newtonian impact flow method were employed in developing the final GHAME aerodynamic data. In order to maintain the realistic nature of the data, certain aerodynamic anomalies contained in some of the sources were retained. Lateral-directional derivatives for Mach numbers above 8 were taken exclusively from Space Shuttle data. Below this speed, the lateral-directional derivatives are an equal combination of the Space Shuttle and a swept double delta

configuration. The effect of the tip fins from the swept double delta configuration was included with the justification that the larger vertical tail of the GHAME vehicle would have a larger effect on the aerodynamics than the small vertical tail of the Space Shuttle Orbiter. The data at the higher Mach numbers was also adjusted in order to insure a smooth transition in the derivatives. The longitudinal aerodynamic coefficients are an equal mix of various sources at all Mach numbers. The drag coefficients were modified through multiplication factors and biases in order to provide L/D numbers which are realistic when compared with the Space Shuttle. Both the lateral-directional and longitudinal sets of data were adjusted for reference span and reference area.

The GHAME data was developed for a flight regime typical of a single stage-to-orbit mission. Such a mission would entail a powered horizontal take-off from conventional runways, and accelerating to orbital velocities with air-breathing engines until achieving a low-Earth-orbit. Upon completing its mission in orbit, the GHAME vehicle would reenter the Earth's atmosphere and maneuver to an unpowered horizontal landing.

The sources employed to model the aerodynamic data result in a physical configuration of the GHAME vehicle which is analogous to the X-24B or the X-24C with a more slender fuselage. The GHAME configuration is a delta wing vehicle with mixed elevons serving both as ailerons and elevators. Provisions were made in the data for a single rudder, however no aerodynamic considerations were given to control jets, speed brake, landing gear, and other variable physical elements.

Mass properties of the GHAME vehicle were estimated by approximating the vehicle geometry through the use of simple shapes. The fuselage was modeled as a cylinder 20 ft. in diameter and 120 ft. in length. This allows enough volume for the liquid hydrogen fuel. Two 10 degree half cones were attached to the cylinder to complete the fuselage structure. Both the delta wings and the vertical tail were modeled as thin triangular plates, with the wings containing no dihedral. The engine module was wrapped around the bottom surface of the fuselage. The complete vehicle configuration is shown in Fig.2-1. The reference area of the vehicle is 6000 ft^2 and

Length, l	233.4 ft.
Ref. Area, S	6000 ft.^{2}
Ref. Span, b	80 ft.
Ref. Chord, c	75 ft.
Mass, m	120,000 lbs.
I_{xx}	$.87 \times 10^6$ slugs-ft.^{2}
I_{yy}	14.2×10^6 slugs-ft.^{2}
I_{zz}	14.9×10^6 slugs-ft.^{2}
I_{xz}	$.28 \times 10^6$ slugs-ft.^{2}

Table 2.1: GHAME Vehicle Parameters

the reference span is 80 ft. Overall vehicle length is 233.4 ft. while the reference chord is 70 ft.

The mass properties of the GHAME vehicle which were estimated employing the simple configuration shown in Fig.2-1 were assumed to be on the same order of magnitude as current existing supersonic cruise aircraft. Most of the GHAME vehicle estimates were derived from the XB-70 aircraft. The gross take-off weight was estimated to be approximately 300,000 lbs, of which 60% was assumed to be the liquid hydrogen fuel. For the purposes of this study of reentry dynamics, the GHAME vehicle is considered to be at the fuel burnout mass of 120,000 lbs. Also, the moments of inertia are taken at fuel burnout values. All of the critical GHAME vehicle parameters employed in this study are shown in Table 2.1.

2.2 Trajectory

In this study, the dynamics of the Generic Hypersonic Aerodynamic Model Example vehicle are examined as it traverses a prescribed trajectory returning it into the Earth's atmosphere. The trajectory employed is one which was originally designed to minimize the thermal-protection-system(TPS) weight of the Space Shuttle Orbiter 049 vehicle[2]. The TPS of the Shuttle Orbiter consists of a collection of 22 metallic panels of varying composition and thickness. In order to obtain the optimal trajectory, the method of steepest descent was applied iteratively to minimize the total heat load

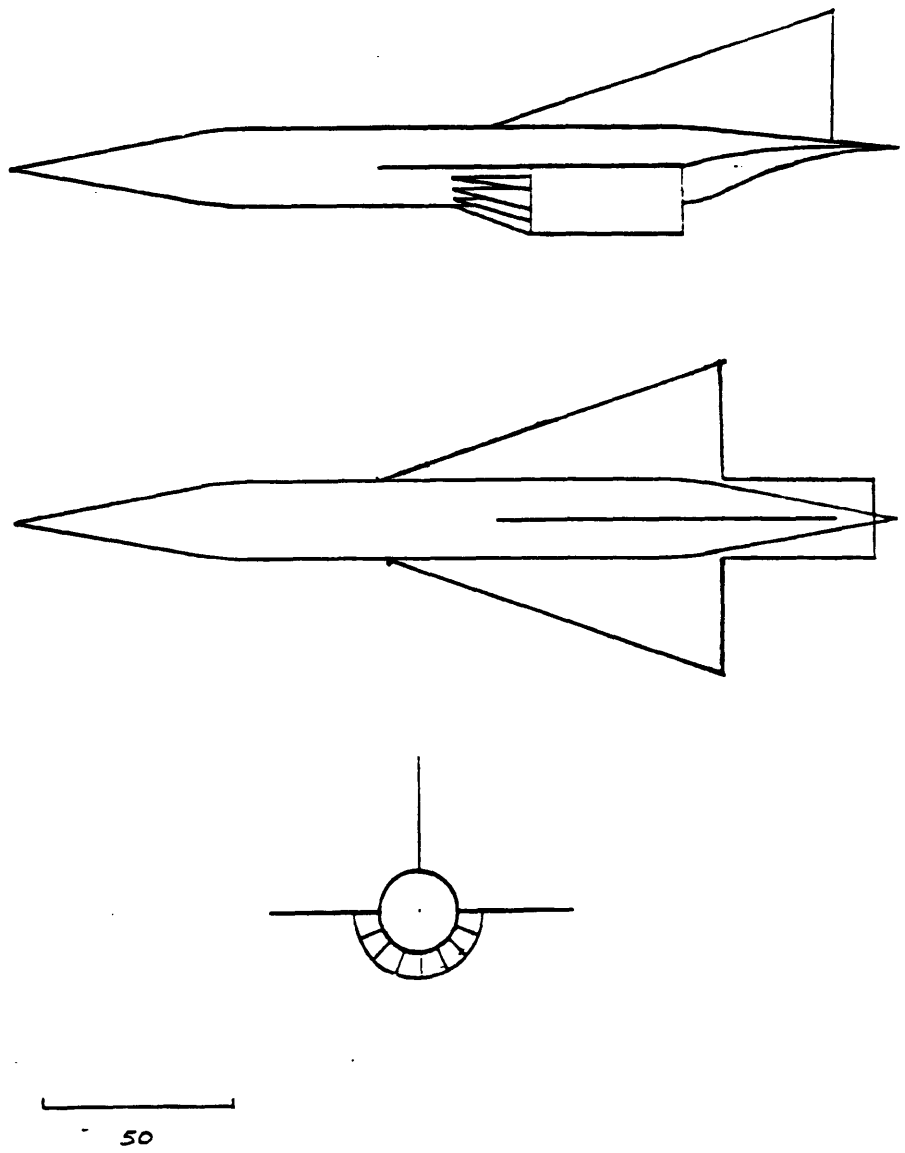

Figure 2-1: GHAME Vehicle Configuration

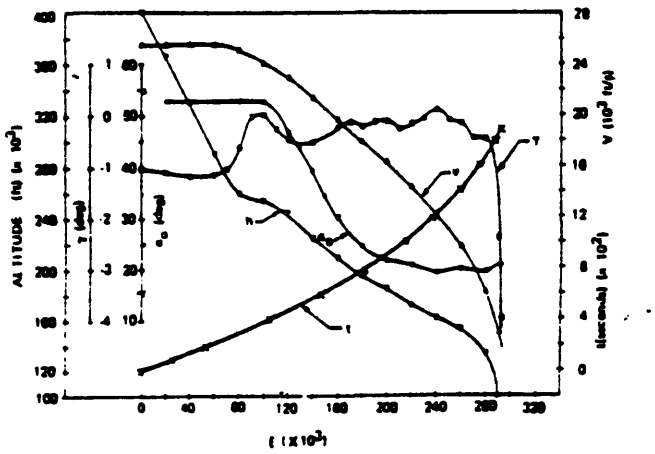

Figure 2-2: Trajectory Parameters

at the stagnation point. The optimal trajectory produced a minimum TPS weight of 30,700 lbs.

Following Ramnath[3], the optimal Shuttle trajectory is detailed in Fig.2-2 where angle of attack, velocity, altitude, and flight path angle are all shown as functions of the non-dimensional variable ξ. This non-dimensional variable is the number of vehicle lengths traversed along the trajectory and is discussed further in Chapter 3. The Space Shuttle reentry trajectory covers a range of 0 to 290,000 vehicle lengths traversed and a descent from 400,000 ft. to 100,000 ft. The terminal down range distance is 5400 nautical miles, and the cross track distance is 1100 nautical miles. The maximum acceleration does not exceed 3 g's. Angle-of-attack values are very large along the trajectory while flight path angles vary from 0° to -4°. It should be noted that the variation of real time with respect to ξ is non-linear as seen in Fig.2-2. The total time required to fly the optimal trajectory is approximately 1900 seconds.

Chapter 3

Generalized Multiple Scales Theory

3.1 Theory

This chapter and the techniques contained within closely follow the development of the Generalized Multiple Scales(GMS) theory by Ramnath[7, 8]. The GMS method is an asymptotic approach for approximating solutions to a variety of complex systems. The concept of asymptotic solutions is based on the original work of Poincarè and has been employed to obtain engineering approximations in fields such as mechanics and astrodynamics. The complete generalization of the multiple scales asymptotic analysis was achieved by Ramnath in his development of GMS theory, and his approach has been successfully applied to a large number of problems including the investigation of the behavior of vehicles such as VTOL aircraft and the Space Shuttle.

One particular application of GMS theory is the approximation of solutions to a class of linear ordinary differential equations having variable coefficients. While first order linear equations of such kind are solved in the form of an exponential, higher order equations cannot be resolved in this way. Often, the exact solutions to higher order equations only exist in the form of transcendental functions such as those of Bessel which cannot be expressed as simple analytic functions of the coefficients. However, it is very often desirable to have approximate solutions in such analytic

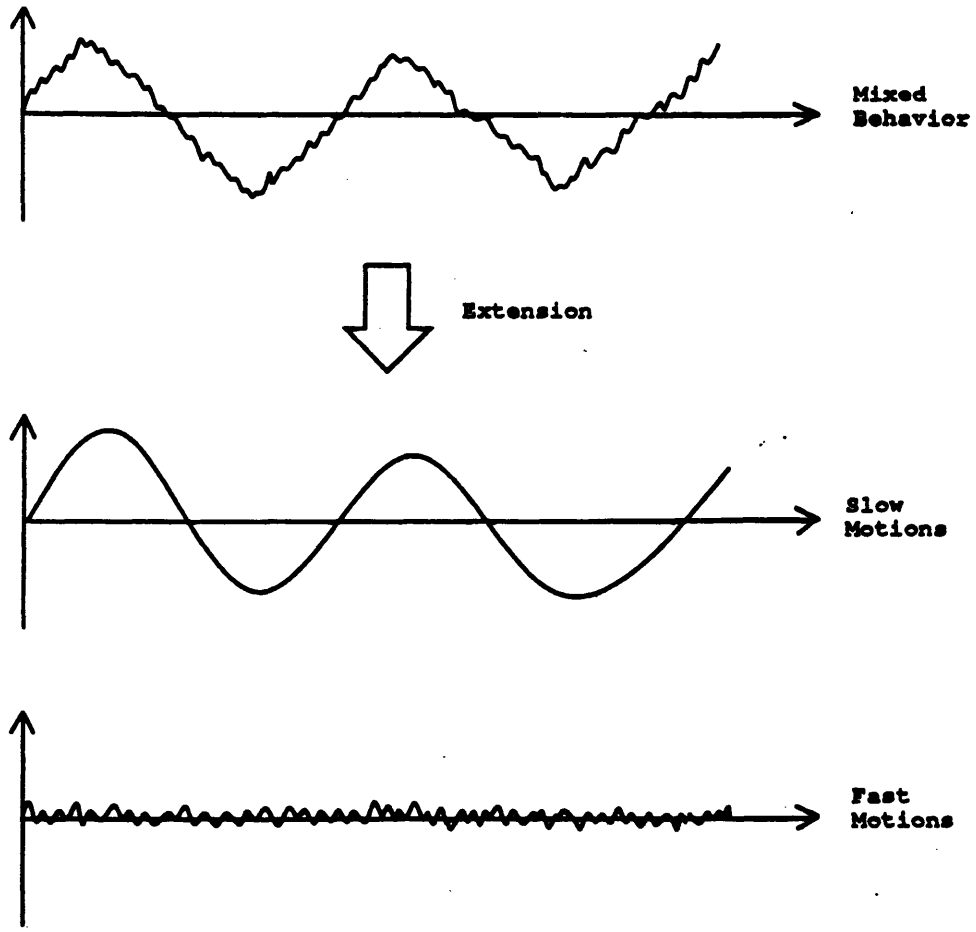

Figure 3-1: Concept of Extension

forms which allow for simple manipulations and sensitivity analysis.

As developed by Ramnath, the Generalized Multiple Scales method is based on the premise that the variable coefficients of the linear differential equations contain a small parameter. Often, direct expansion in powers of this parameter leads to a misrepresentation of the true solution over a particular range of the independent variable. Such a misrepresentation is called a nonuniformity in the perturbation expansion and is avoided by the GMS approximations through the concept of extension. The fundamental idea behind the concept of extension is to enlarge the domain of the independent variable to a space of higher dimension. This is achieved by the introduction of general scale functions which reparameterize the independent variable into

a set of new independent clocks. The scale functions can in general be both complex and nonlinear. If the original independent variable is time, qualitatively, extension is similar to having a particular motion be recorded by a set of independent observers each with time pieces running at different rates. In this way, the general solution is separated into characteristic motions which occur at different rates or on different scales. The scaling functions are chosen such that the non-uniformities of direct perturbation theory are eliminated. The complete generalization of this technique was achieved by Ramnath[7, 8] and has been fruitfully applied to a large number of complex problems. The concept of extension is illustrated in Fig.3-1.

Generalized Multiple Scales theory employs the concept of extension in order to provide asymptotic approximations to ordinary differential equations. Extension allows the dynamics to be separated into motions on different scales after which they are combined to produce an approximation to the full solution. Mathematically, applying extension to ordinary differential equations results in sets of partial differential equations with a new independent variables. These equations are solved, and the approximation is completed by returning the problem to its original independent variable. Ramnath's Generalized Multiple Scales theory is applied and detailed in the next two sections.

3.2 Second Order GMS Solution

In this section, the Generalized Multiple Scales theory is demonstrated on a second order linear differential equation with varying coefficients[3]. The GMS theory approximates the full solution through separation of natural motions. Consider the following equation.

$$\frac{d^2x}{dt^2} + \omega_1(t)\frac{dx}{dt} + \omega_0(t)x = 0 \tag{3.1}$$

In order to employ the GMS approximation, it is necessary to assume that the coefficients of the above equation vary slowly. That is to say the variations in the

coefficients are slow in comparison to the time constant of the dynamic motion. Mathematically, this is equivalent to stating that the coefficients of Eq.3.1 vary on a new slow variable $\bar{t}$ defined as

$$\bar{t} = \epsilon t \tag{3.2}$$

The small parameter ϵ in the above equation is a measure of the ratio of time constants of the solution and coefficient variation. Asymptotic solutions are obtained as $\epsilon \rightarrow 0$. As developed by Ramnath, asymptotic solutions of the form $x = x_s(\tau_0)x_f(\tau_1)$ are sought for Eq.3.1 by the GMS method. The final GMS solution is given by

$$x = x_s(t)x_f(t) \tag{3.3}$$

where the slow solution x_s is

$$x_s(t) = |\omega_1(t)^2 - 4\omega_0(t)|^{-\frac{1}{4}} \tag{3.4}$$

and the fast solution is given by

$$\begin{aligned} x_f(t) = {} & C_1 exp\left(\int_{t_0}^{t} k_r(t)dt\right) sin\left(\int_{t_0}^{t} k_i(t)dt\right) + \\ & C_2 exp\left(\int_{t_0}^{t} k_r(t)dt\right) cos\left(\int_{t_0}^{t} k_i(t)dt\right) \end{aligned} \tag{3.5}$$

k_r and k_i are respectively the real and imaginary parts of the characteristic roots of Eq.3.1. C_1 and C_2 are arbitrary constants which depend on the initial conditions of the original differential equation. The above approach was developed by Ramnath in order to solve such systems of any order. This general theory is applied to a fourth order system in the next section.

3.3 Fourth Order GMS Solution

The GMS approximation to a fourth order linear differential equation with varying coefficients is detailed in this section. The full GMS solution is obtained by first obtaining approximations to the dynamics associated with each of the modes of motion.[7, 8] Consider the fourth order equation

$$\frac{d^4x}{dt^4} + \omega_3(t)\frac{d^3x}{dt^3} + \omega_2(t)\frac{d^2x}{dt^2} + \omega_1(t)\frac{dx}{dt} + \omega_0(t)x = 0 \tag{3.6}$$

The characteristic roots which describe the solution of the equation are them given by the fourth order algebraic equation

$$s^4 + \omega_3 s^3 + \omega_2 s^2 + \omega_1 s + \omega_0 = 0 \tag{3.7}$$

Since the coefficients of this equation vary with time, it is clear that the characteristic roots of this system also change with time. Depending on the nature of the coefficients, the four roots of the algebraic equation are comprised of pairs of complex conjugates or real roots. A particular mode of motion is represented by either a pair of complex conjugates roots or a single real root. As shown by Ramnath, the GMS solution to Eq.3.6 is obtained by first approximating the motion associated with each of the modes. If a mode is represented by a single real root, k, then the GMS approximation to its characteristic motion is given by

$$x(t) = exp\left(\int_{t_0}^{t_f} k(t)dt\right) \tag{3.8}$$

If a particular mode is represented by a complex conjugate pair of roots given by $k(t) = k_r \pm ik_i$ then the GMS fast and slow solutions to the characteristic motion are given by

$$x(t) = x_s(t)x_f(t) \tag{3.9}$$

where the slow solution is

$$x_s(t) = exp\left(\int_{t_0}^{t_f} \left|\frac{\dot{k_r}(t)}{2ik_i(t)}\right| dt\right) \tag{3.10}$$

and the fast solution is given by

$$\begin{aligned} x_f(t) &= C_1 exp\left(\int_{t_0}^{t} k_r(t)dt\right) sin\left(\int_{t_0}^{t} k_i(t)dt\right) + \\ & C_2 exp\left(\int_{t_0}^{t} k_r(t)dt\right) cos\left(\int_{t_0}^{t} k_i(t)dt\right) \end{aligned} \tag{3.11}$$

C_1 and C_2 are arbitrary constants to be determined by initial conditions. The full GMS solution to the fourth order equation shown in Eq.3.6 is obtained by a linear combination of the approximations to each of the mode motions. For example, consider a system which contains three modes consisting of a pair of complex roots and two real roots. If the complex roots are given by $k_r + ik_i$ and the real roots are k_1 and k_2 respectively, then the full GMS solution to the system is given by

$$\begin{aligned} x(t) &= C_1 exp\left(\int_{t_0}^{t_f} \left|\frac{\dot{k_r}(t)}{2ik_i(t)}\right| dt\right) exp\left(\int_{t_0}^{t} k_r(t)dt\right) sin\left(\int_{t_0}^{t} k_i(t)dt\right) + \\ & C_2 exp\left(\int_{t_0}^{t_f} \left|\frac{\dot{k_r}(t)}{2ik_i(t)}\right| dt\right) exp\left(\int_{t_0}^{t} k_r(t)dt\right) cos\left(\int_{t_0}^{t} k_i(t)dt\right) + \\ & C_3 exp\left(\int_{t_0}^{t_f} k_1(t)dt\right) + C_4 exp\left(\int_{t_0}^{t_f} k_2(t)dt\right) \end{aligned} \tag{3.12}$$

The constants C_1, C_2, C_3, and C_4 are determined by initial conditions of the original differential equation.

Chapter 4

Second Order Longitudinal Dynamics

4.1 Overview

The second order longitudinal dynamics of the GHAME vehicle flying along the Space Shuttle trajectory are studied through the use of second order GMS solutions developed in section 3.1. The GMS solutions to angle-of-attack perturbations during reentry are compared to numerical approximations. The sensitivity of longitudinal motions to various aerodynamic coefficients is obtained by the differentiation of the analytical approximations provided by GMS theory. This is based on Ramnath's sensitivity theory of variable systems. Second order longitudinal stability is assessed through a GMS stability criterion developed by Ramnath. One possible way to display such stability information to a flight crew is considered.

4.2 Equations of Motion

The following equations describing the longitudinal motions of an aircraft are developed under the assumption that the vehicle experiences lift, but does not exhibit a rolling or yawing motion. The coordinate system is such that the x-axis is always tangential to the instantaneous flight path. Under such conditions, the equations of

motion in the plane of symmetry are described by[4, 3, 10, 11]

$$\dot{V} = -\rho S C_D V^2/(2m) - g sin\gamma \tag{4.1}$$

$$V\dot{\gamma} = \frac{\rho S C_L V^2}{2m} - \left(g - \frac{V^2}{R}\right) cos\gamma \tag{4.2}$$

$$\dot{q} = \frac{\rho S l C_m V^2}{2I_{yy}} - \frac{3g}{2R}\left(\frac{I_{xx} - I_{yy}}{I_{yy}}\right) sin2\theta \tag{4.3}$$

and the kinematic relations

$$\dot{\theta} = q + (V/R)cos\gamma \tag{4.4}$$

$$\dot{R} = V sin\gamma \tag{4.5}$$

$$\theta = \gamma + \alpha \tag{4.6}$$

The dot in the equations above denotes differentiation with respect to time.

Assuming that the slope of the lift curve is approximately independent of flight speed and Mach number at high supersonic speeds, the aerodynamic coefficients in Eqs.4.1-4.3 are linearized through a Taylor Series expansion about the nominal trajectory. After eliminating θ and V from the equations, a change of variable is made. The independent variable time is replaced by a non-dimensional parameter ξ according to the relationship

$$l\xi = \int_0^t V(t)dt \tag{4.7}$$

The new independent variable is the non-dimensional number of vehicle lengths traversed along the trajectory. This variable transformation leads to the following general equation for transient angle-of-attack perturbation.

$$\bar{\alpha}'' + \omega_1(\xi)\bar{\alpha}' + \omega_0(\xi)\bar{\alpha} = 0 \tag{4.8}$$

where

$$\omega_1(\xi) = \delta[C_{L_\alpha} - \sigma(C_{m_\alpha} + C_{m_q})] + V'/V \tag{4.9}$$

$$\begin{aligned}\omega_0(\xi) \;=\; & -\delta\left(\sigma C_{m_\alpha} + \frac{gl}{V^2} C_{D_\alpha} cos\gamma\right) + \delta' C_{L_\alpha} + \\ & \delta\frac{V'}{V} C_{L_\alpha} - \delta^2[C_{L_\alpha}(\sigma C_{m_q} + C_{D_0}) + C_{L_0} C_{D_\alpha}] + \\ & \frac{3l}{R}\left(\frac{gl}{V^2}\right)\nu cos2(\gamma + \alpha_0)\end{aligned} \tag{4.10}$$

The non-dimensional parameters are defined by

$$\delta = \frac{\rho S l}{2m} \qquad \nu = \frac{I_{xx} - I_{zz}}{I_{yy}} \qquad \sigma = \frac{ml^2}{I_{yy}} \tag{4.11}$$

The primes in Eqs.4.8-4.10 represent differentiation with respect to the new independent variable ξ. It can be seen from Eqs.4.9 and 4.10 that both the coefficients ω_1 and ω_0 are functions of parameters which depend on instantaneous flight conditions, and can be calculated only if the trajectory is explicitly known. It is clear that Eq.4.8 is a second order linear differential equation containing coefficients which vary with the independent variable. In its most general form, Eq.4.8 cannot be solved exactly. In the next section, Ramnath's Generalized Multiple Scales theory is employed to obtain approximate solutions to Eq 4.8 with only mild restrictions on the vehicle or trajectory.

4.3 GMS Solutions to Dynamics

Approximate solutions to angle-of-attack perturbations of the GHAME vehicle flying along the shuttle trajectory are developed by applying Ramnath's GMS solutions detailed in section 3.1. The GMS solutions are employed under the assumption that the coefficients of Eq.4.8 vary slowly. During reentry from an altitude of 400,000 ft., the variations in the coefficients of Eq.4.8 are primarily caused by the changes in density, velocity, and moment parameters. These changes are slow when compared

to the time constant of vehicle motion.[3, 8] From the equations developed in section 3.2, the GMS solution to Eq.4.8 is given by

$$\begin{aligned}\bar{\alpha}(\xi) &= (4\omega_0 - \omega_1^2)^{-\frac{1}{4}} \left[C_1 exp\left(\int_{\xi_0}^{\xi} k_r(\xi) d\xi \right) sin\left(\int_{\xi_0}^{\xi} k_i(\xi) d\xi \right) \right. \\ &\quad \left. + C_2 exp\left(\int_{\xi_0}^{\xi} k_r(\xi) d\xi \right) cos\left(\int_{\xi_0}^{\xi} k_i(\xi) d\xi \right) \right] \end{aligned} \tag{4.12}$$

The coefficients of Eq.4.8 as defined in Eqs.4.9 and 4.10 are calculated along the Shuttle trajectory employing the aerodynamic data included in the GHAME model. Since nominal angle-of-attack values of the prescribed trajectory are so large, a least-squares analysis is required to extrapolate aerodynamic data for the GHAME vehicle at the flight conditions desired. The values of the coefficients ω_1 and ω_0 are plotted along the trajectory in Figs.4-1 and 4-2. Again, the independent variable ξ is the number of vehicle lengths traversed along the trajectory. From the coefficients shown in Figs.4-1 and 4-2, the characteristic roots of Eq.3.1 are calculated. Variations of these roots as the GHAME vehicle progresses along the reentry trajectory are shown in Fig.4-3. Finally, this information is substituted into Eq.4.12 in order to obtain final GMS approximations to the angle-of-attack perturbation dynamics.

Two sets of solutions are developed for different sets of initial conditions. In order to obtain a solution of a sine wave nature, the initial conditions are set at $\bar{\alpha}(\xi_0) = 0$ and $\bar{\alpha}'(\xi_0) = k_i(\xi_0)$. A solution of a cosine wave form is obtained with the initial conditions $\bar{\alpha}(\xi_0) = 1$ and $\bar{\alpha}'(\xi_0) = 0$. For the purposes of comparison, a numerical approximation to Eq.4.8 is also generated by means of a Runge-Kutta integration scheme. In addition to the numerical approximation, an exact solution to a 'frozen' system is obtained for further comparison. The coefficients of Eq.4.8 are assumed to be constant at their initial reentry values, and a constant coefficient analysis is employed to generate solutions to the 'frozen' system. The GMS approximations are plotted for the two sets of initial conditions in Fig.4-4 and 4-5 along with their respective numerical and 'frozen' counterparts. The fast scale solution of the GMS approximation is also included.

As seen in Figs.4-4 and 4-5, the angle-of-attack perturbations of the GHAME

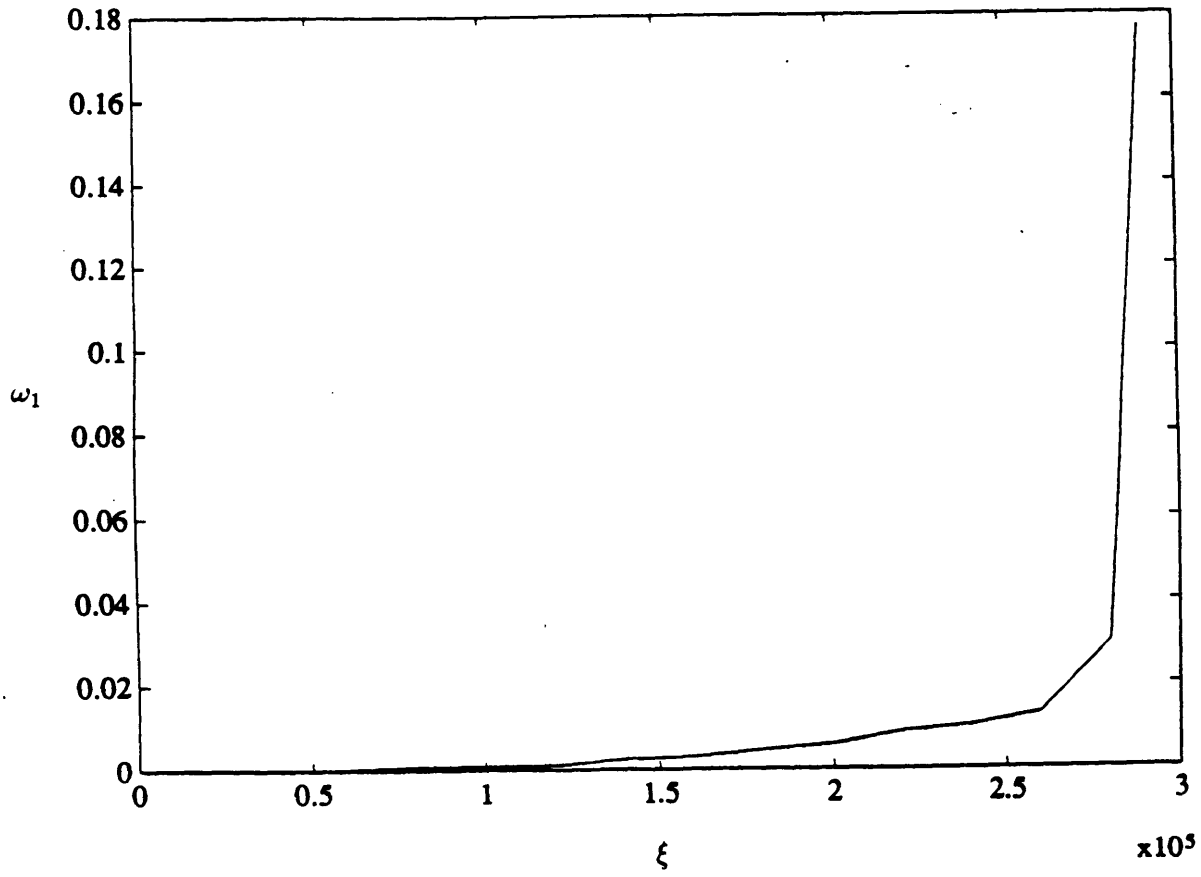

Figure 4-1: Variation of Coefficient ω_1 Along Trajectory

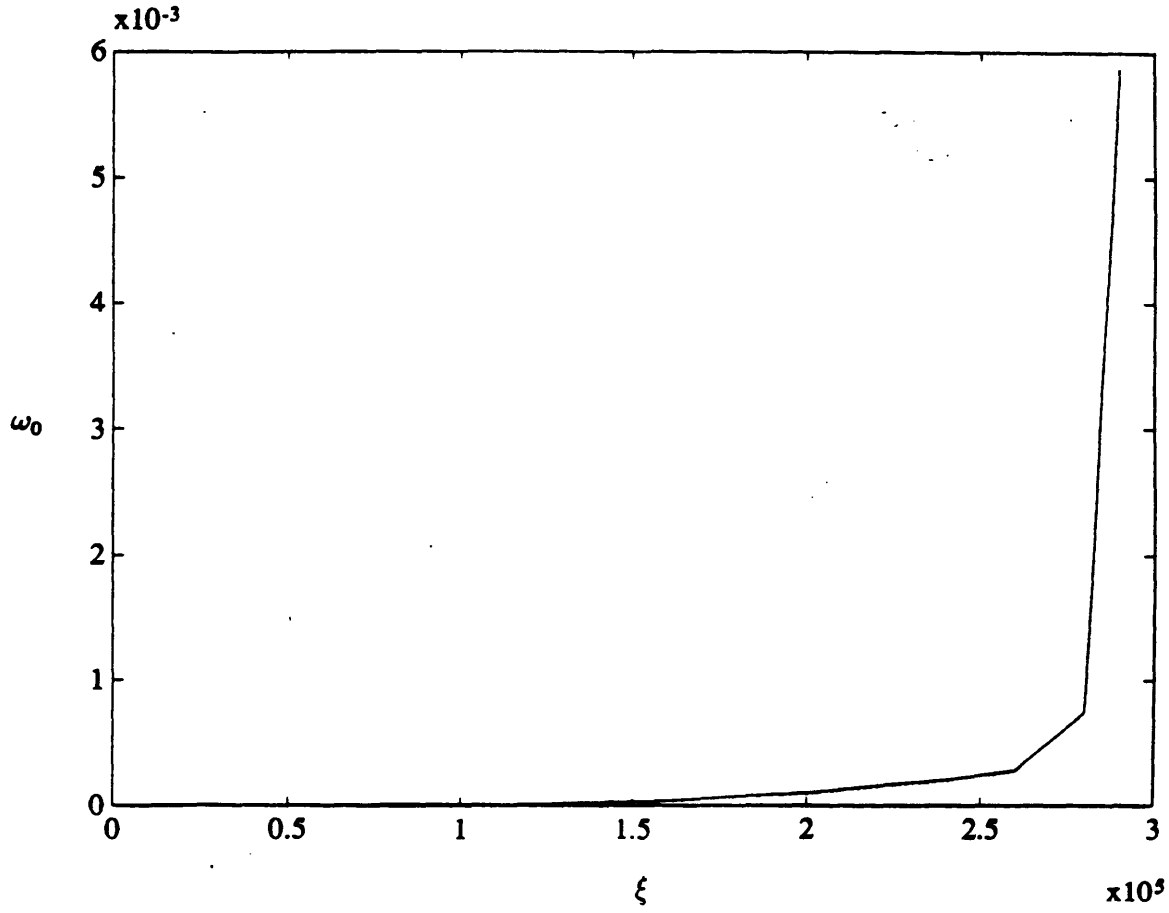

Figure 4-2: Variation of Coefficient ω_0 Along Trajectory

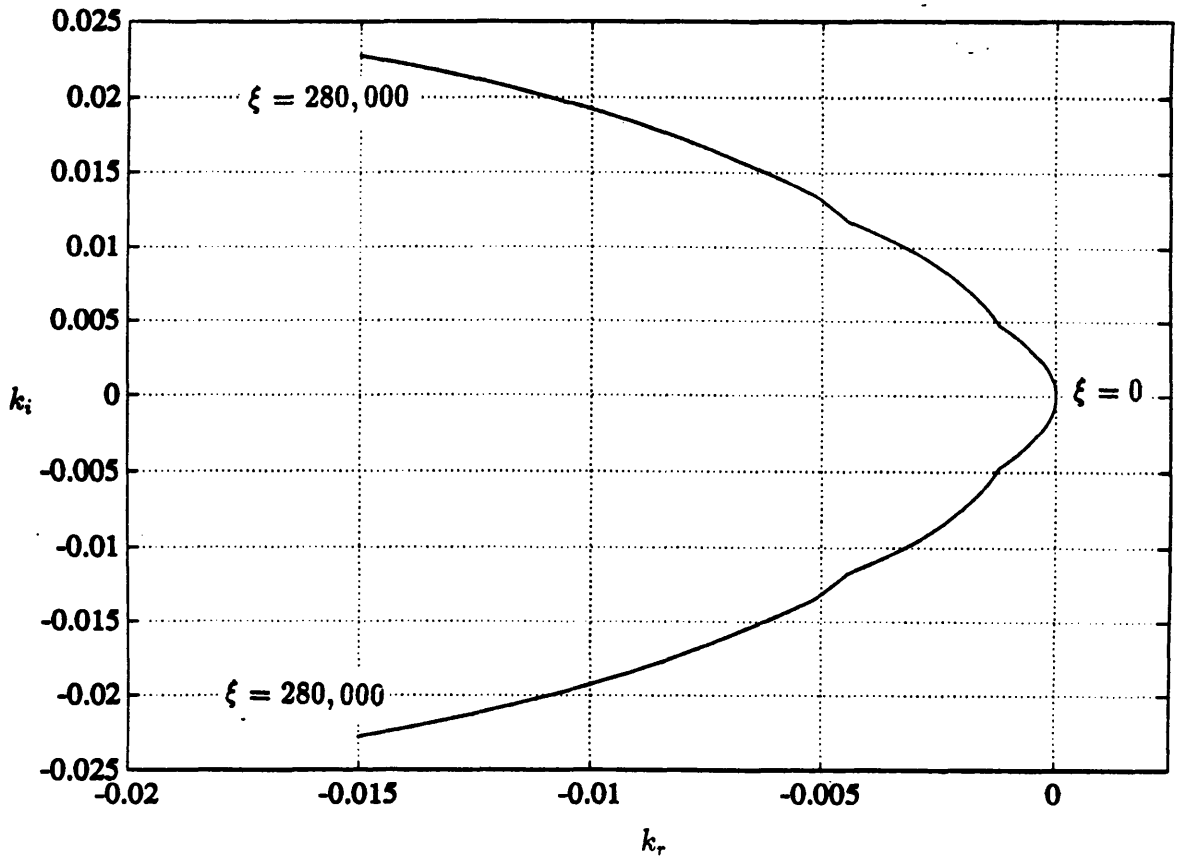

Figure 4-3: Clock Function Variations Along Trajectory

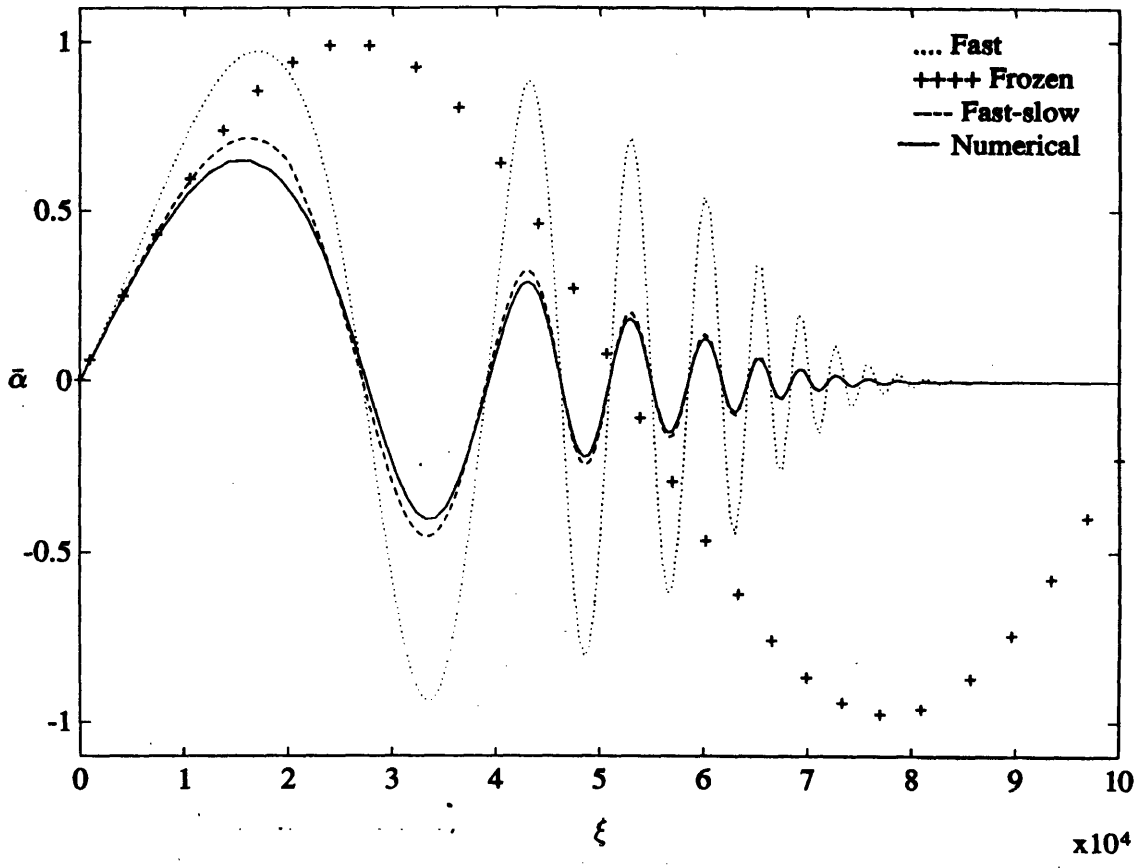

Figure 4-4: Sine-like Solutions to Angle-of-Attack Perturbations

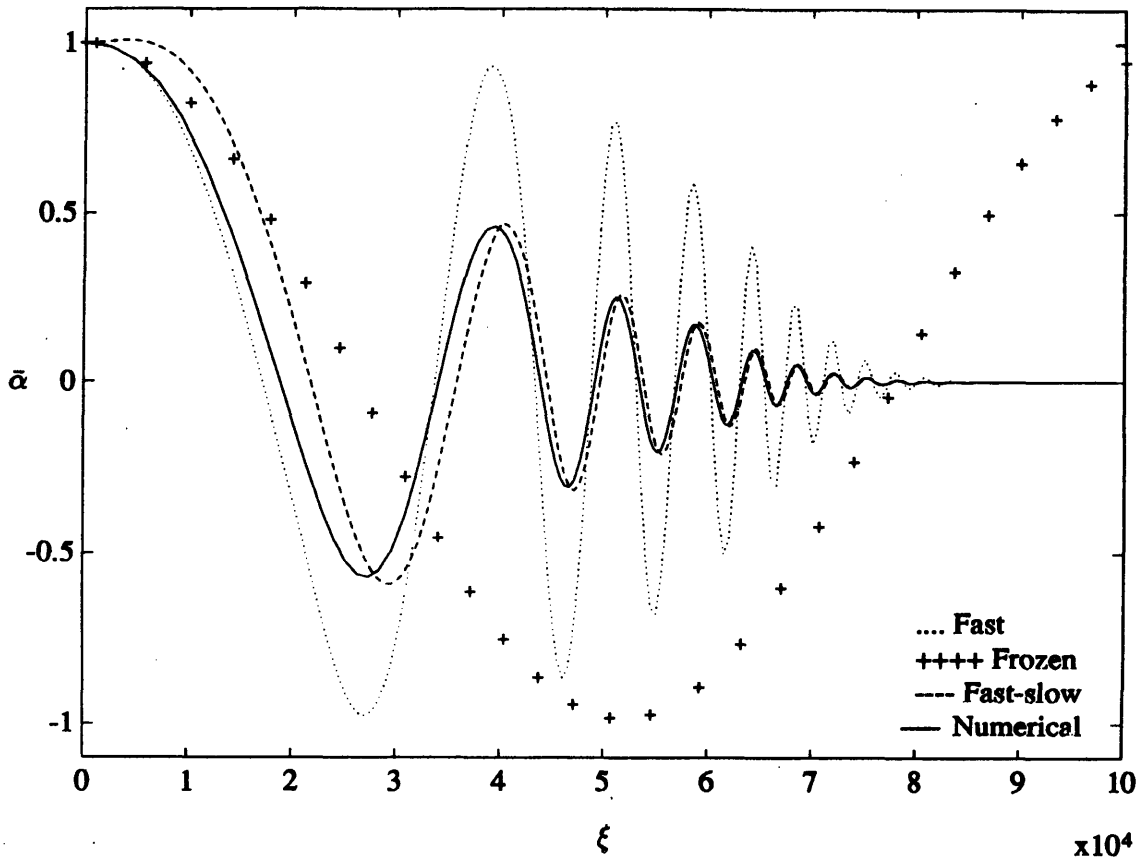

Figure 4-5: Cosine-like Solutions to Angle-of-Attack Perturbations

vehicle during reentry behave as damped oscillations with increasing frequency. Upon comparison to the numerical solutions, the GMS fast scale solution predicts these frequency changes of the angle-of-attack perturbation dynamics quite accurately. In both the sine and cosine-like cases, the zero-crossings of the fast scale solutions and the numerical solutions occur virtually at the same instant. When the slow scale solution is incorporated to form the full GMS approximation, the complete dynamics are predicted with great accuracy. For both sets of initial conditions, the fast scale solutions predict the frequency changes yet consistently overshoot the magnitude variations. When the slow scale solution is included, the magnitude of the dynamics is also predicted accurately. In the sine-like dynamics, the full GMS solution overshoots the amplitude of the numerical solution by a negligible margin, and matches the frequency completely. In the cosine-like case, both the GMS and numerical solutions exhibit the same amplitude behavior, while the frequency appears to have a phase shift towards the beginning of the trajectory. This may be due to the proximity of the clock function roots to the real axis early in the trajectory.

The 'frozen' approximation is one that is often employed in the engineering analysis of slowly varying systems. Despite its use, it can clearly be seen that by freezing the system at the initial point, the dynamics of the vehicle are totally misrepresented. In both sets of initial conditions, the frozen approximation becomes quite invalid after approximately half a cycle. The dynamics of angle-of-attack perturbations are clearly better predicted by GMS theory.

4.4 Sensitivity Analysis

In the study of vehicle dynamics, it is often useful to determine how certain physical parameters of the aircraft can affect its motion. Since the GMS method provides solutions to vehicle dynamics in simple analytical forms, a sensitivity analysis can be performed by simple partial differentiation with respect to various physical parameters. Sensitivity of the GHAME vehicle second order angle-of-attack perturbations to certain aerodynamic coefficients is studied in this manner. The aerodynamic coef-

ficients C_{L_α}, C_{m_α}, and C_{m_q} are chosen due to their importance in the determination of longitudinal dynamics.

It should be noted that partial differentiation of the GMS angle-of-attack solutions with respect to the aerodynamic coefficients does not provide a true sensitivity analysis. Partial differentiation with respect to the aerodynamic coefficients assumes that these parameters are constant. In reality, these aerodynamic coefficients also vary along the trajectory, and in order to conduct a true sensitivity study, variational principles should be utilized. However, Ramnath has shown that the partial differentiation is a suitable approximation to variational methods, and vehicle sensitivity to physical parameters can be studied by treating the aerodynamic coefficients as if they are constant.

The GMS approximation to angle-of-attack perturbation can be written in the form

$$\bar{\alpha}(\xi) = \bar{\alpha}_s(\xi)\bar{\alpha}_f(\xi) \tag{4.13}$$

where the fast and slow solutions are as shown in Eq.4.12. Partial differentiation with respect to the aerodynamic coefficient C_{L_α} is now carried out. The GMS solution shown above is not only a function of the variable ξ, but also a function of the the aerodynamic coefficients in question. Thus, differentiating Eq.4.13 with respect to C_{L_α} gives

$$\frac{\partial\bar{\alpha}}{\partial C_{L_\alpha}} = \bar{\alpha}_s\frac{\partial\bar{\alpha}_f}{\partial C_{L_\alpha}} + \bar{\alpha}_f\frac{\partial\bar{\alpha}_s}{\partial C_{L_\alpha}} \tag{4.14}$$

It now must be determined how the fast and slow GMS solutions each vary with respect to changes in $C_{L\alpha}$. From Eq.4.12, the fast solution, $\bar{\alpha}_f$, can be written in the form

$$\bar{\alpha}_f = C_1 e^A sin(B) + C_2 e^A cos(B) \tag{4.15}$$

where A and B are defined by

$$A = \int_{\xi_0}^{\xi} k_r(\xi)d\xi = -\frac{1}{2}\int_{\xi_0}^{\xi}\omega_1(\xi)d\xi \tag{4.16}$$

$$B = \int_{\xi_0}^{\xi} k_i(\xi)d\xi = \frac{1}{2}\int_{\xi_0}^{\xi}[4\omega_0(\xi) - \omega_1(\xi)^2]^{\frac{1}{2}}d\xi \tag{4.17}$$

Without considering the dependence of initial or boundry conditions on the parameter, differentiating Eq.4.15 with respect C_{L_α} leads to the equation

$$\frac{\partial \bar{\alpha}_f}{\partial C_{L_\alpha}} = \left(C_1\frac{\partial A}{\partial C_{L_\alpha}} - C_2\frac{\partial B}{\partial C_{L_\alpha}}\right)e^A sin(B) + \left(C_2\frac{\partial A}{\partial C_{L_\alpha}} + C_1\frac{\partial B}{\partial C_{L_\alpha}}\right)e^A cos(B) \tag{4.18}$$

where from Eqs.4.16 and 4.17

$$\frac{\partial A}{\partial C_{L_\alpha}} = -\frac{1}{2}\int_{\xi_0}^{\xi}\frac{\partial \omega_1}{\partial C_{L_\alpha}}d\xi \tag{4.19}$$

and

$$\frac{\partial B}{\partial C_{L_\alpha}} = \frac{1}{4}\int_{\xi_0}^{\xi}\left[(4\omega_0 - \omega_1^2)^{-\frac{1}{2}}\left(4\frac{\partial \omega_0}{\partial C_{L_\alpha}} - 2\omega_1\frac{\partial \omega_1}{\partial C_{L_\alpha}}\right)\right]d\xi \tag{4.20}$$

Now the slow GMS solution is differentiated with respect to the aerodynamic coefficient. The slow solution is given by

$$\bar{\alpha}_s(\xi) = (4\omega_0 - \omega_1^2)^{-\frac{1}{4}} \tag{4.21}$$

Partial differentiation with respect to C_{L_α} leads to the following.

$$\frac{\partial \bar{\alpha}_s}{\partial C_{L_\alpha}} = -\frac{1}{4}(4\omega_0 - \omega_1^2)^{-\frac{5}{4}}\left(4\frac{\partial \omega_0}{\partial C_{L_\alpha}} - 2\omega_1\frac{\partial \omega_1}{\partial C_{L_\alpha}}\right) \tag{4.22}$$

In order to calculate the sensitivity of the full GMS angle-of-attack perturbations to C_{L_α}, it is now required to determine the sensitivity of the coefficients ω_1 and ω_0 to the aerodynamic parameter. Once this is obtained, the information is substituted into the above equations, and the effect of C_{L_α} on vehicle dynamics is obtained. The effect of other aerodynamic coefficients such as C_{m_α} and C_{m_q} on vehicle dynamics

can also be determined in a similar matter. All of the sensitivity equations developed above are rendered valid for any vehicle parameter by simply replacing C_{L_α} with the desired aerodynamic coefficient. Sensitivity solutions for C_{m_α} and C_{m_q} can also be obtained by determining their respective effects on ω_1 and ω_2 and substituting the information into Eqs.4.14-4.22.

Differentiating Eqs.4.9 and 4.10 with respect to the aerodynamic parameters mentioned above leads to the following.

$$\frac{\partial \omega_1}{\partial C_{L_\alpha}} = \delta' + \delta v'/v - \delta^2 \sigma C_{m_q} \tag{4.23}$$

$$\frac{\partial \omega_0}{\partial C_{L_\alpha}} = \delta \tag{4.24}$$

$$\frac{\partial \omega_1}{\partial C_{m_\alpha}} = -\delta\sigma \tag{4.25}$$

$$\frac{\partial \omega_0}{\partial C_{m_\alpha}} = -\delta\sigma \tag{4.26}$$

$$\frac{\partial \omega_1}{\partial C_{m_q}} = -\delta\sigma \tag{4.27}$$

$$\frac{\partial \omega_0}{\partial C_{m_q}} = -\delta^2 \sigma C_{L_\alpha} \tag{4.28}$$

By substituting the above expressions and the trajectory information into Eqs.4.14-4.22, the sensitivity of the GHAME vehicle angle-of-attack perturbations to C_{L_α}, C_{m_α}, and C_{m_q} is determined.

Sensitivity solutions are calculated for the same initial conditions employed in section 4.3. Sensitivity of a cosine-like solution is obtained with the initial conditions $\bar{\alpha}(\xi_0) = 1$, $\bar{\alpha}'(\xi_0) = 0$ while sine-like solution sensitivity is studied with the initial conditions $\bar{\alpha}(\xi_0) = 0$, $\bar{\alpha}'(\xi_0) = k_i(\xi_0)$. GHAME vehicle sensitivity to the three aerodynamic parameters along the Shuttle trajectory for both sets of initial conditions is shown in Figs.4-6 through 4-14. Sensitivity of the slow GMS solution to the various parameters is also included.

It can be seen from these plots that the angle-of-attack perturbation sensitivity

to the three aerodynamic parameters all exhibit a similar behavior. For both sets of initial conditions, the reentry sensitivity to C_{L_α}, C_{m_α}, and C_{m_q} oscillates with the same frequency that was evident in the solutions to the actual angle-of-attack dynamics. Also, the amplitude of vehicle sensitivity behaves in a similar manner for all cases. Initially, the values are relatively small, after which they

increase to a maximum at approximately 50,000 to 60,000 vehicle lengths into the trajectory. This is followed by an amplitude decay until sensitivity values reach zero at approximately 90,000 vehicle lengths. Since the sensitivity of the angle-of-attack perturbations reaches a maximum for all three aerodynamic parameters at virtually the same time, this particular section of the trajectory is crucial to the longitudinal dynamics. When the GHAME vehicle reaches the point in the trajectory where it has traveled 50,000 to 60,000 vehicle lengths, changes in the three aerodynamic parameters could have profound effects on the longitudinal dynamics.

It is important to note that the three aerodynamic parameters do not all affect the vehicle dynamics to the same degree. Although each parameter's effect on the dynamics reaches a maximum at approximately the same time, the actual sensitivity of angle-of-attack perturbations to each differs greatly. As can be seen from the plots, angle-of-attack perturbations are least sensitive to changes in the moment due to pitch rate parameter, C_{m_q}, while they are most sensitive to C_{m_α}. In fact, angle-of-attack dynamics are approximately 2000 times more sensitive to C_{m_α} than they are to C_{m_q}. Similarly, a change in C_{m_α} will have about 500 times a greater affect on the longitudinal dynamics than the same change in C_{L_α} might produce. The relative effects that each of the aerodynamic parameters has on the longitudinal dynamics of the GHAME vehicle is result of the GMS slow solution sensitivity to the parameters. The plots of the GMS slow solution sensitivity show that C_{m_α} has a much greater impact on the full GMS solution than either of the other two parameters. It is clearly evident that when concerned with the effect of changes in aerodynamic coefficients on GHAME vehicle longitudinal dynamics, greater consideration should be given to C_{m_α} than the other aerodynamic parameters.

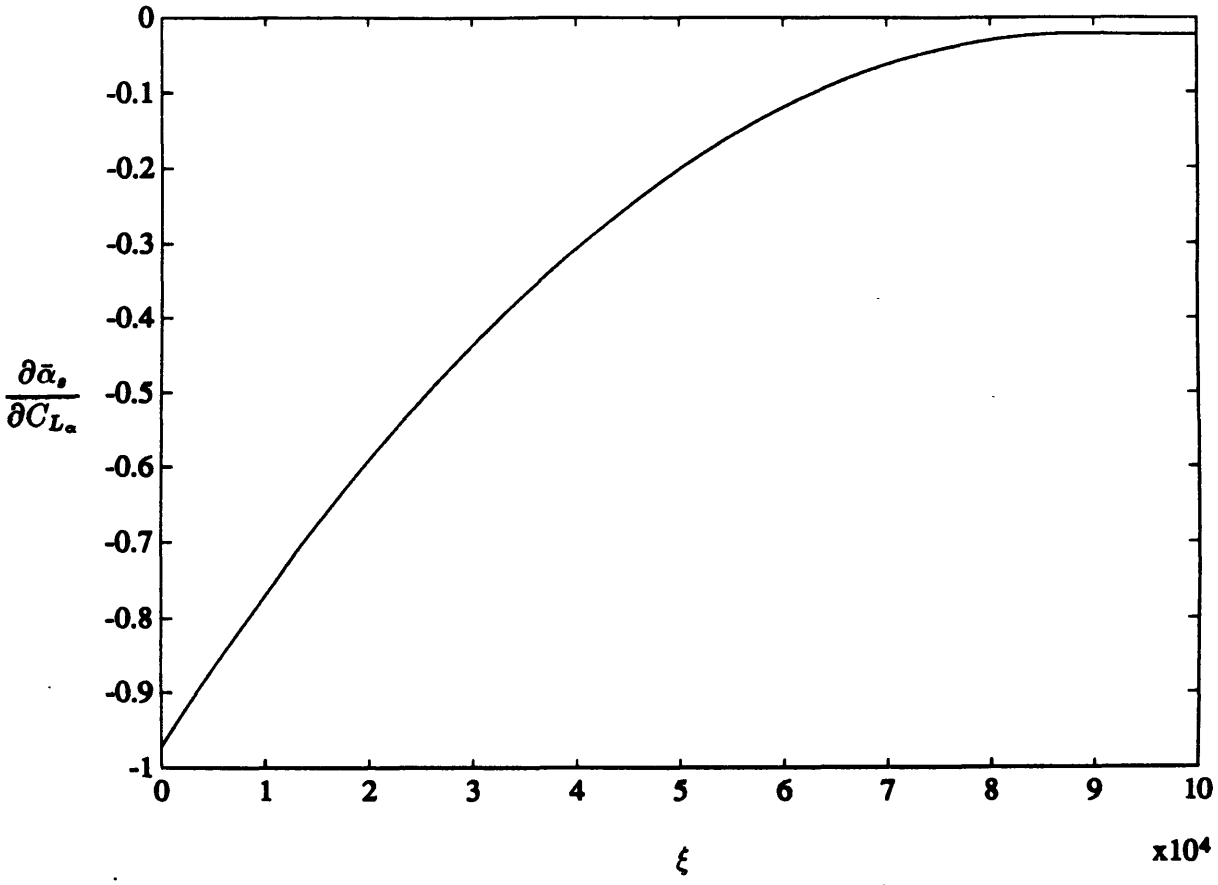

Figure 4-6: GMS Slow Solution Sensitivity to C_{L_α}

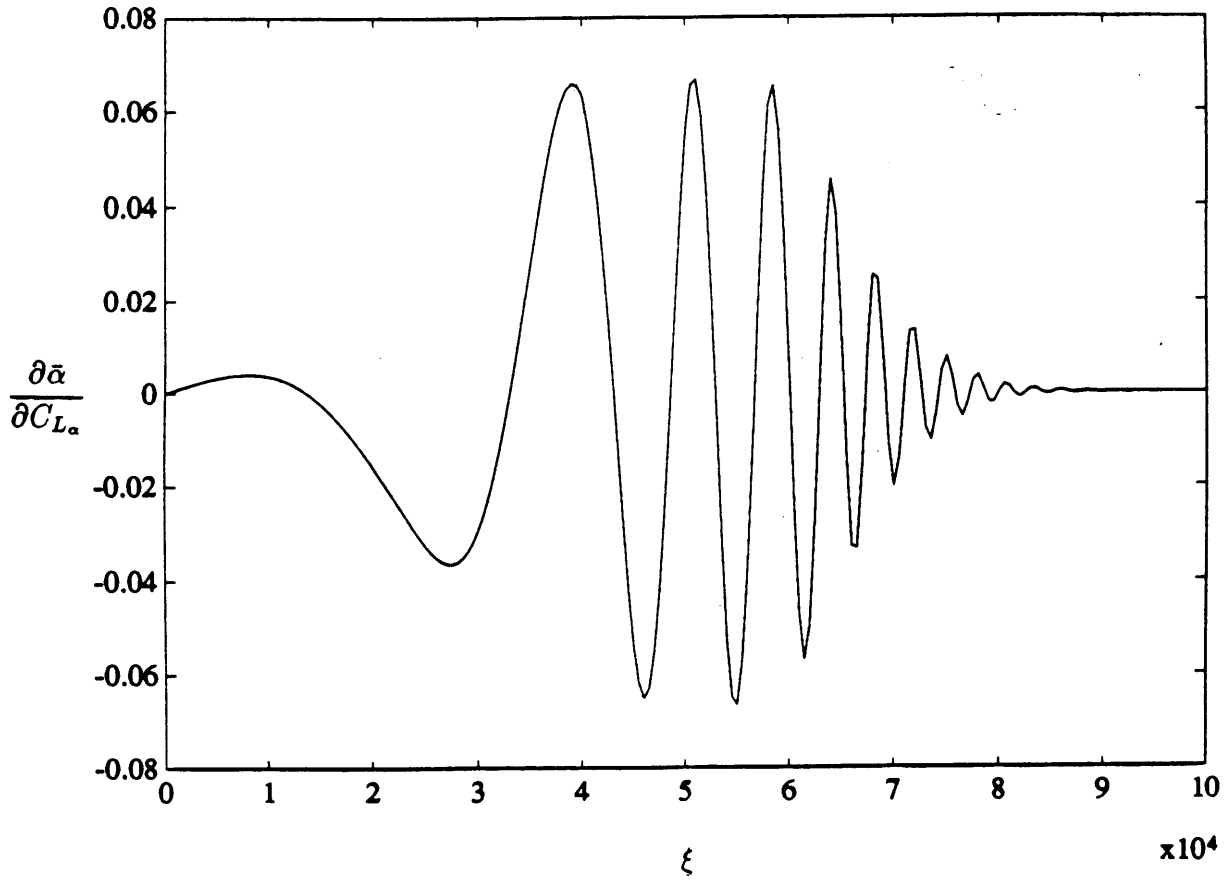

Figure 4-7: GMS Sine-like Solution Sensitivity to C_{L_α}

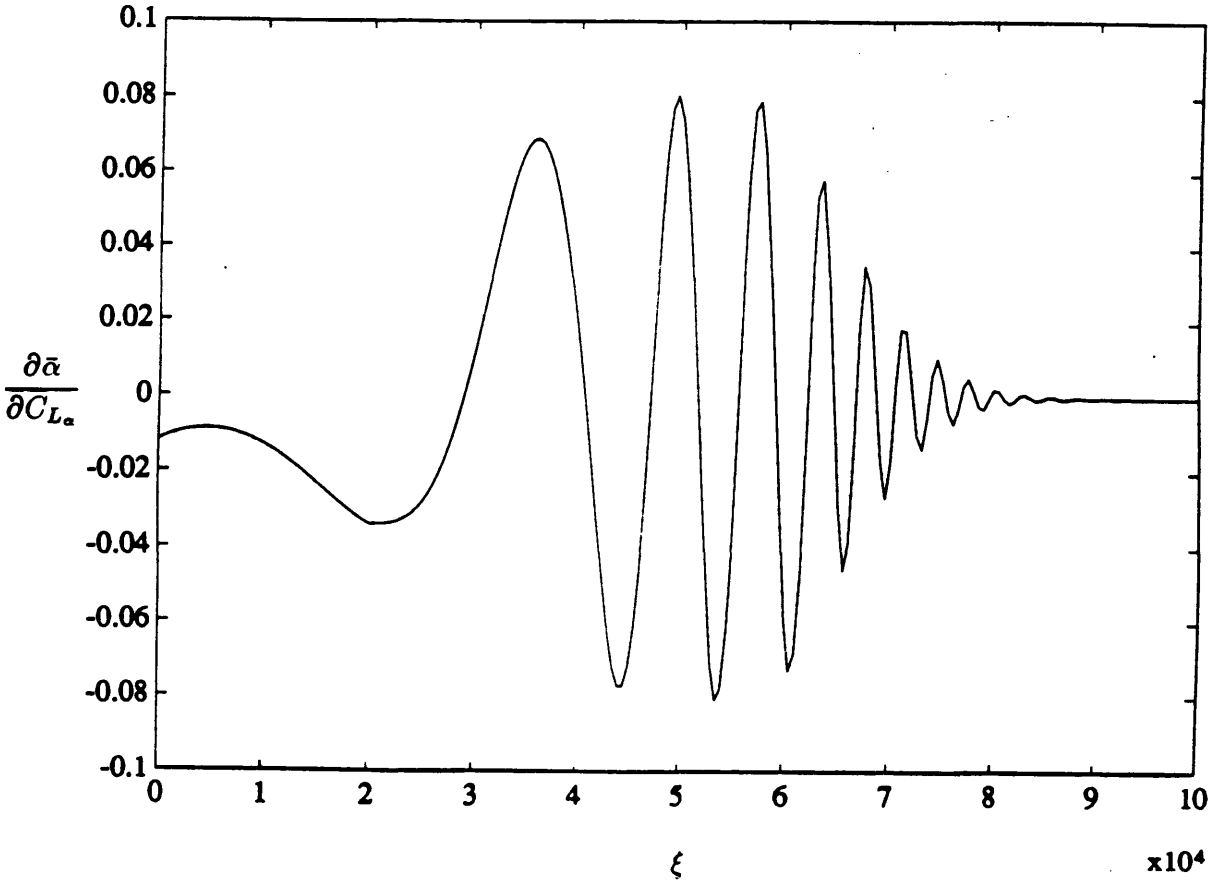

Figure 4-8: GMS Cosine-like Solution Sensitivity to C_{L_α}

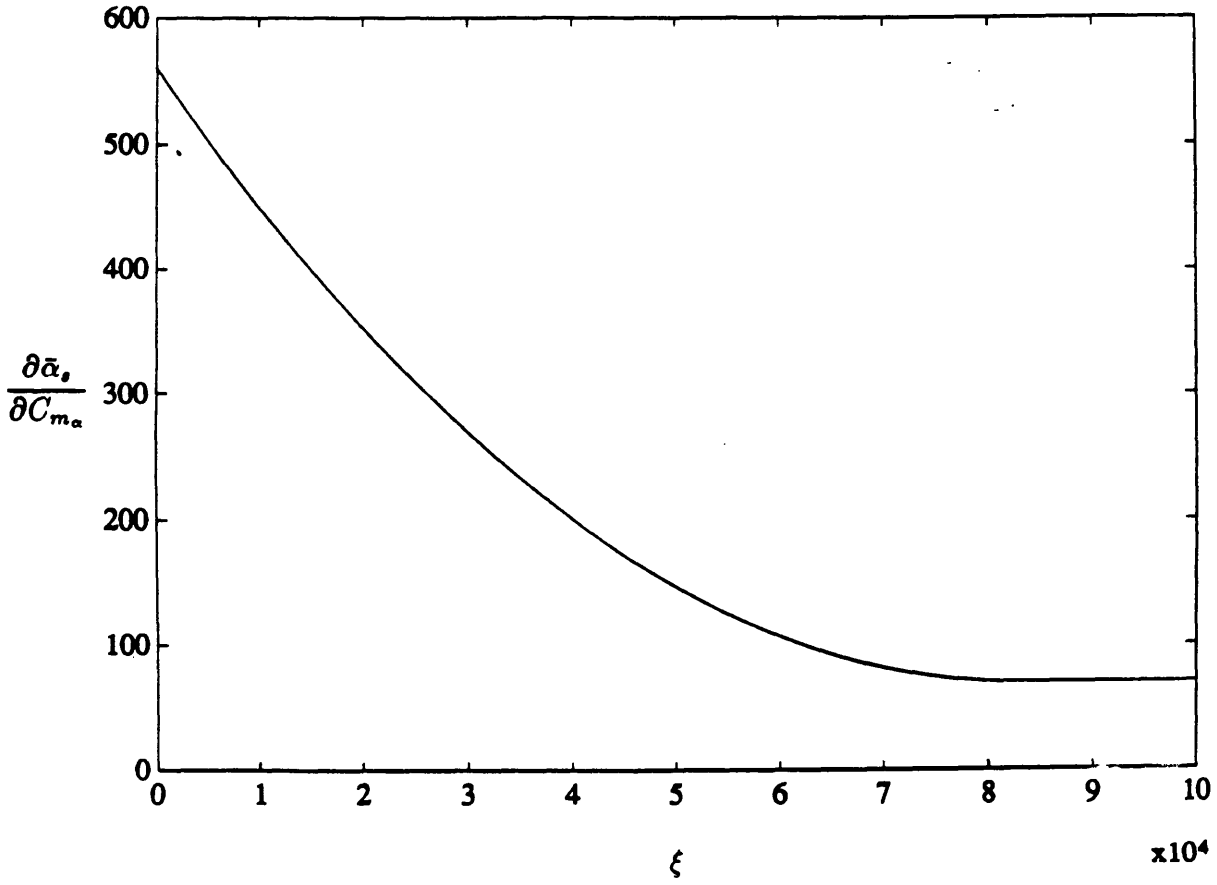

Figure 4-9: GMS Slow Solution Sensitivity to C_{m_α}

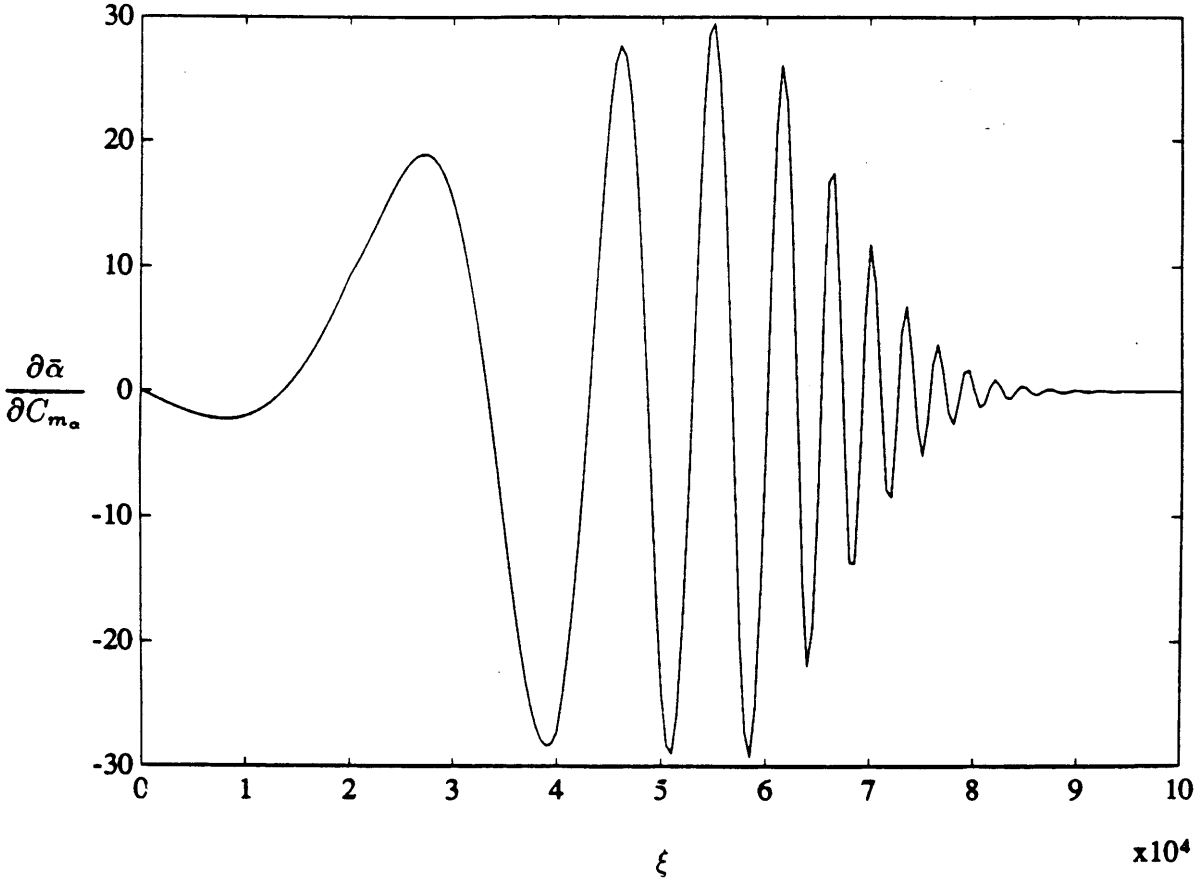

Figure 4-10: GMS Sine-like Solution Sensitivity to C_{m_α}

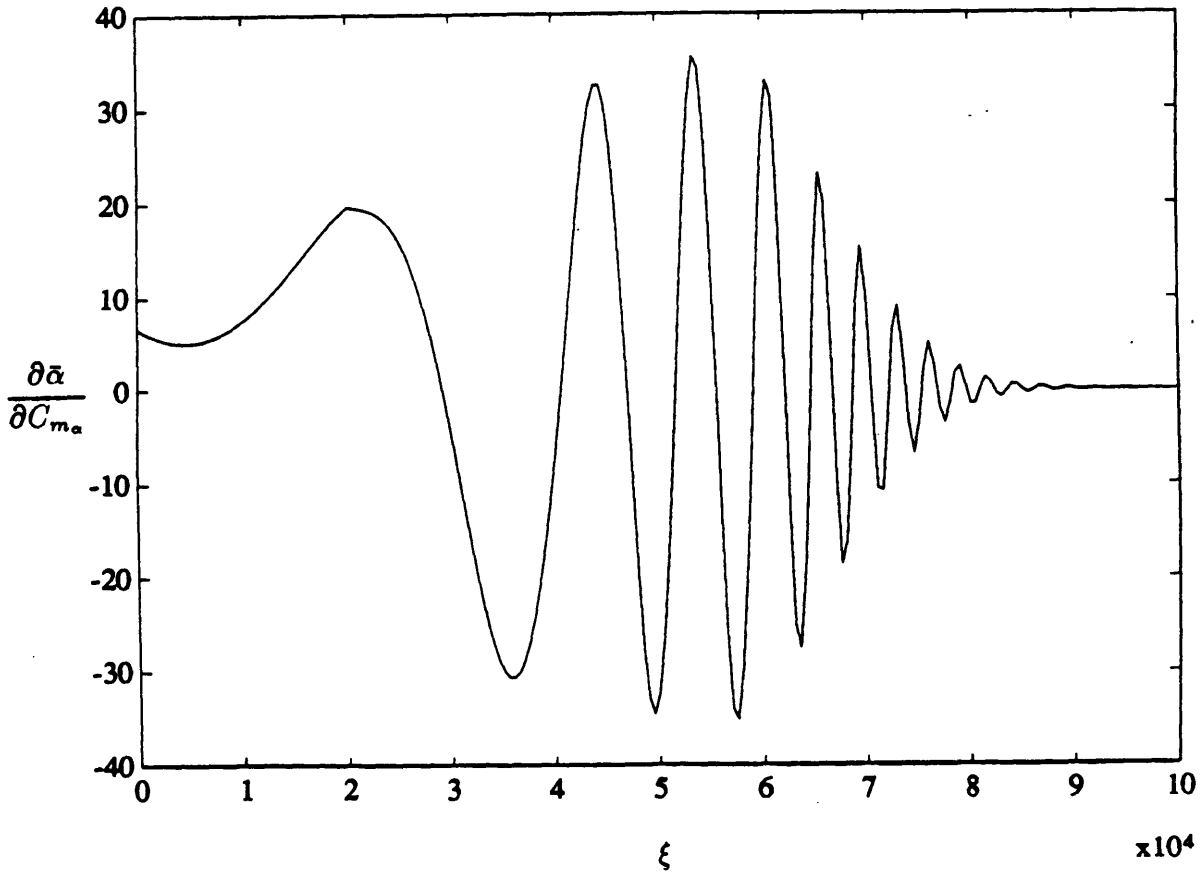

Figure 4-11: GMS Cosine-like Solution Sensitivity to C_{m_α}

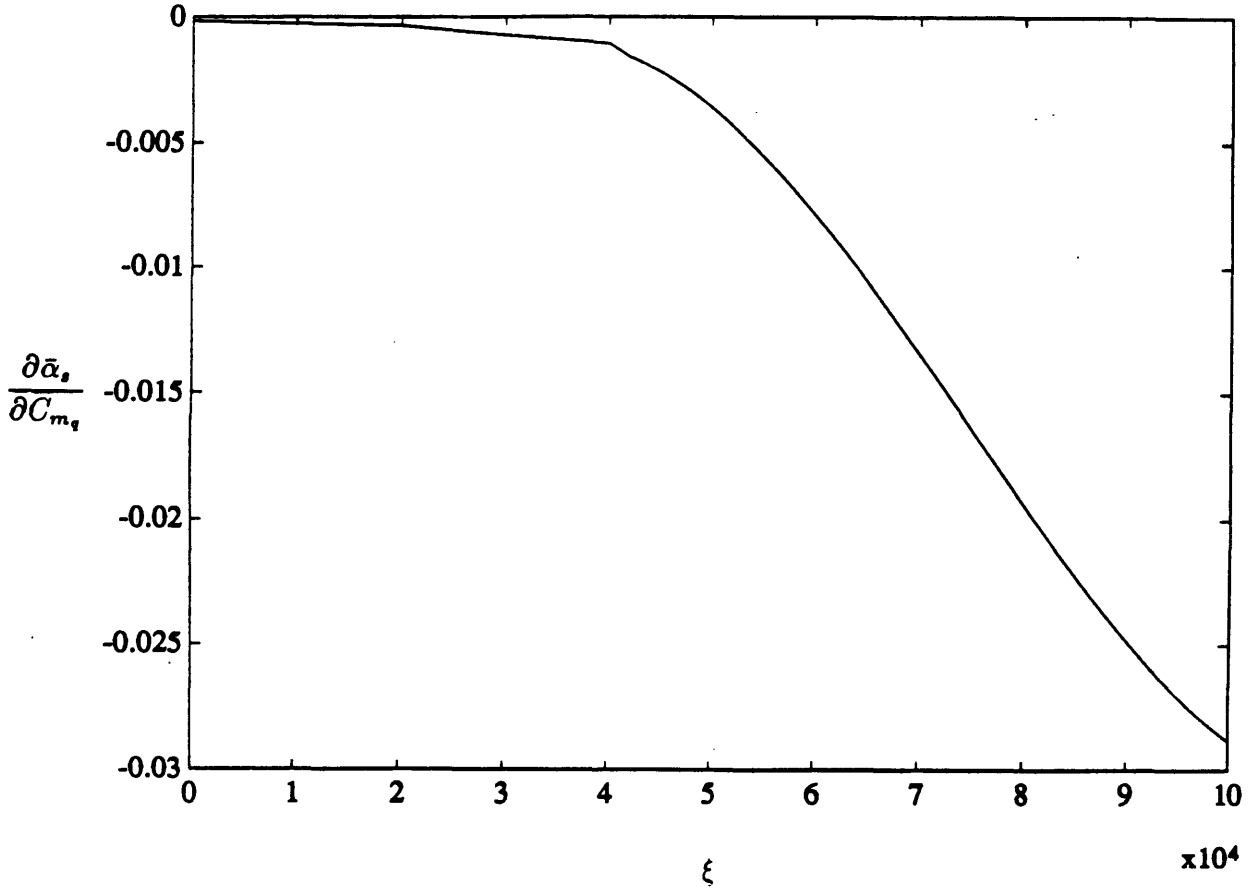

Figure 4-12: GMS Slow Solution Sensitivity to C_{m_q}

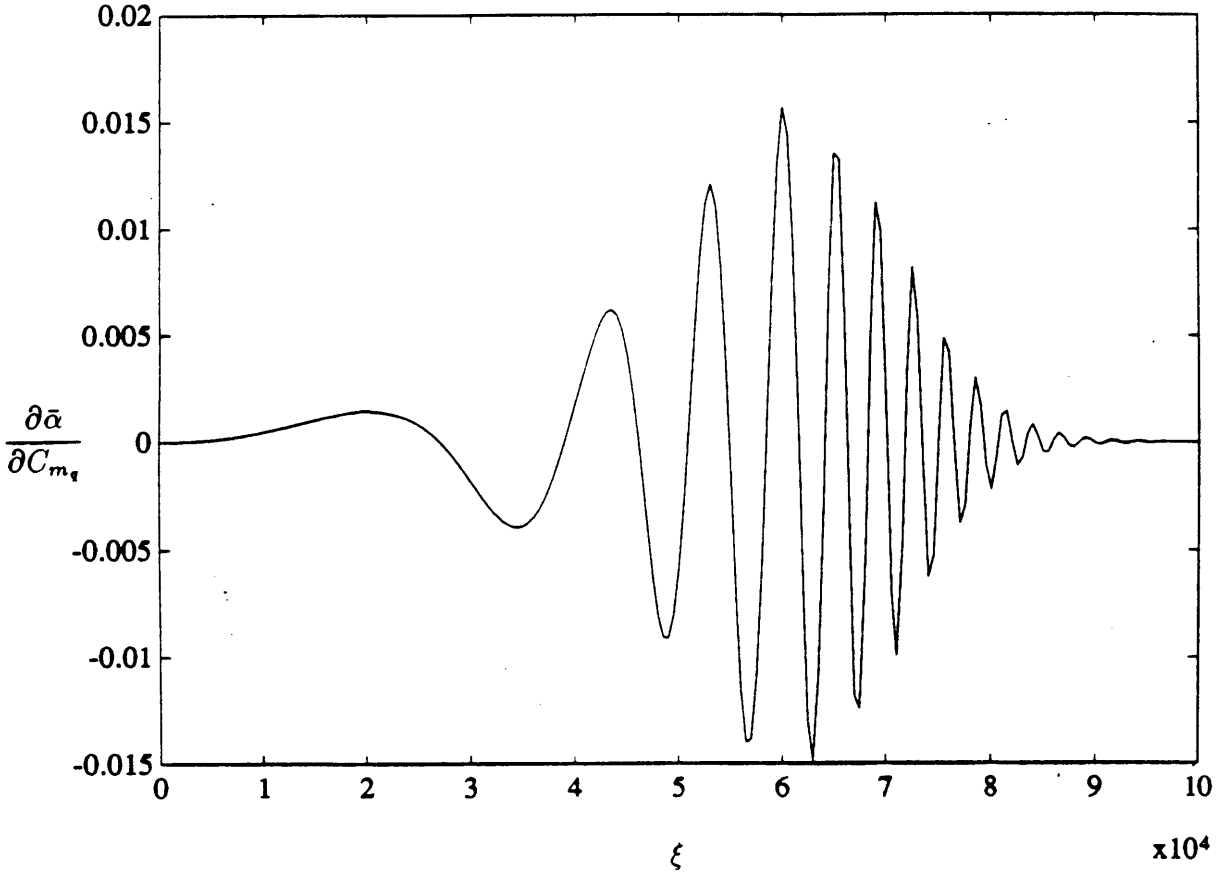

Figure 4-13: GMS Sine-like Solution Sensitivity to C_{m_q}

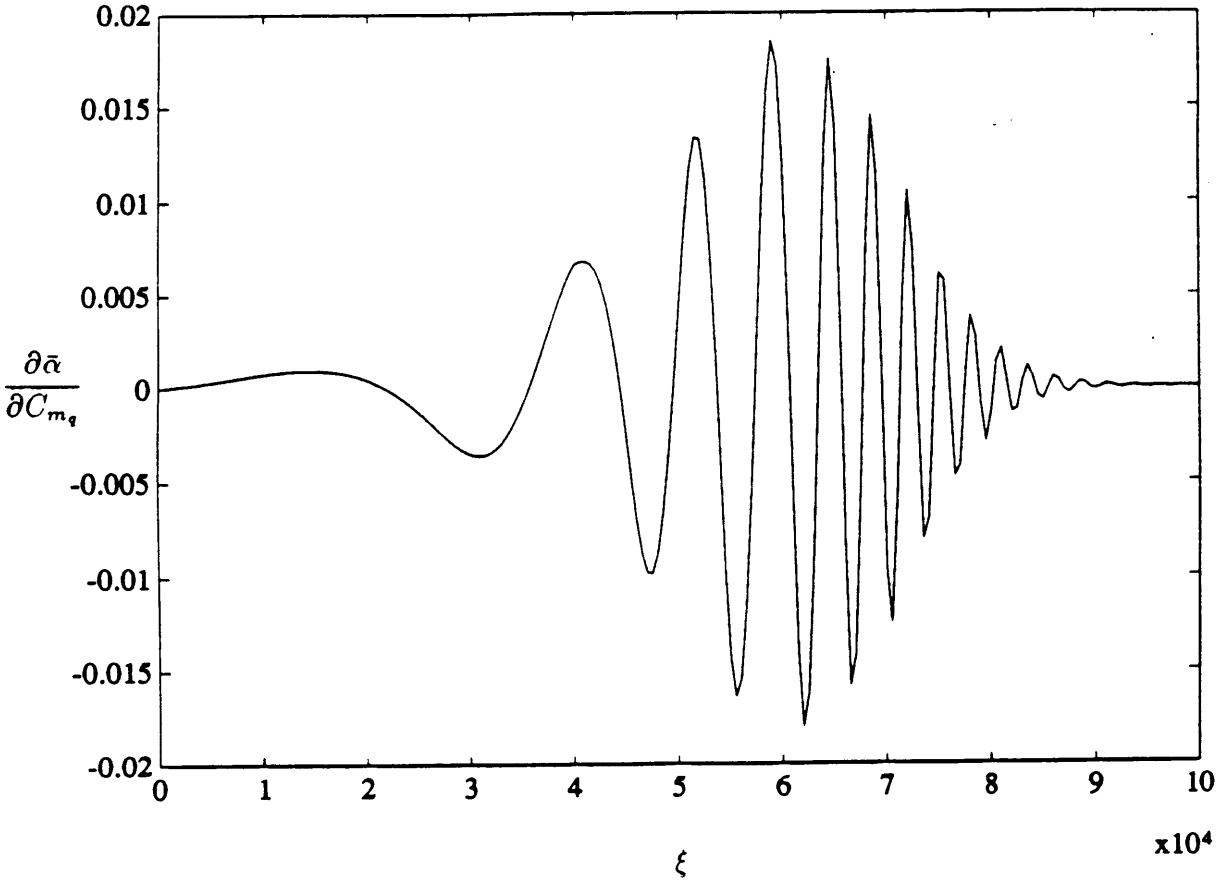

Figure 4-14: GMS Cosine-like Solution Sensitivity to C_{m_q}

4.5 Stability Analysis and Displays

The stability of the second order longitudinal GHAME vehicle dynamics is investigated in this section. The stability of variable systems such as the GHAME vehicle is, in general, very difficult to predict. Simple stability criteria applicable to this case have been developed by Ramnath. This approach is used to predict the longitudinal stability of the GHAME vehicle as it traverses the Space Shuttle reentry trajectory. The effectiveness of such a criterion to provide useful information to the GHAME vehicle flight crew is explored by presenting the stability information in the form of a flight display.

An GMS criterion for longitudinal dynamics of an aircraft was developed by Ramnath as

$$P = C_{L_\alpha} - C_{D_T} - \sigma C_{m_\alpha} \tag{4.29}$$

where C_{D_T} is the trim drag coefficient value and σ is as defined in Eq.4.11. If the stability parameter, P, is greater than zero, the vehicle's second order longitudinal motions can be considered stable. If the expression in the Eq.4.29 is of negative value, than the aircraft is longitudinally unstable. Substituting the GHAME vehicle data into the above expression, longitudinal second order stability along the shuttle trajectory is predicted. The stability parameter for the GHAME vehicle is plotted versus vehicle lengths into the trajectory as well as time elapsed in Figs.4-15 and 4-16.

It can be seen from these plots that the stability parameter never becomes negative as the GHAME vehicle travels along the Space Shuttle trajectory. Therefore, the second order longitudinal dynamics remain stable for the entire reentry. Figs.4-15 and 4-16 show that at approximately 60,000 vehicle lengths or 225 seconds into the trajectory, the stability parameter is at a minimum and the GHAME vehicle is close to becoming longitudinally unstable. It should be noted that this particular section of the trajectory is also the time at which the GHAME vehicle was found to be most sensitive to the aerodynamic parameters C_{m_α}, C_{L_α}, and C_{m_q}. The second order longitudinal dynamics are most affected by changes in the three aerodynamic coefficients at the approximately the same time that the GHAME vehicle is closest to becoming

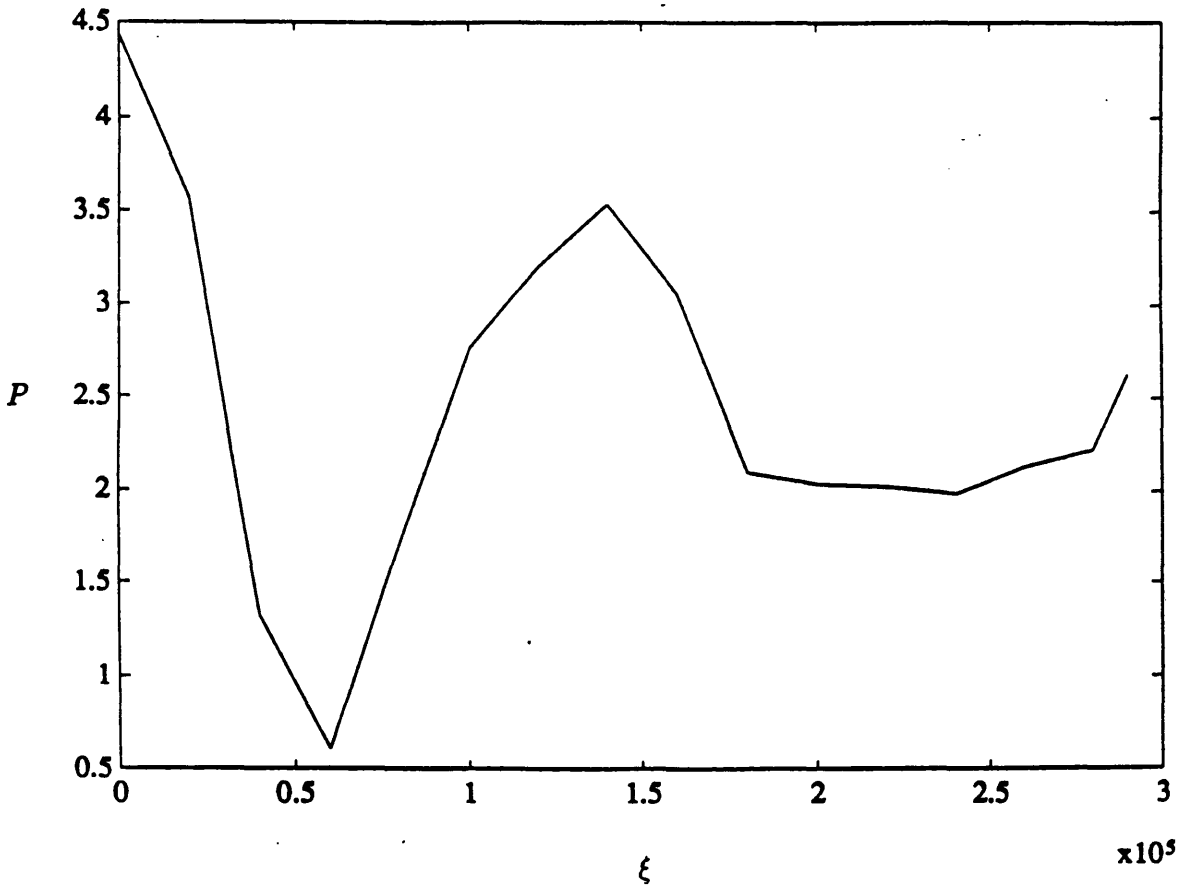

Figure 4-15: Stability Parameter vs. Vehicle Lengths Along Trajectory

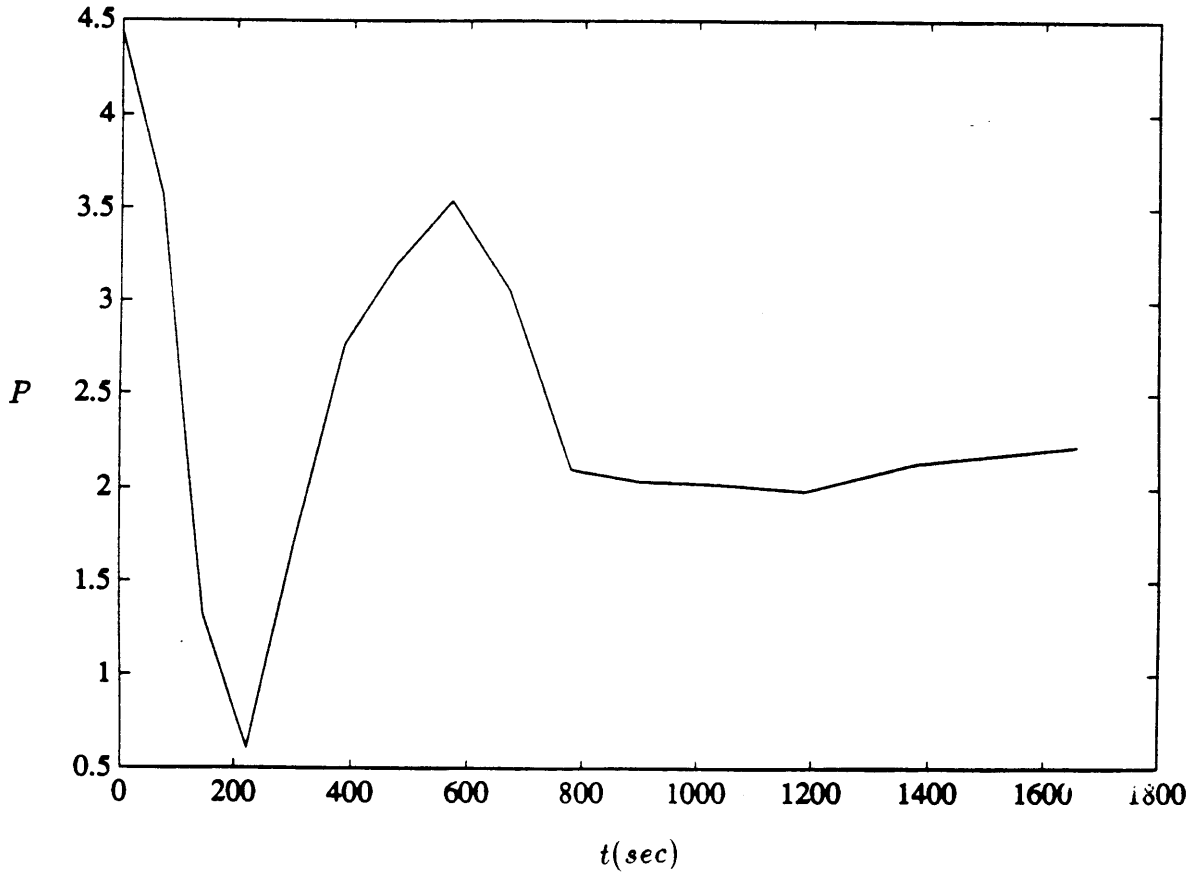

Figure 4-16: Stability Parameter vs. Elapsed Time Along Trajectory

longitudinally unstable. It is obvious that particular attention should be paid when traversing this particular area of the reentry trajectory.

In order to alert the flight crew of such critical sections in the trajectory, it may be desirable to display stability information in the form of a display in the cockpit. If it is assumed that all of the trajectory and vehicle information is known prior to the flight, than the stability parameter, P, can be displayed in a manner such that the flight crew is presented with its immediate past, present, and future values. As suggested by Ramnath[15], a possible display of such a nature is shown in Fig.4-17 through 4-19. As seen in the figures, a bar graph concept is employed to show the values of the stability parameter in the neighborhood of a particular instant along the trajectory. Stability values are displayed for up to 60 seconds into the immediate future and for 30 seconds of the immediate past. The display is updated continuously and the elapsed time readout provides the flight crew with their relative location along the entire trajectory. The displays in Figs.4-17 through 4-19 are the actual values of the stability parameter, P, for the GHAME vehicle as it flies along the Shuttle trajectory. The display in Fig.4-17 in which the vehicle has been flying along the trajectory for 200 seconds, shows the area discussed above where the longitudinal stability parameter is at its minimum. Using displays as the ones shown, it may be possible to effectively inform the flight crew as to when the vehicle is traversing sensitive and critical sections of the reentry trajectory.

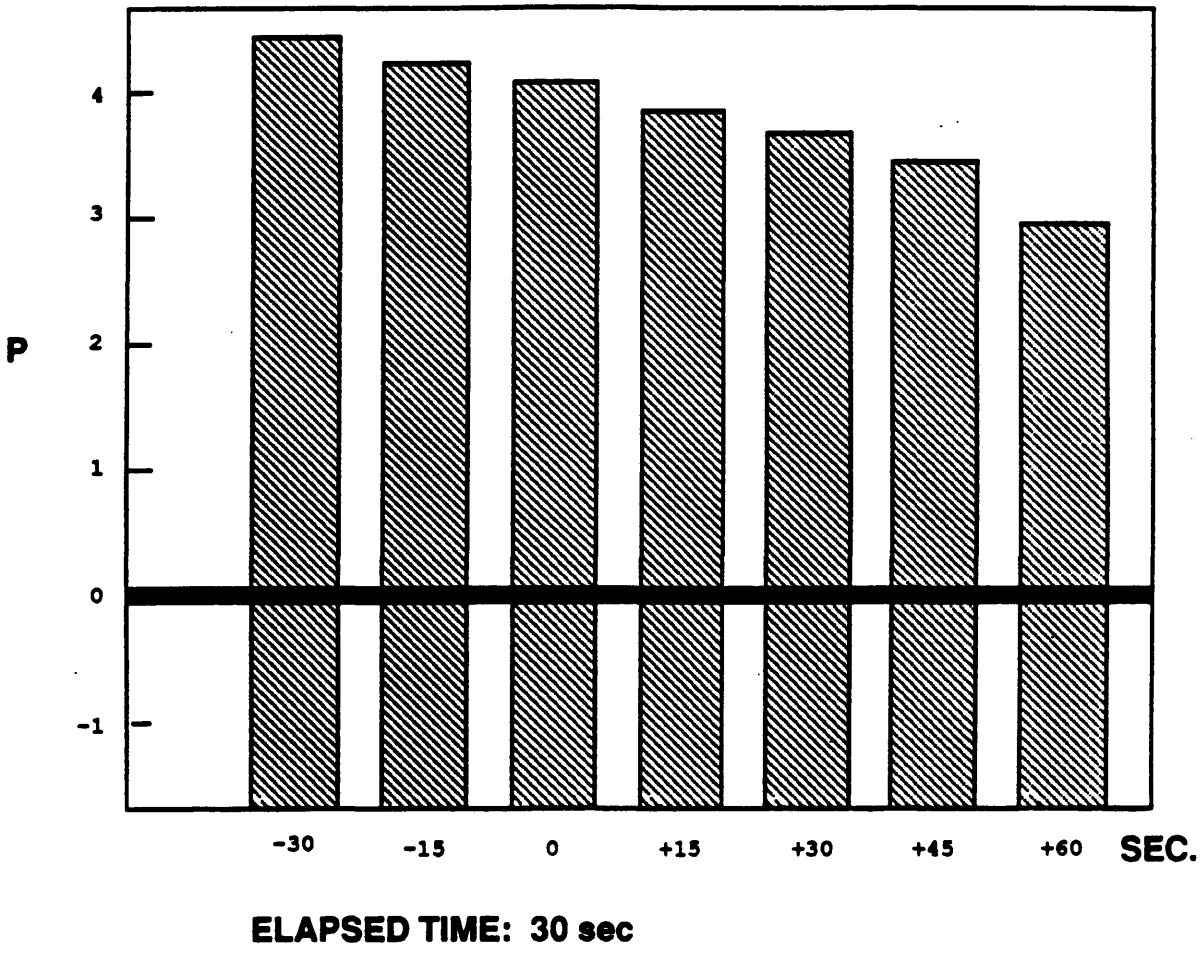

Figure 4-17: Stability Parameter Display at 30 Seconds into Trajectory

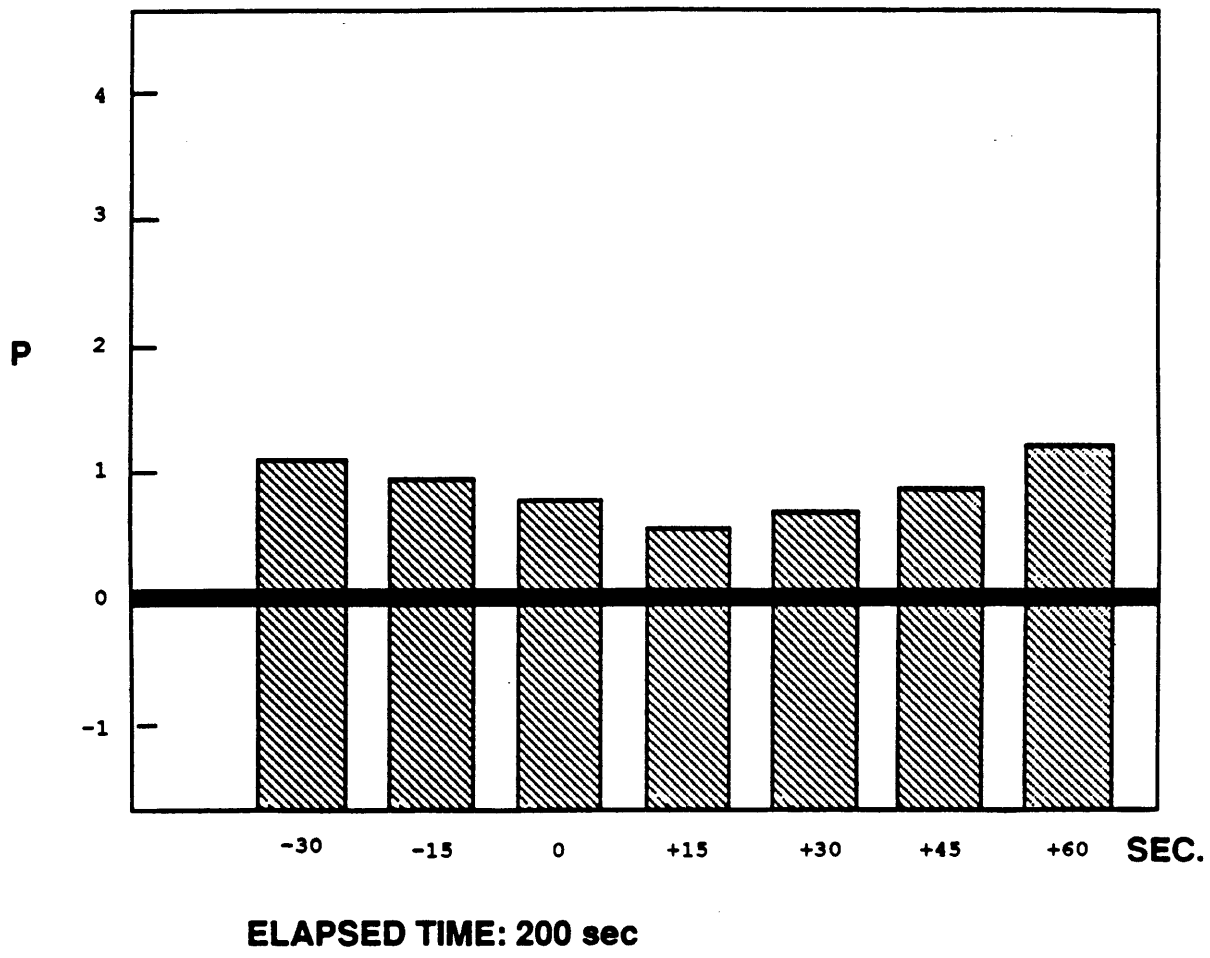

Figure 4-18: Stability Parameter Display at 200 Seconds into Trajectory

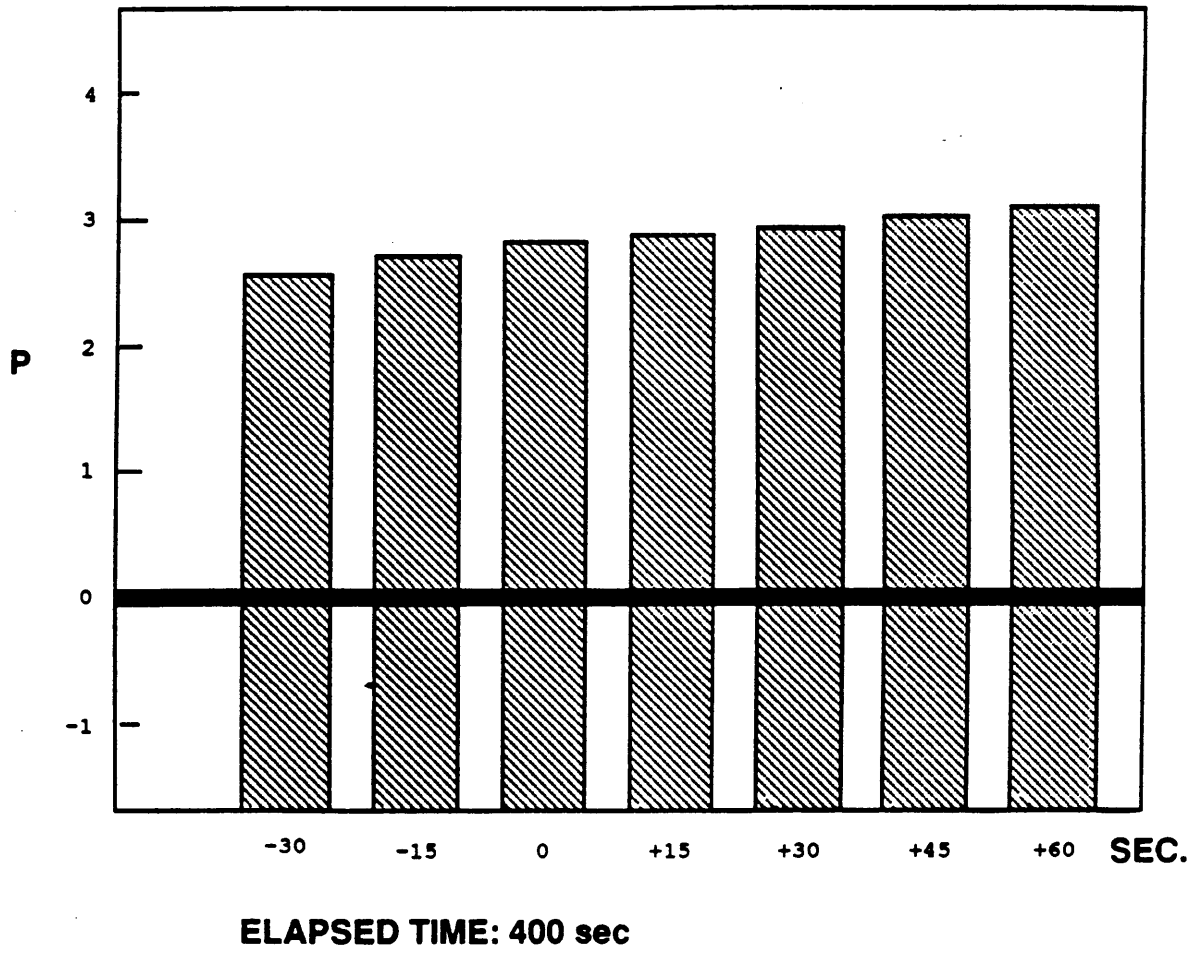

Figure 4-19: Stability Parameter Display at 400 Seconds into Trajectory

Chapter 5

Fourth Order Longitudinal Dynamics

5.1 Overview

The fourth order longitudinal dynamics of the GHAME vehicle flying along the Space Shuttle reentry trajectory are studied in this section. Attempts to approximate the solutions to the longitudinal equations of motion are made through the use of the fourth order Generalized Multiple Scales solutions as developed by Ramnath. These approximations are again compared to numerical integration solutions in order to determine the accuracy of GMS methods.

5.2 Equations of Motion

The longitudinal equations of motion for a vehicle in flight are in general non-linear and time varying. The longitudinal reentry dynamics of the GHAME vehicle are investigated in this chapter by developing approximate solutions to the equations of motion linearized about a steady flight condition. This is justified by the Poincarè-Lyapunov Theorem which states that in most cases, the local stability of a non-linear system is described exactly in the same manner as the behavior of its linearized form. Insight into the longitudinal dynamics of the GHAME vehicle can be obtained by

simply developing solutions to the equations of motion linearized about some nominal steady flight condition.

The general longitudinal dynamics of a flight vehicle are described by the following three equations which are obtained through balancing the lift and drag forces as well as the moments acting on the aircraft[9-11].

$$-m\dot{V} + (T - D) - W(\theta - \alpha) = 0 \tag{5.1}$$

$$L - W - mV(\dot{\theta} - \dot{\alpha}) = 0 \tag{5.2}$$

$$M_y - I_{yy}\ddot{\theta} = 0 \tag{5.3}$$

Eq.5.1 is the drag equation and represents a balancing of forces in the direction of flight, while the lift equation shown in Eq.5.2 describes the sum of forces in a direction perpendicular to the flight path. The moment equation shown in Eq.5.3 balances the moments experienced by the aircraft around its center of mass. In order to linearize these equations of motion, the flight parameters α, V, and θ are represented as perturbations about some steady flight value. They are given by

$$\alpha = \alpha_0 + \Delta\alpha \tag{5.4}$$

$$V = V_0 + \Delta V \tag{5.5}$$

$$\theta = \theta_0 + \Delta\theta \tag{5.6}$$

where α_0, V_0, and θ_0 are the equilibrium steady state values. The forces of thrust, lift, and drag as well as the aerodynamic moment are expressed about some nominal steady state value through expansion in a Taylor series. Taylor series expansion allows the forces and moment to be written as

$$L = L_0 + \frac{\partial L}{\partial \alpha}\Delta\alpha + \frac{\partial L}{\partial V}\Delta V + ... \tag{5.7}$$

$$T = T_0 + \frac{\partial T}{\partial V}\Delta V + ... \tag{5.8}$$

$$D = D_0 + \frac{\partial D}{\partial V}\Delta V + \frac{\partial D}{\partial \alpha}\Delta\alpha + ... \tag{5.9}$$

$$M = M_0 + \frac{\partial M}{\partial V}\Delta V + \frac{\partial M}{\partial \alpha}\Delta\alpha + \frac{\partial M}{\partial \dot{\theta}}\Delta\dot{\theta} + \frac{\partial M}{\partial \dot{\alpha}}\Delta\dot{\alpha} + ... \tag{5.10}$$

L_0, T_0, D_0, and M_0 are nominal values of the aerodynamic forces and moment which produce the equilibrium flight condition given by α_0, V_0, and θ_0. Eqs.5.4 through 5.10 are substituted into the the general non-linear equations of motion and upon manipulation results in the following.

$$\Delta\dot{V} + \Delta V(D_V - T_V) + \Delta\alpha(D_\alpha - g) + g\Delta\theta = 0 \tag{5.11}$$

$$\left(\frac{L_V}{V_0}\right)\Delta V + \Delta\dot{\alpha} + \left(\frac{L_\alpha}{V_0}\right)\Delta\alpha - \Delta\dot{\theta} = 0 \tag{5.12}$$

$$-M_v\Delta V - M_{\dot{\alpha}}\Delta\dot{\alpha} - M_\alpha\Delta\alpha + \Delta\ddot{\theta} - M_{\dot{\theta}}\Delta\dot{\theta} = 0 \tag{5.13}$$

The parameters D_V, D_α, T_V, L_V/V_0, L_α/V_0, M_V, $M_{\dot{\alpha}}$, M_α, and $M_{\dot{\theta}}$ appearing in the equations above are the longitudinal stability derivatives of the vehicle and vary with time as the flight conditions change along the reentry trajectory. The drag damping term D_V is defined as

$$D_V = \frac{1}{m}\frac{\partial D}{\partial V} \tag{5.14}$$

and all of the other stability derivatives relating the change in flight parameters to drag and lift are defined in the same manner. They are defined as the partial derivative of the lift or drag with respect to the flight parameter in question normalized by the inverse of vehicle mass. Similarly, the stability derivatives involving the moment of the vehicle are defined as the partial derivative of the moment with respect to the flight parameter in question normalized by the inverse of the moment of inertia I_{yy}.

Hence, the speed stability term M_V is defined by the following.

$$M_V = \frac{1}{I_{yy}} \frac{\partial M}{\partial V} \tag{5.15}$$

The longitudinal stability derivatives of the GHAME vehicle and their approximation along the reentry trajectory are detailed in the following section.

The linearized longitudinal equations of motion shown in Eqs.5.11 through 5.13 are simplified and written into the final state space form[9]

$$\begin{bmatrix} s + D_V - T_V & D_\alpha - g & g \\ L_V/V_0 & s + L_\alpha/V_0 & -s \\ -M_V & -(M_{\dot{\alpha}} s + M_\alpha) & s(s - M_{\dot{\theta}}) \end{bmatrix} \begin{bmatrix} \Delta V \\ \Delta \alpha \\ \Delta \theta \end{bmatrix} = \begin{bmatrix} 0 \\ 0 \\ 0 \end{bmatrix} \tag{5.16}$$

where s is the derivative operator $\frac{d}{dt}$. The stability derivatives appearing in the state equation are functions of different flight parameters such as air density and flight velocity which vary with time as the GHAME vehicle reenters the Earth's atmosphere. It is clear that the state equation describing the fourth order longitudinal motions is a time varying system which cannot be solved employing traditional constant coefficient methods. Attempts to develop approximate solution to Eq.5.16 are made using GMS methods in section 5.4.

5.3 Longitudinal Stability Derivatives

From the equations of longitudinal motion developed in the previous section, it is clear that the dynamics of the GHAME vehicle during reentry along the Space Shuttle trajectory are very much dependent on the stability derivatives. The GHAME vehicle stability derivatives along the shuttle reentry trajectory are detailed in this section. For the purposes of dynamics and stability, the thrust velocity derivative, T_V, and the angle-of-attack damping derivative, $M_{\dot{\alpha}}$ often have little effect, and are therefore ignored.

The longitudinal stability derivatives of the GHAME vehicle are approximated by substituting vehicle aerodynamic data and other parameters of the Shuttle reentry trajectory into equations available for estimating stability derivatives. The actual equations used for the approximations are left to be detailed in Appendix A. The longitudinal stability derivatives of the GHAME vehicle along the Shuttle reentry trajectory are shown in Figs.5-1 through 5-7. Each of the parameters is plotted against the ξ, the number of vehicle lengths traversed along the trajectory.

There are certain tendencies exhibited by longitudinal stability derivatives which are a result of the inherent nature of aircraft and the conventions of definitions. For example, in a typical aircraft, the parameters D_α, D_V, L_α/V_0, and L_V/V_0 are usually of positive value, and it can be seen that this is in fact the case for the GHAME vehicle. Similarly, due to convention, the pitch damping derivative, $M_{\dot{\theta}}$, is usually negative for conventional aircraft. Again, as can be seen in Fig.5-7, the GHAME vehicle pitch damping derivative conforms and is always negative during the reentry flight. It is clear that the longitudinal stability derivatives of the GHAME vehicle during reentry do not exhibit strange anomalies. It should be noted that certain stability derivatives exhibit similar behavior as the vehicle progresses along the trajectory. The derivatives D_V, L_α/V_0, and L_V/V_0 increase in in a very similar manner along the trajectory, while the drag angle-of-attack derivative, D_α, and the speed stability term, M_V exhibit the same behavior. This may be due to the fact that these stability derivatives are functions of trajectory characteristics such as air density in similar ways.

Two of the longitudinal stability derivatives involved in the equations of motion have significant roles in determining the longitudinal stability of the aircraft. The angle-of-attack stability parameter, M_α, determines the static stability of longitudinal motions. If M_α is negative than the vehicle is statically stable. As seen in Fig.5-5, throughout the entire reentry trajectory, the GHAME vehicle angle-of-attack stability parameter remains negative, and the aircraft becomes statically more stable as it progresses further. M_α is closer to zero at initial parts of the reentry, and the vehicle is less statically stable at these sections.

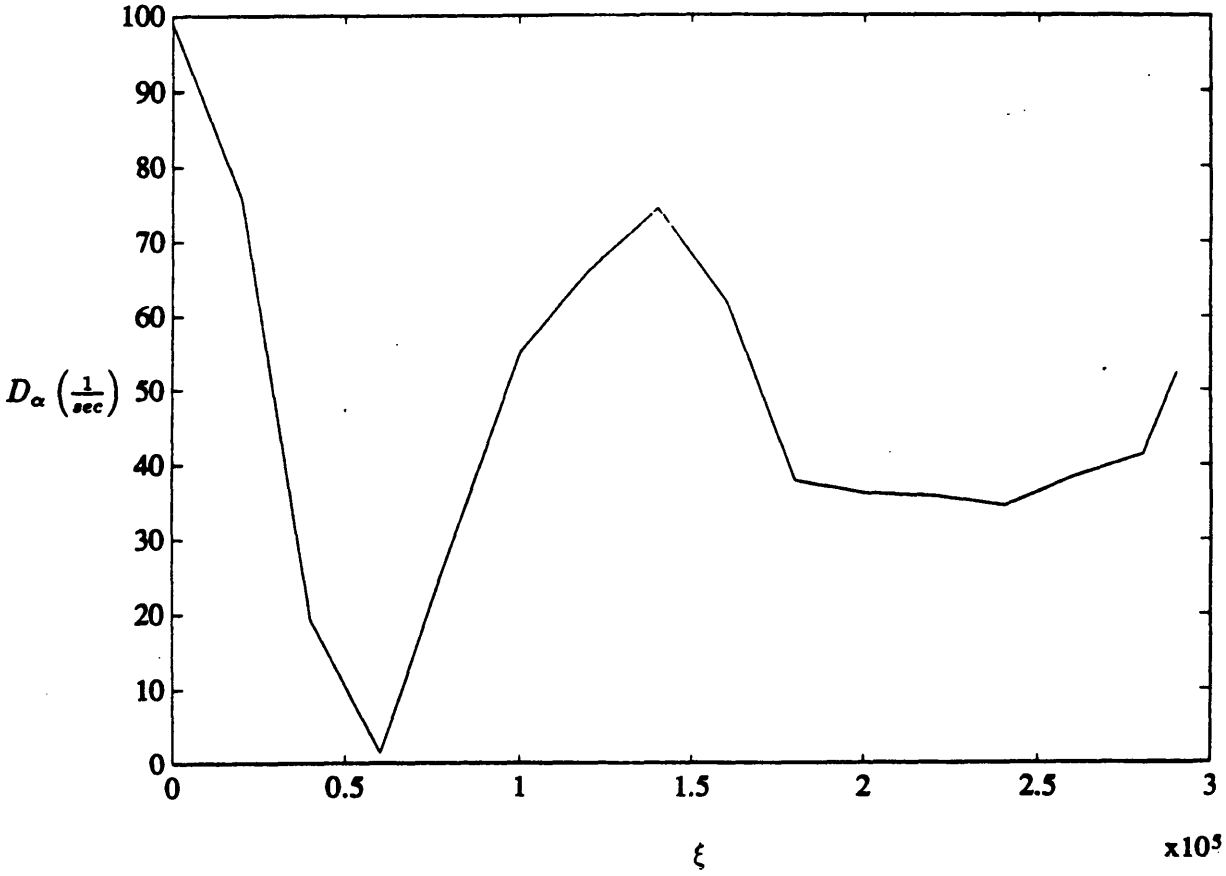

Figure 5-1: Drag Angle-of-Attack Derivative vs. Vehicle Lengths Along Trajectory

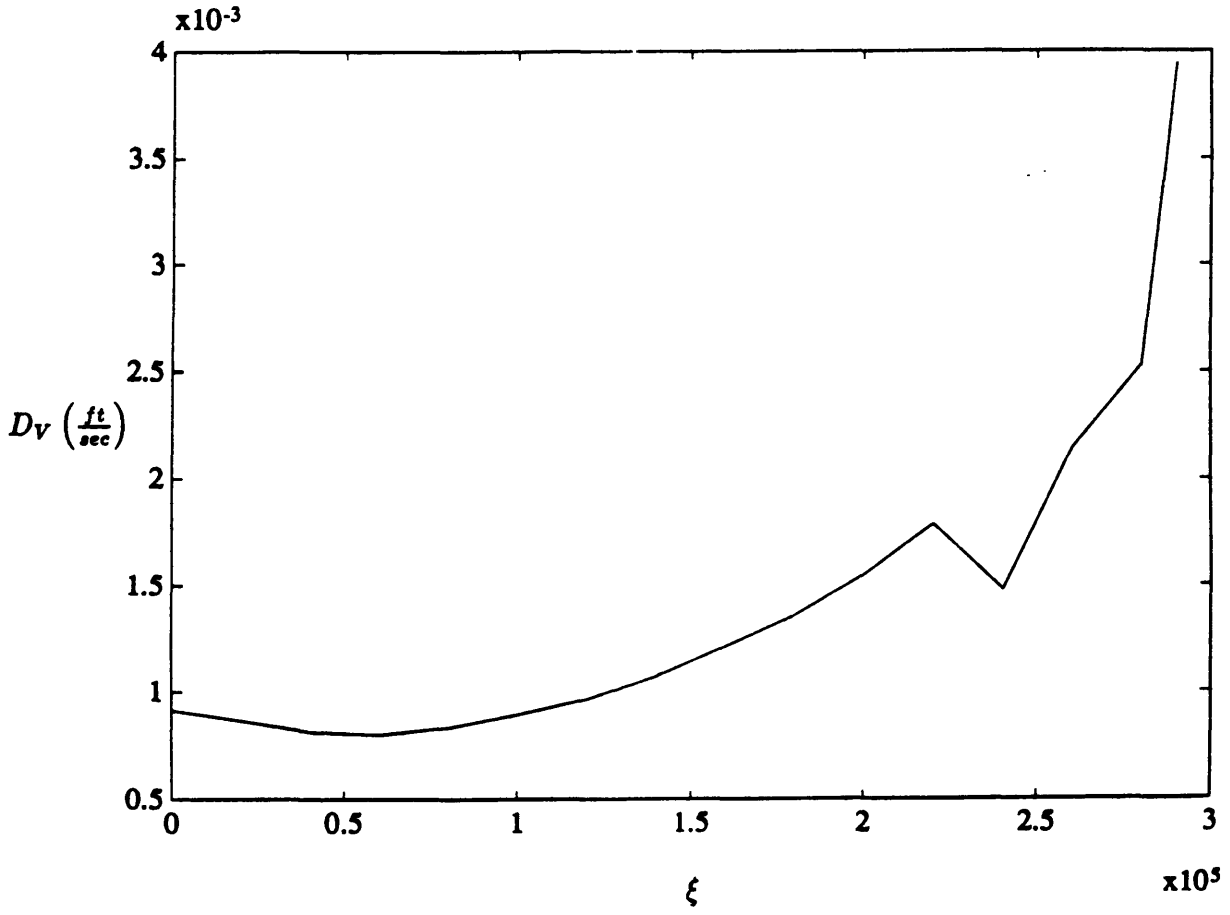

Figure 5-2: Drag Damping Derivative vs. Vehicle Lengths Along Trajectory

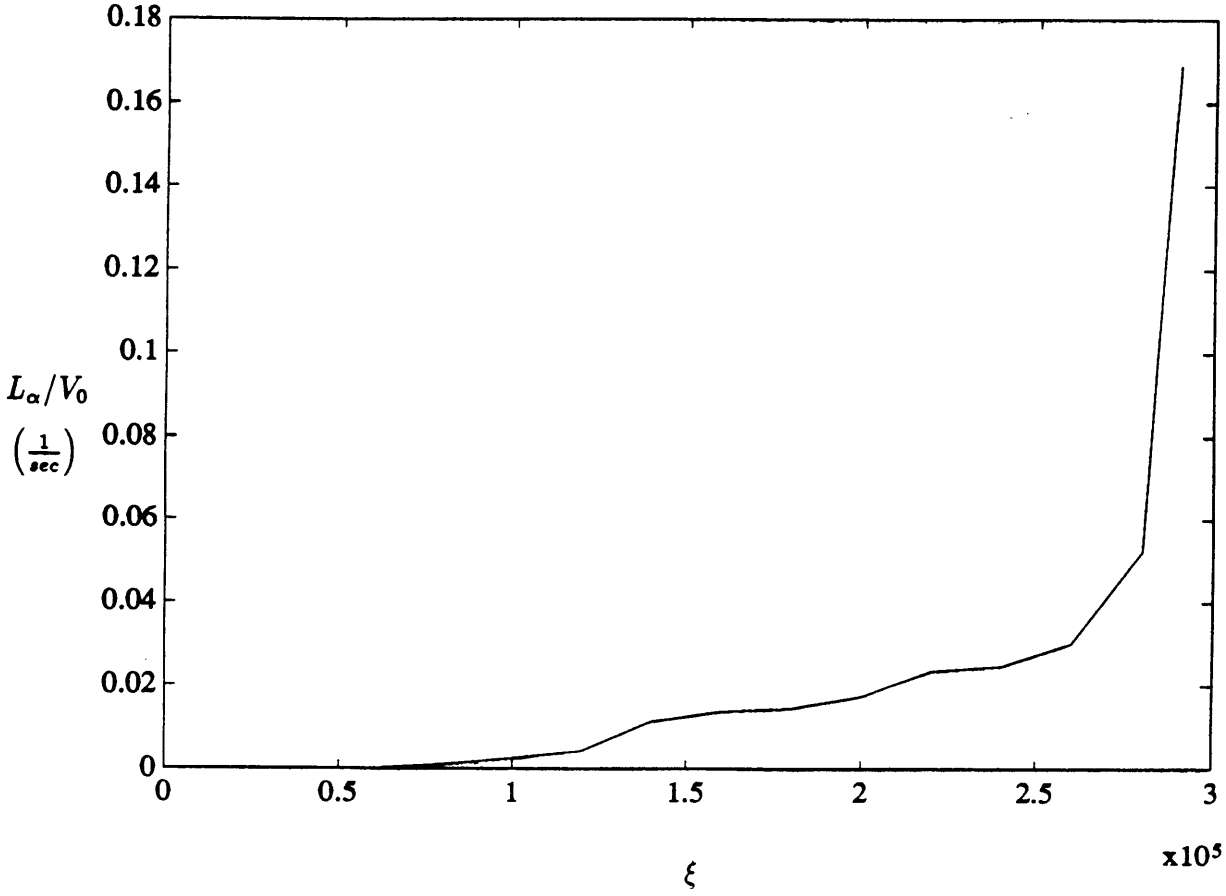

Figure 5-3: Vertical Damping Derivative vs. Vehicle Lengths Along Trajectory

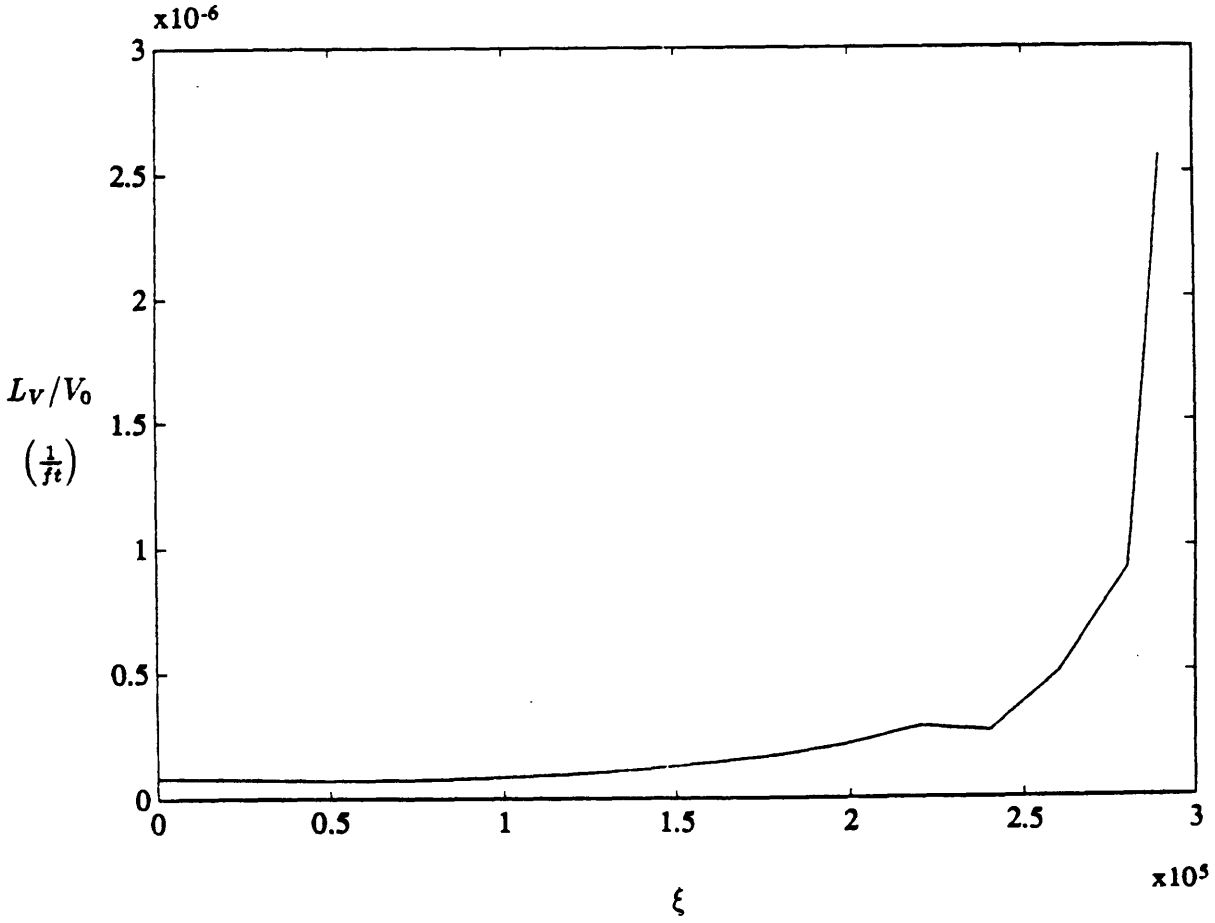

Figure 5-4: Lift Velocity Derivative vs. Vehicle Lengths Along Trajectory

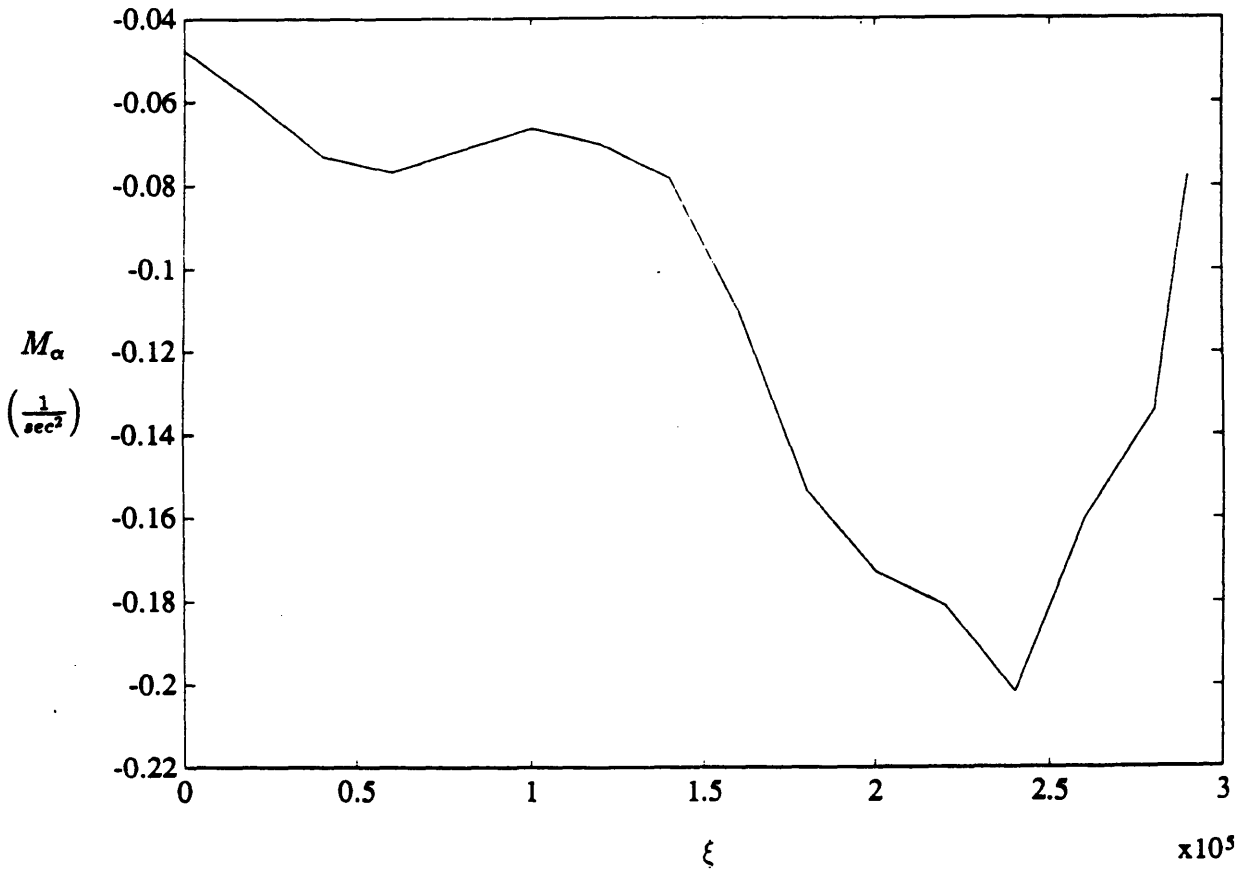

Figure 5-5: Angle-of-Attack Static Stability Derivative vs. Vehicle Lengths Along Trajectory

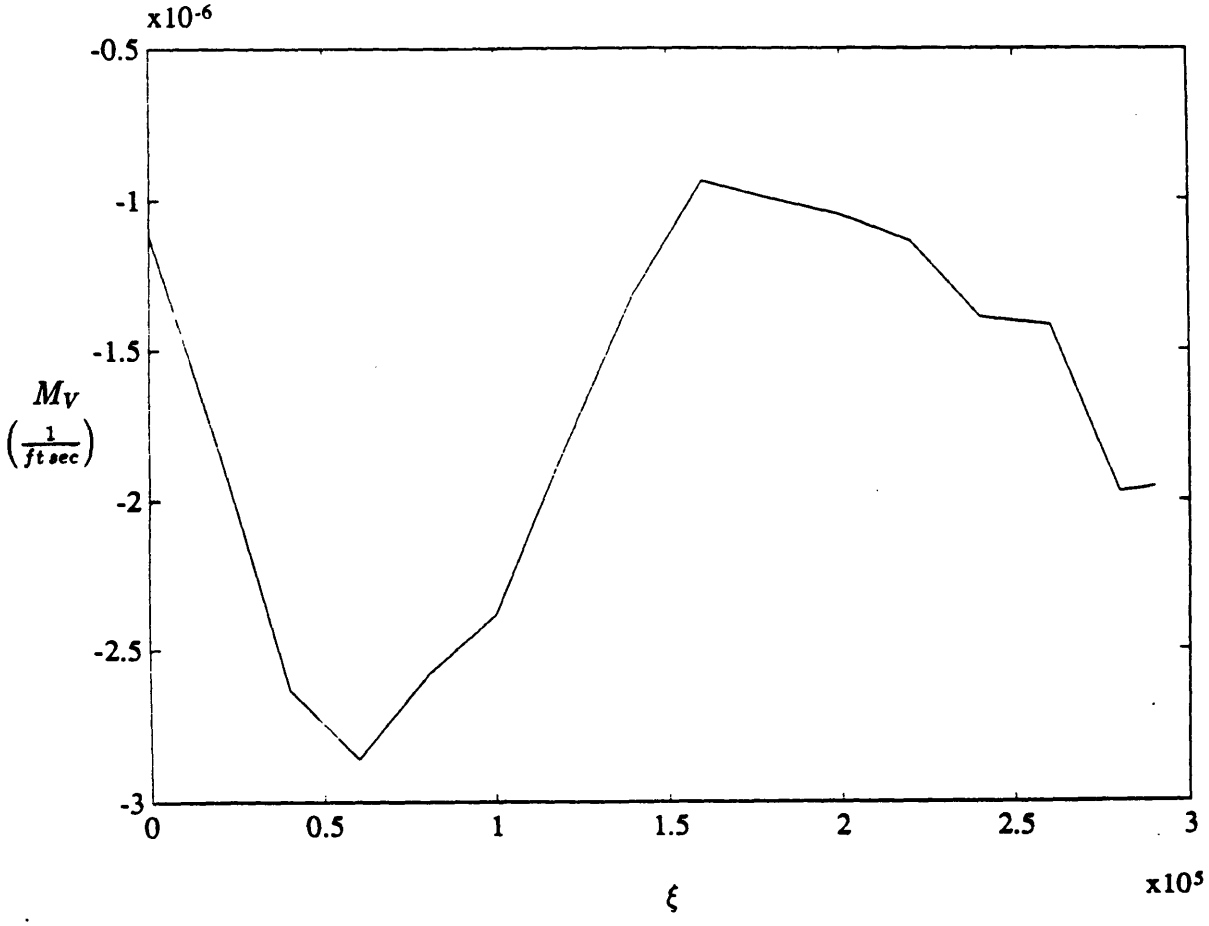

Figure 5-6: Speed Stability Derivative vs. Vehicle Lengths Along Trajectory

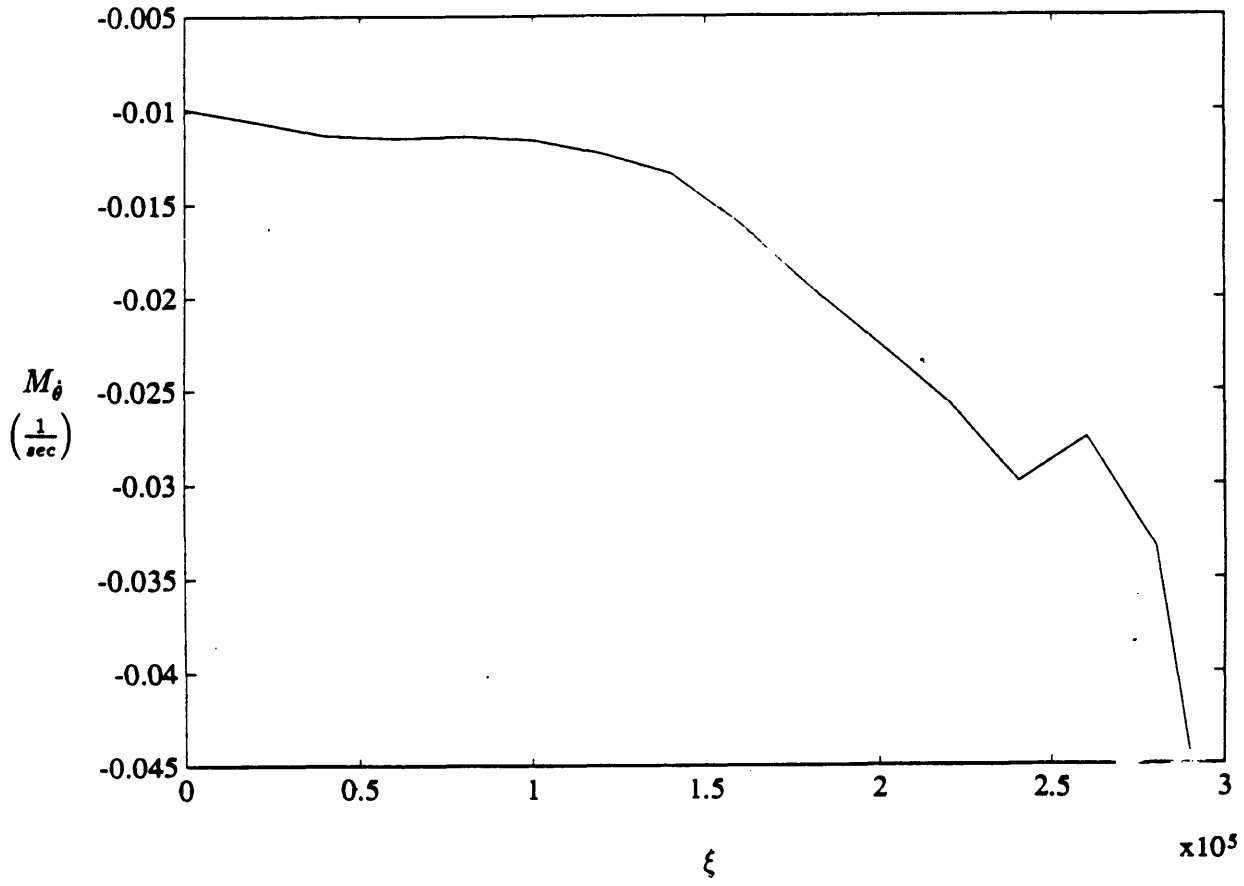

Figure 5-7: Pitch Damping Derivative vs. Vehicle Lengths Along Trajectory

Another important stability derivative with regards to dynamics is the speed stability term, M_V. If M_V is positive than it has a dynamically destablizing effect on the aircraft while if it is negative than the tendency is to statically destabalize the vehicle. Therefore, it is usually desirable to maintain M_V as close to zero as possible, and as seen in Fig.5-6, the speed stability parameter values for the GHAME vehicle are extremely small. The speed stability term is statically most destablizing at approximately 60,000 vehicle lengths into the trajectory and is dynamically most destablizing after traveling 160,000 vehicle lengths.

As shown, it is possible to obtain some insight into the longitudinal dynamics of the GHAME vehicle by analyzing the stability derivatives. The fourth order longitudinal reentry dynamics of the GHAME vehicle described by these stability derivatives is studied through the use of GMS theory in the next section.

5.4 GMS Solutions to Dynamics

The Generalized Multiple Scales theory is utilized in this section to study the fourth order longitudinal dynamics of the GHAME vehicle as it reenters the atmosphere along the optimal Shuttle trajectory. The linearized state equations which describe the longitudinal vehicle motions are given in Eq.5.16. Since the stability derivatives contained in the state equations vary along the trajectory as detailed in section 5.2, it is clear that the fourth order systems is time-varying. In order to apply the GMS solutions shown in section 3.3 to this time-varying system, the equations of motion must be written as a fourth order linear differential equation. The transformation of the linearized state equations into such a form is accomplished by making a dominant approximation to the actual longitudinal equations of motion.

For the purposes of transforming the state equations into a fourth order linear differential equation, it is assumed for a moment that the stability derivatives contained in Eq.5.16 are all of constant value along the trajectory. If this is the case, than solutions to the dynamics of the three independent variables, ΔV, $\Delta\alpha$, and $\Delta\theta$, are identical, and their response is described by solving an equation obtained

by calculating the determinant of the main matrix in Eq.5.16. Ignoring the stability derivatives T_V and $M_{\dot{\alpha}}$, we have

$$det \begin{bmatrix} s + D_V & D_\alpha - g & g \\ L_V/V_0 & s + L_\alpha/V_0 & -s \\ -M_V & -M_\alpha & s(s - M_{\dot{\theta}}) \end{bmatrix} = s^4 + \omega_3 s^3 + \omega_2 s^2 + \omega_1 s + \omega_0 \qquad (5.17)$$

where

$$\omega_3 = L_\alpha/V_0 - M_{\dot{\theta}} + D_V \qquad (5.18)$$

$$\omega_2 = D_V(L_\alpha/V_0) - D_V M_{\dot{\theta}} - M_{\dot{\theta}}(L_\alpha/V_0) - M_\alpha - D_\alpha(L_\alpha/V_0) + g(L_V/V_0) \qquad (5.19)$$

$$\omega_1 = M_V D_\alpha - M_\alpha D_V - D_v M_{\dot{\theta}}(L_\alpha/v_0) + D_\alpha M_{\dot{\theta}}(L_V/V_0) - g M_{\dot{\theta}}(L_V/V_0) \qquad (5.20)$$

$$\omega_0 = g[M_V(L_\alpha/V_0) - M_\alpha(L_V/V_0)] \qquad (5.21)$$

and s again is the derivative operator $\frac{d}{dt}$. Under the assumption that the longitudinal stability derivatives in the above equations are constant, the full longitudinal response of the vehicle is described by setting the above determinant equal to zero and replacing the higher order s terms with their respective higher order derivatives. Since the independent variables, ΔV, $\Delta\theta$, and $\Delta\alpha$ have the same response, all three will be replaced by a generic variable y, and the longitudinal dynamics of the GHAME vehicle are represented by the expression

$$\frac{d^4y}{dt^4} + \omega_3\frac{d^3y}{dt^3} + \omega_2\frac{d^2y}{dt^2} + \omega_1\frac{dy}{dt} + \omega_0 y = 0 \qquad (5.22)$$

As shown by Ramnath, this equation is a dominant approximation to the actual longitudinal behavior and is made under the assumption that the stability derivatives in Eqs.5.18-21 are constant. However, it is recognized that the coefficients in Eq.5.22 and the stability derivatives actually do vary with time, and they are now allowed to do so. This finally results in the longitudinal dynamics of the GHAME vehicle being

represented by the fourth order linear time-varying equation

$$\frac{d^4t}{dt^4} + \omega_3(t)\frac{d^3t}{dt^3} + \omega_2(t)\frac{d^2t}{dt^2} + \omega_1(t)\frac{dy}{dt} + \omega_0(t)y = 0 \tag{5.23}$$

where the coefficients ω_3, ω_2, ω_1, and ω_0 are as defined in Eqs.5.18 through 5.21.

The fourth order GMS solutions shown in section 3.3 require that the each mode of motion and its corresponding roots be identified before an approximation to the dynamics can be made. The roots associated with the longitudinal equation of motion are determined by solving the algebraic equation

$$s^4 + \omega_3 s^3 + \omega_2 s^2 + \omega_1 s + \omega_0 = 0 \tag{5.24}$$

Since the coefficients of the above expression vary with time, the roots of the equation will move as the vehicle traverses along the trajectory. The roots associated with the longitudinal motions of the GHAME vehicle and their movement with time are shown in Figs.5-8 and 5-9. Fig. 5-8 clearly shows the roots of the short period mode and the way they vary as the vehicle travels 1657 seconds into the Shuttle trajectory. As expected, the short period mode is a complex conjugate pair and remains in the left-half plane throughout the entire trajectory. As the GHAME vehicle progresses further into the atmosphere, the short period damping as well as the frequency increases. Due to the fact that the phugoid mode and the short period mode of the vehicle occur on such differing frequency scales, in Fig.5-8, the roots representing the phugoid mode appear as a set of unresolvable points near the origin. The movement of the phugoid roots along the trajectory is plotted in detail in Fig.5-9.

It is clear that the roots of the phugoid mode do not behave in a conventional manner. As the GHAME vehicle begins its reentry, the phugoid roots are a pair of complex conjugates in the right-half plane. As the vehicle progresses along the trajectory, the pair of roots move into the left-half plane and then once again return toward the right-half plane. At approximately 400 seconds into the reentry trajectory, the complex phugoid roots abruptly become a pair of real roots, one negative and the other positive. These real roots move towards the origin until approximately 600

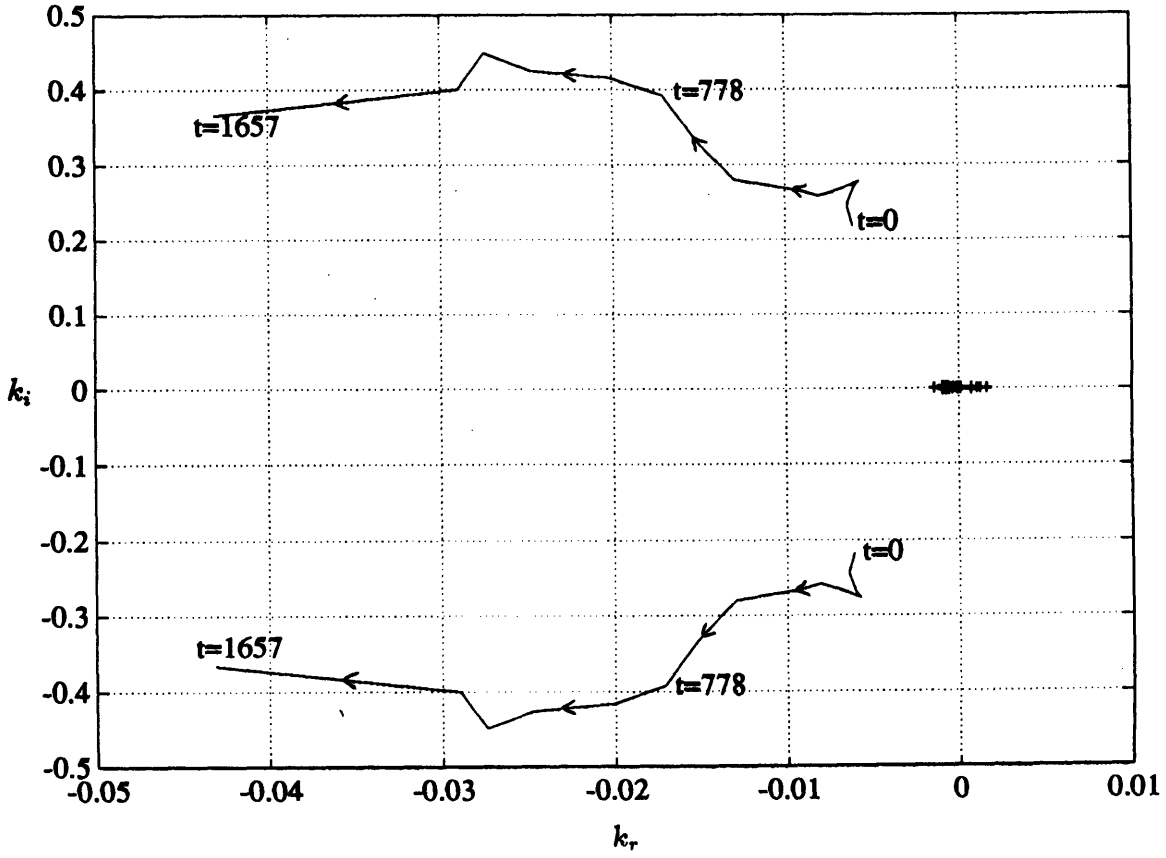

Figure 5-8: Short Period Roots Along Trajectory

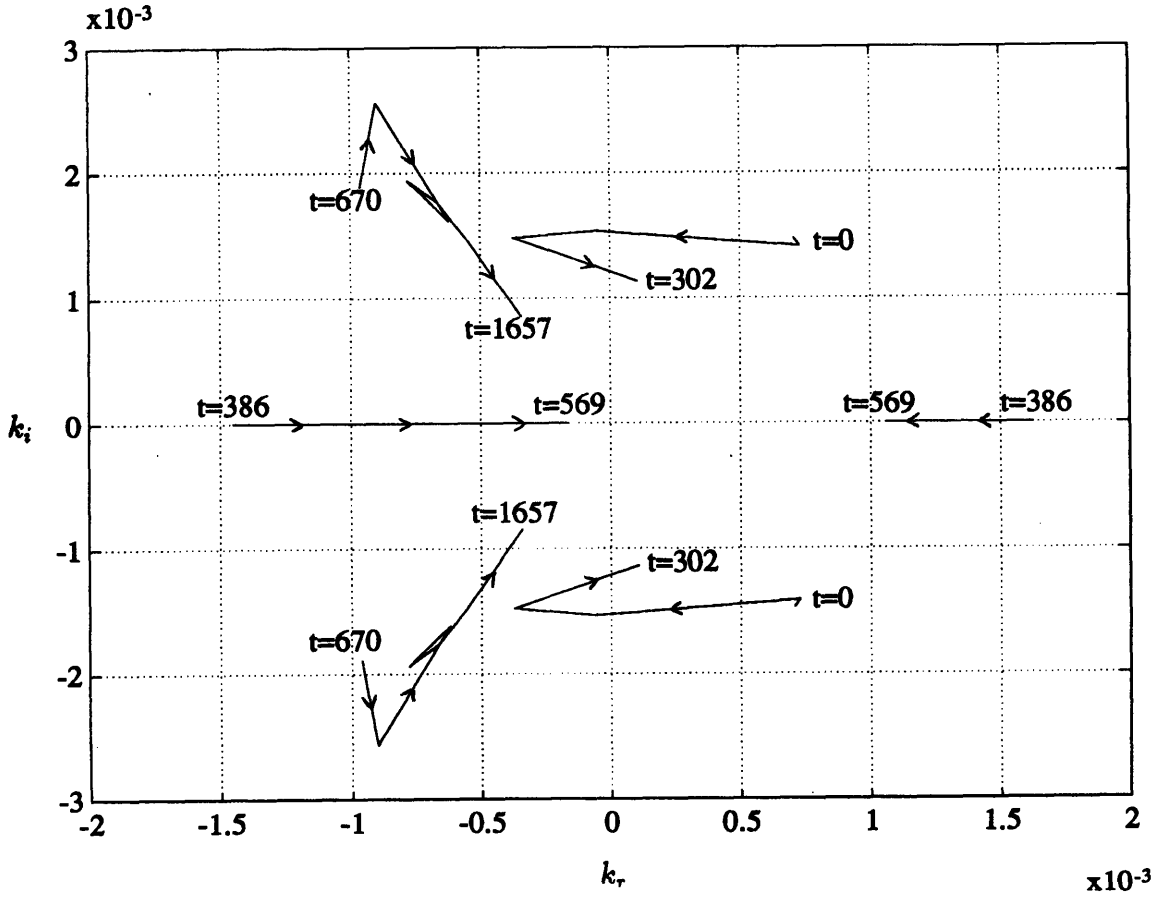

Figure 5-9: Phugoid Mode Roots Along Trajectory

seconds into the trajectory at which point they once again become complex.

The peculiar behavior of the phugoid mode roots requires greater rigor and a more careful use of Generalized Multiple Scales to study the GHAME vehicle dynamics. The points at which the phugoid roots change from complex conjugates to real roots and vice versa are known as 'turning points' and represent a change in the nature of the mode between oscillatory and non-oscillatory behavior. In regard to the GMS theory, these 'turning points' present additional mathematical difficulties. When a 'turning point' is present, greater care is needed in generating the GMS approximations. Because of this, the study of GHAME vehicle longitudinal dynamics as it travels along the Shuttle reentry trajectory is restricted to predicting only the short period behavior of the vehicle.

The GHAME vehicle root information shown in Fig.5-8 is substituted into the fourth order GMS solutions given in section 3.3 in order to approximate the nature of the short period mode motions. Once again, two sets of initial conditions are chosen to produce solutions of different forms. In order to simulate a sine-like solution, the initial conditions are set at $y(0) = 0$, $y'(0) = .2181$, while a cosine-like solution is obtained with the initial conditions $y(0) = 1$, $y'(0) = 0$. The fast GMS solution as well as the full GMS solution to the short period behavior for both sets of initial conditions are shown in Fig.5-10 and 5-11. Unlike the GMS solutions to the second order angle-of-attack perturbations obtained in Chapter 4, these approximations exhibit virtually no difference between the fast solution and the complete solution. The fast GMS solution contains all of the frequency and magnitude information to be obtained by GMS theory and the addition of the slow solution has virtually no effect on the approximation. Once again, to determine the degree of accuracy with which the GMS theory predicts the dynamics of the GHAME vehicle, a Runge-Kutta integration scheme was employed to obtain numerical solutions to the short period mode. The numerical solutions to the short period behavior along with the full GMS approximations for both sets of initial conditions are plotted in Figs.5-12 and 5-13. As with the angle-of-attack perturbations in Chapter 4, the GMS approximations coincide extremely well with their numerical counterparts. In both the sine-like and

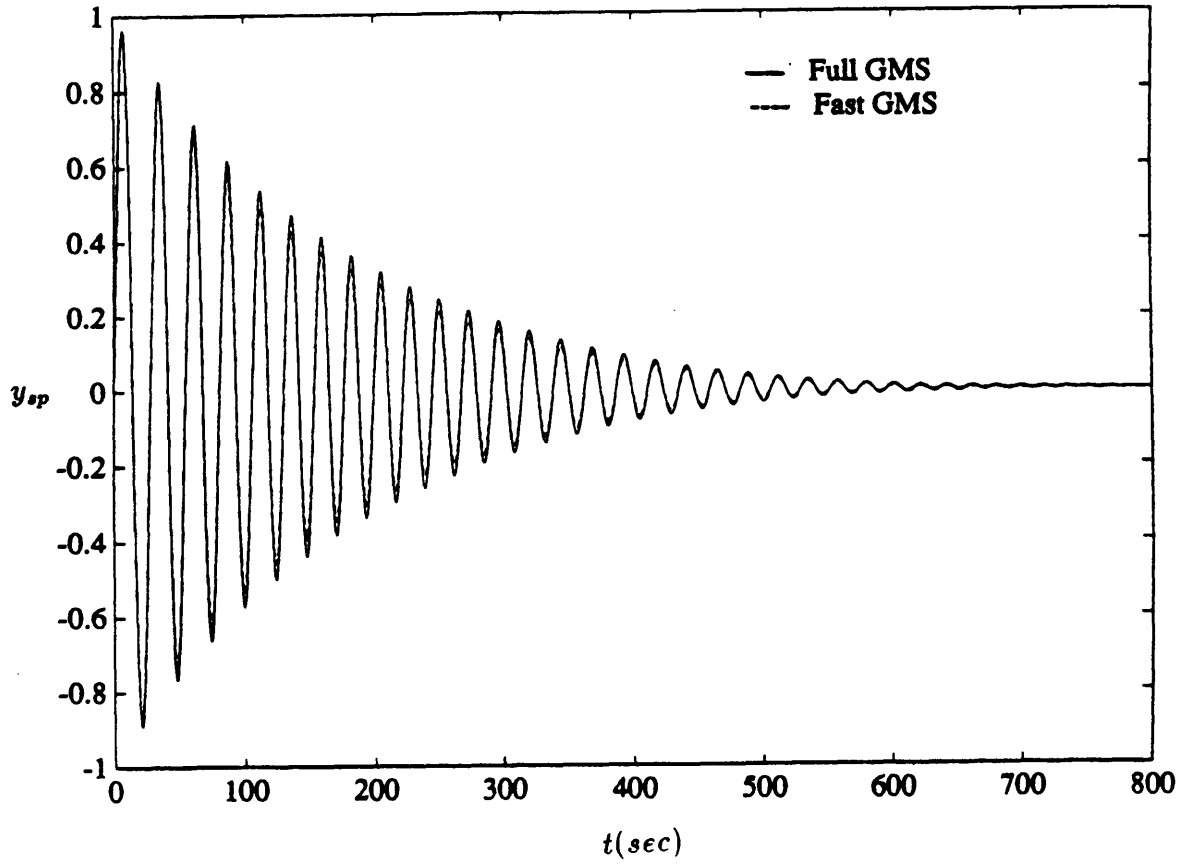

Figure 5-10: Sine-like GMS Solutions to Short Period Mode

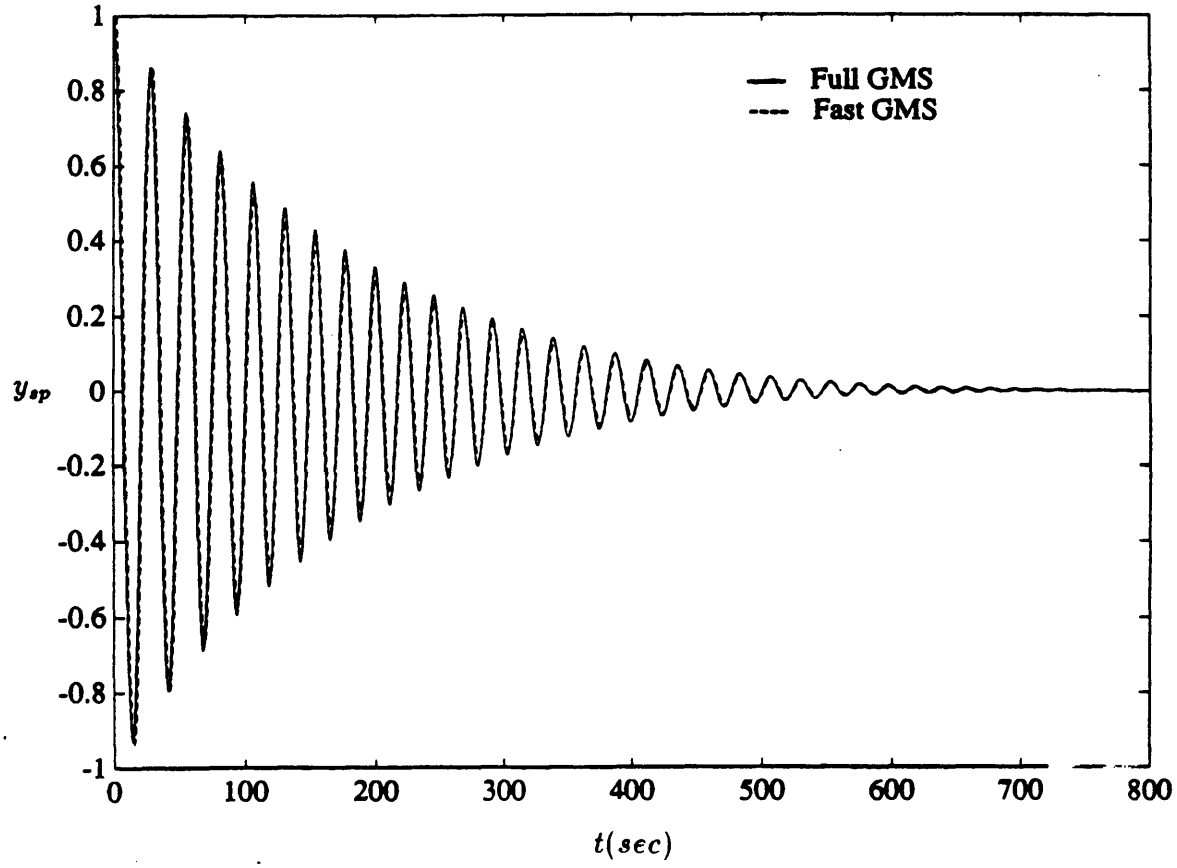

Figure 5-11: Cosine-like GMS Solutions to Short Period Mode

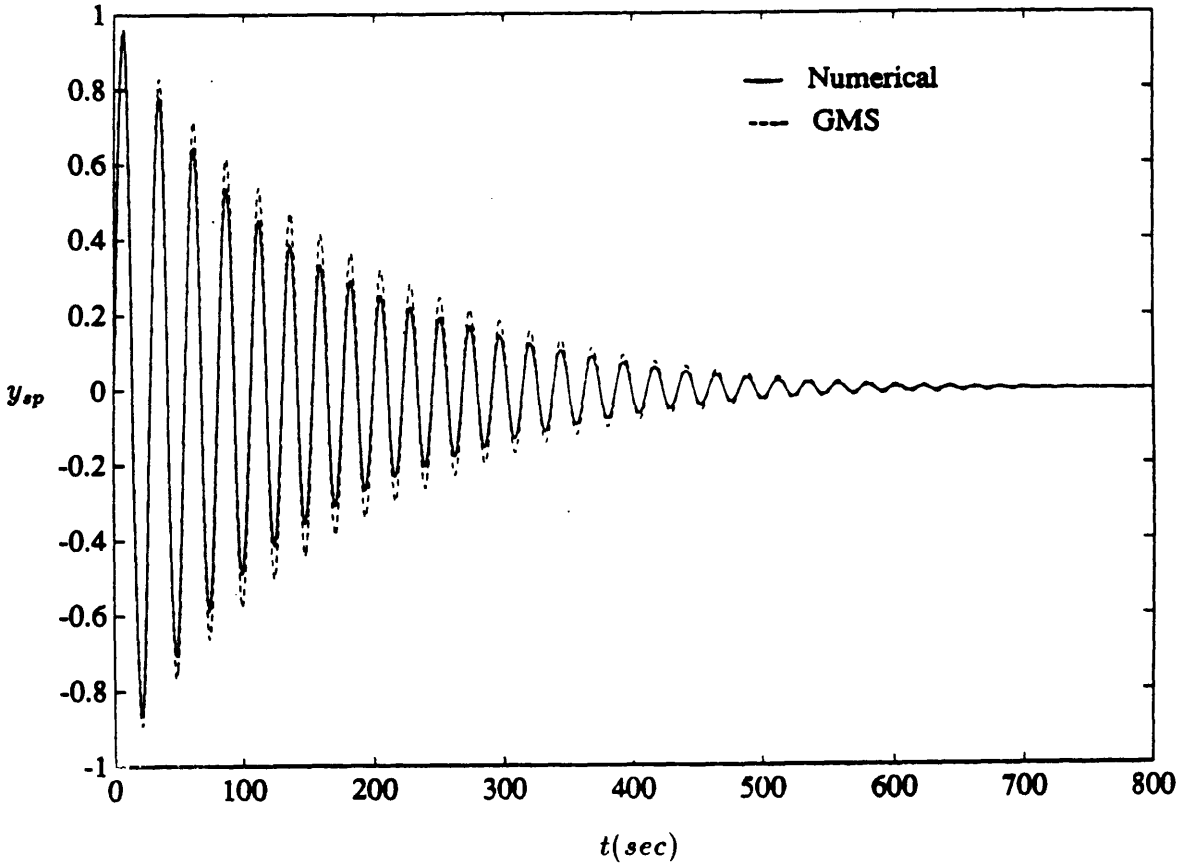

Figure 5-12: Sine-like Numerical and GMS Solutions to Short Period Mode

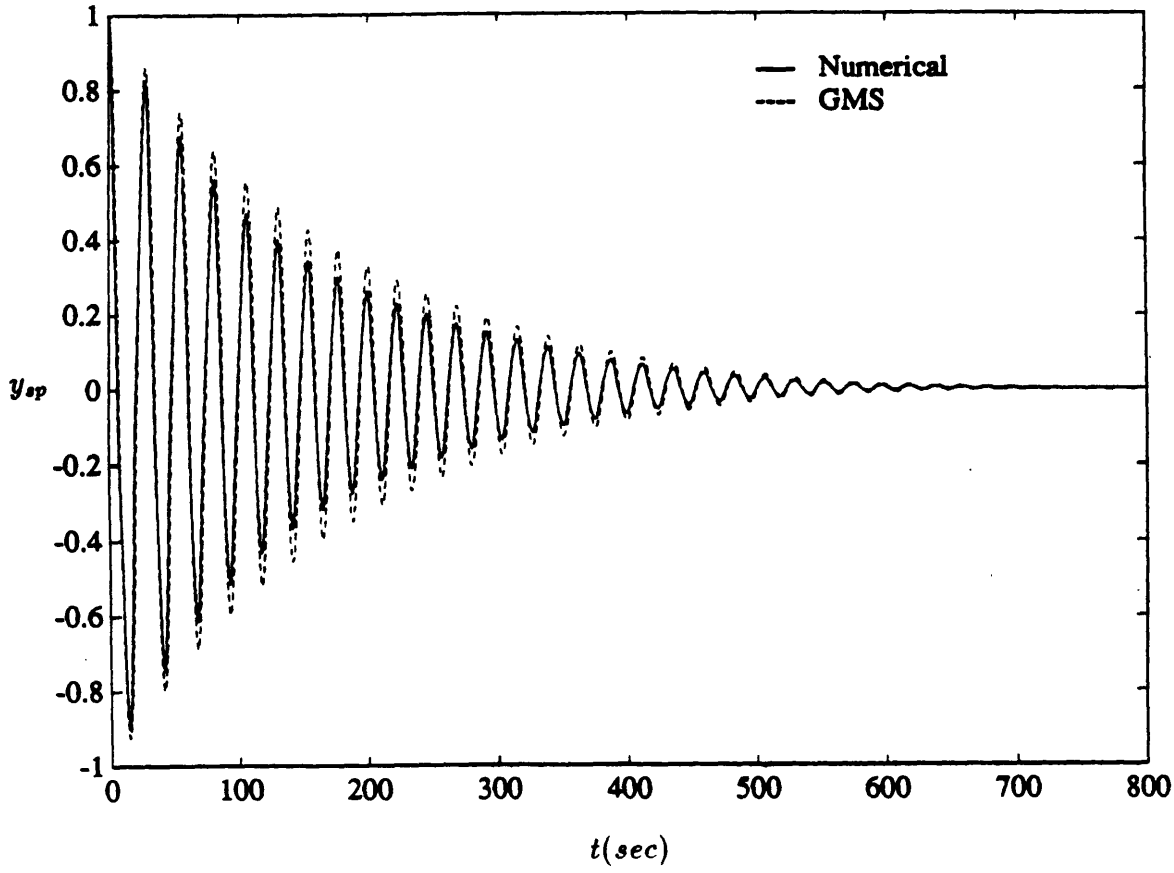

Figure 5-13: Cosine-like Numerical and GMS Solutions to Short Period Mode

cosine-like solutions, the amplitude of the short period behavior is overshot by the GMS approximations, however, the discrepancy is small and disappears as the vehicle progresses further into the trajectory. Unfortunately, due to the presence of the turning points in the phugoid mode, a complete study of the fourth order longitudinal reentry dynamics of the GHAME vehicle could not be accomplished in this study. However, the accuracy of the asymptotic method is again demonstrated in predicting the short period behavior of the vehicle.

Chapter 6

Fourth Order Lateral-Directional Dynamics

6.1 Overview

In this chapter, the lateral-directional dynamics of the GHAME vehicle as it traverses the Space Shuttle reentry trajectory are studied. As before, the motions of the hypersonic vehicle are investigated through the use of Generalized Multiple Scales theory which provides approximation to non-autonomous differential equations. The GMS solutions obtained to the lateral-directional dynamics of the GHAME vehicle are once again compared to numerical solutions in order to determine the accuracy of such approximations. Finally, a sensitivity analysis of the lateral-directional motions is conducted by differentiating the GMS solutions with respect to the lateral-directional stability derivatives.

6.2 Equations of Motion

Similar to their longitudinal counterparts, the equations of motion describing the lateral-directional dynamics of a flight vehicle are generally non-linear. The Poincarè-Lyapunov theorem is again invoked, and in order to gain insight into the behavior of the GHAME vehicle, GMS theory is employed to approximate solutions to the lateral-

directional equations of motion linearized about a nominal steady flight condition.

The non-linear equations describing the lateral-directional motions of the GHAME vehicle are given by[9, 10, 11]

$$Y - m\dot{v} - mVr + mg\phi = 0 \tag{6.1}$$

$$L - I_{xz}\dot{r} + I_{xx}\ddot{\phi} = 0 \tag{6.2}$$

$$N - I_{zz}\dot{r} + I_{xz}\ddot{\phi} = 0 \tag{6.3}$$

where Y, L, and N are respectively the aerodynamic side force, rolling moment, and yawing moment on the vehicle. The variable v represents the component of velocity perpendicular to the flight path while r and ϕ are the yaw rate and roll angle of the vehicle. The three equations shown above are a result of balancing aerodynamic and inertial forces as well as moments which affect lateral-directional motions. Eq.6.1 is developed through the equating of forces in the direction perpendicular to the flight path. Eqs.6.2 and 6.3 are the result of balancing the rolling and yawing moments of the aircraft. These three equations are now linearized using the exact same process employed to linearize the longitudinal equations of motion. The three parameters v, r, and ϕ are represented as perturbations about some nominal steady state value, while the aerodynamic force and moments are rewritten in the form a Taylor expansion given by

$$Y = Y_0 + \frac{\partial Y}{\partial v}\Delta v + ... \tag{6.4}$$

$$L = L_0 + \frac{\partial L}{\partial v}\Delta v + \frac{\partial L}{\partial r}\Delta r + \frac{\partial L}{\partial p}\Delta p + ... \tag{6.5}$$

$$N = N_0 + \frac{\partial N}{\partial v}\Delta v + \frac{\partial N}{\partial r}\Delta r + \frac{\partial N}{\partial p}\Delta p + ... \tag{6.6}$$

where p is the roll rate and the other variables are as defined before. These Taylor series representations and the perturbation forms of v, r, and ϕ are substituted into the nonlinear equations of motion given in Eq.6.1 through 6.3. Upon manipulation, the resulting linearized lateral-directional equations of motion given in state space

form are[9]

$$\begin{bmatrix} s - Y_v & V & -g \\ -L_v & -L_r & s^2 - L_p s \\ -N_v & s - N_r & -N_p s \end{bmatrix} \begin{bmatrix} \Delta v \\ \Delta r \\ \Delta \phi \end{bmatrix} = \begin{bmatrix} 0 \\ 0 \\ 0 \end{bmatrix} \tag{6.7}$$

where s is once again the derivative operator $\frac{d}{dt}$. The parameters Y_v, L_v, L_r, L_p, N_v, N_r, and N_p appearing in the linearized state equation are the lateral-directional stability derivatives of the aircraft and vary with time as the GHAME vehicle travels along the reentry trajectory. The stability derivative Y_v is defined as

$$Y_v = \frac{1}{m} \frac{\partial Y}{\partial v} \tag{6.8}$$

The stability derivatives involving the rolling and yawing moments are defined as the partial derivative of the moment with respect to the particular parameter normalized by the inverse of the relevent moment of inertia. For example, the dihederal term L_v, is given by

$$L_v = \frac{1}{I_{xx}} \frac{\partial L}{\partial v} \tag{6.9}$$

All of the other derivatives involving rolling moment are defined in the same manner. Similarly, the yawing moment derivatives are normalized by the inverse of I_{zz} and can be written in the same form as N_v which is defined as

$$N_v = \frac{1}{I_{zz}} \frac{\partial N}{\partial v} \tag{6.10}$$

The lateral-directional stability derivatives of the GHAME vehicle during reentry along the optimal trajectory are detailed in the next section. As with the longitudinal derivatives, these parameters vary along the trajectory as the flight conditions change, and the linearized equations of motion in Eq.6.7 are time-varying. GMS theory is employed in section 6.3 to develop approximate solutions to this system and gain insight into the lateral-directional reentry behavior of the GHAME vehicle.

6.3 Lateral-Directional Stability Derivatives

It is clear by examining the lateral-directional equations of motion shown in Eq. 6.7 that the stability derivatives of the GHAME vehicle primarily determine its lateral-directional behavior. Similar to their longitudinal counterparts, these lateral-directional stability derivatives are functions of a variety of parameters and vary with the changing flight conditions during reentry. The lateral-directional stability derivatives of the GHAME vehicle along the Shuttle trajectory are shown in Figs.6-1 through 6-7. The derivatives are plotted against ξ, the number of vehicle lengths traversed along the trajectory by the GHAME vehicle. The equations employed to approximate the lateral-directional stability derivatives are left to be detailed in Appendix A.

Although the values of the lateral-directional stability derivatives largely determine the dynamics, insights into the nature of the vehicle and trajectory can be gained by studying the derivatives themselves. For example, due to the dihederal of the main wings, sideslip components of velocity causes most aircraft to experience

a change in local angle-of-attack values between the two wings. Hence, the vehicle experiences a rolling moment due to sideslip velocity. The stability derivative L_v, represents this tendency, and its values for the GHAME vehicle along the optimal reentry trajectory are plotted in Fig.6-2. Since the GHAME vehicle has no dihederal angle in the main wings, the values of L_v are relatively small. Although main contributions to the dihederal effect are due to the main wings, the fuselage and tail can also be factors. They are likely responsible for the small positive values of L_v exhibited by the GHAME vehicle. For stability purposes, it is desirable to keep the dihederal derivative within narrow limits, and as seen in Fig.6-2, L_v remains almost at a constant value through most of the reentry trajectory.

Another important lateral-directional stability derivative is the directional stability term N_v. This parameter represents the tendency of flight vehicles to yaw into the relative wind and is mainly caused by the change in oncoming airflow angle experienced by the vertical tail. The values of N_v for the GHAME vehicle are plotted versus vehicle lengths into the reentry trajectory in Fig.6-5. It can be seen that early

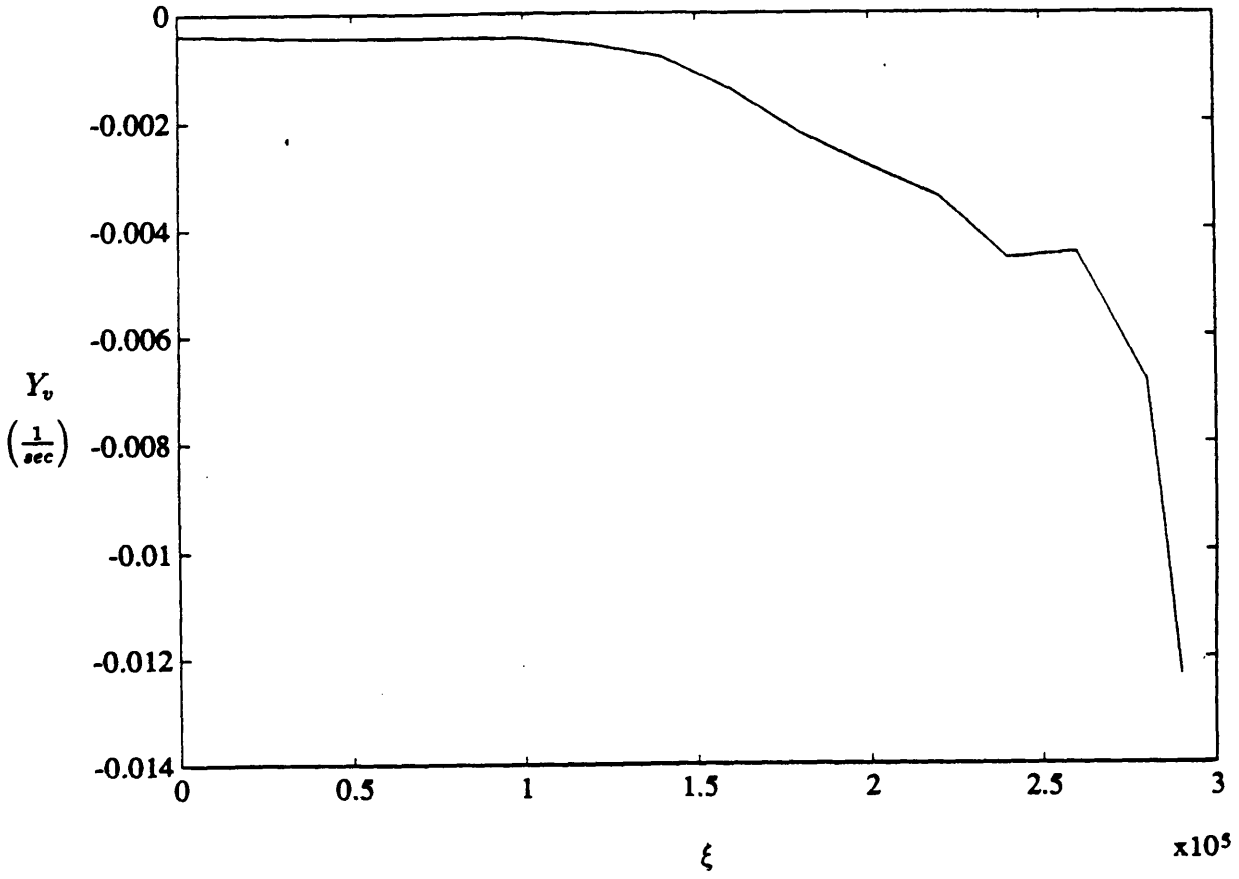

Figure 6-1: Side Force Due to Sideslip vs. Vehicle Lengths Along Trajectory

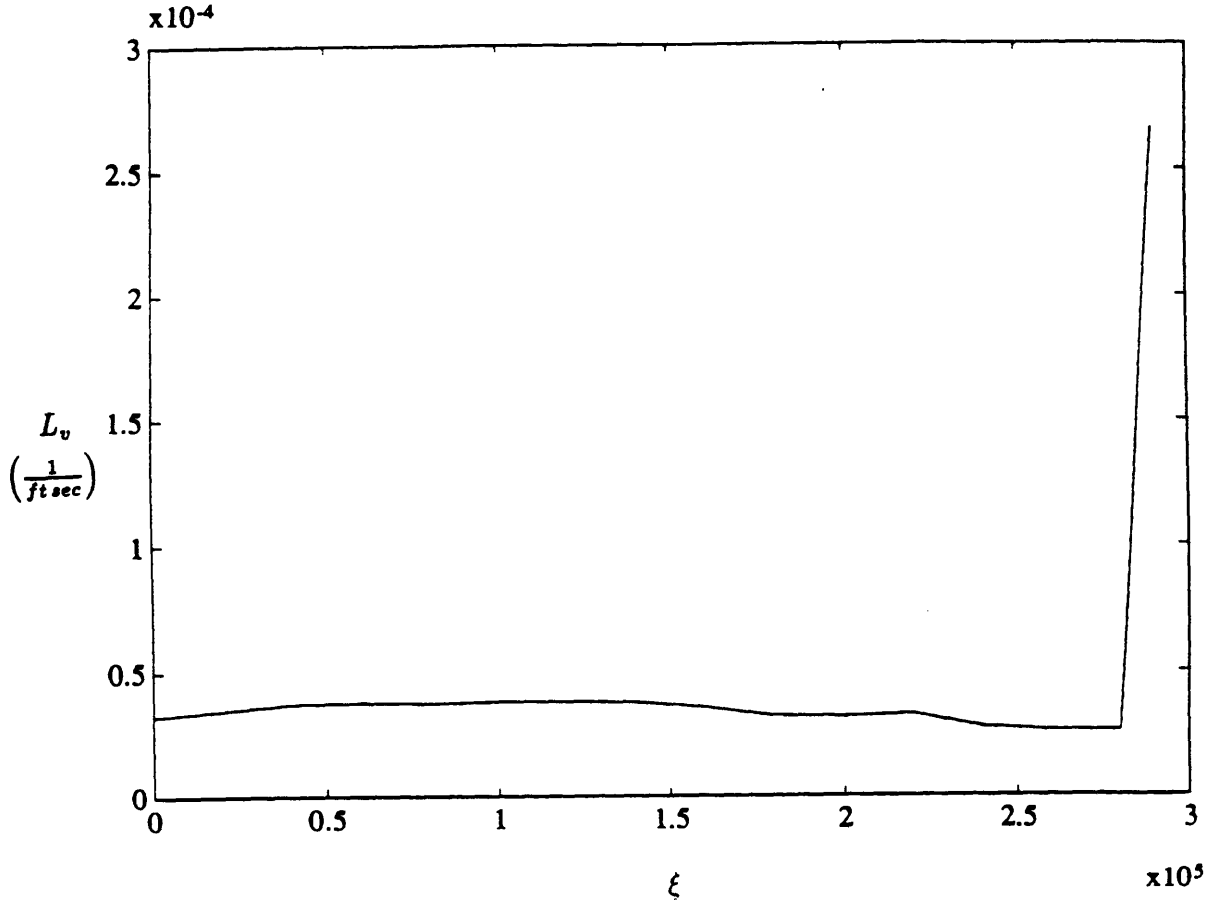

Figure 6-2: Dihederal Effect Derivative vs. Vehicle Lengths Along Trajectory

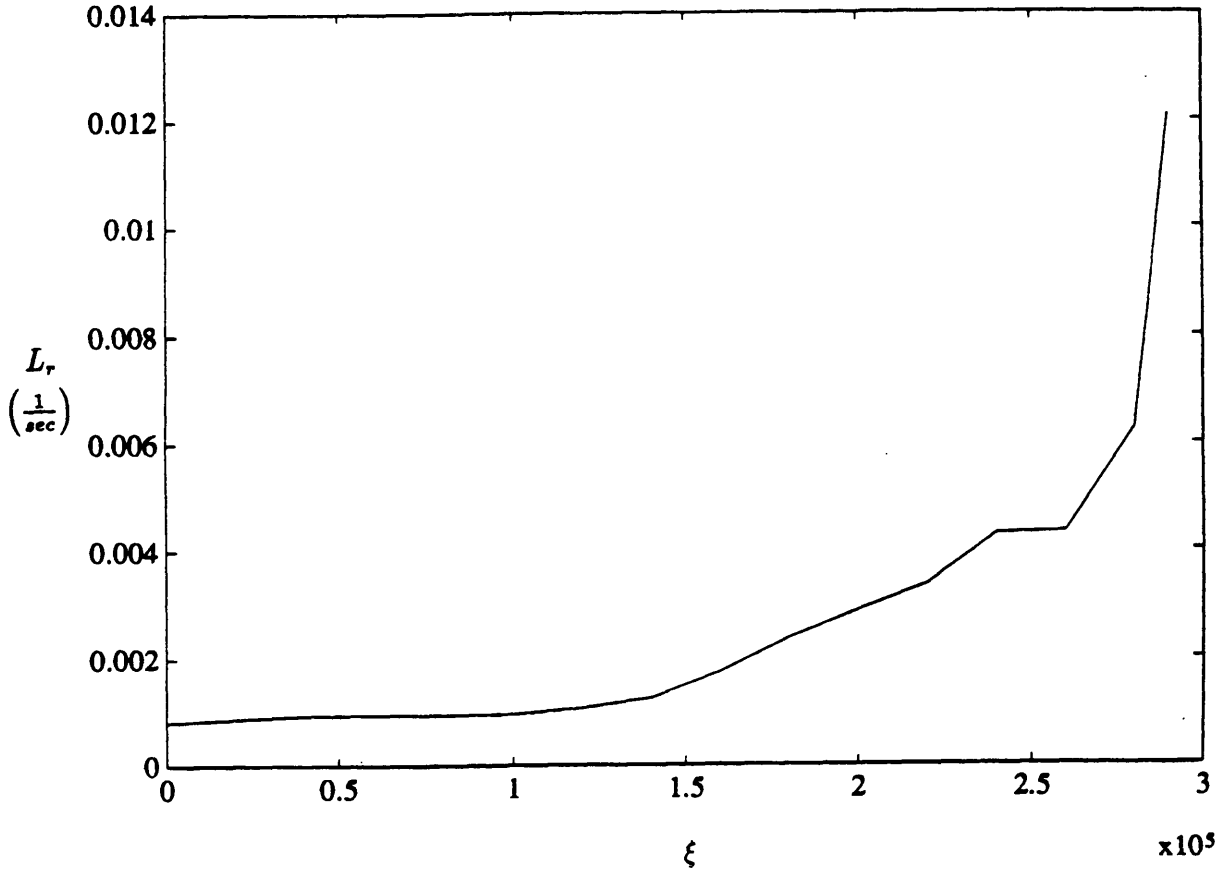

Figure 6-3: Rolling Moment Due to Yaw Rate vs. Vehicle Lengths Along Trajectory

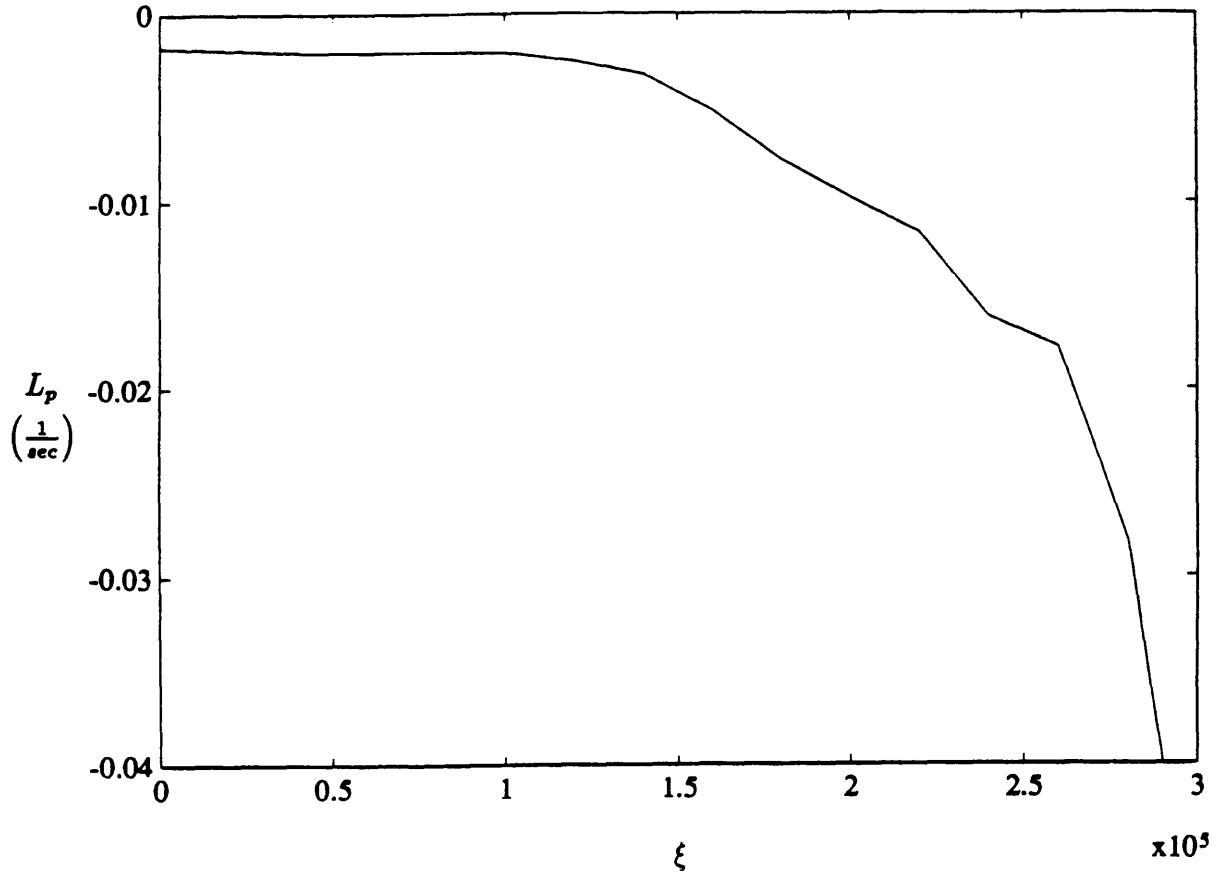

Figure 6-4: Roll Damping Derivative vs. Vehicle Lengths Along Trajectory

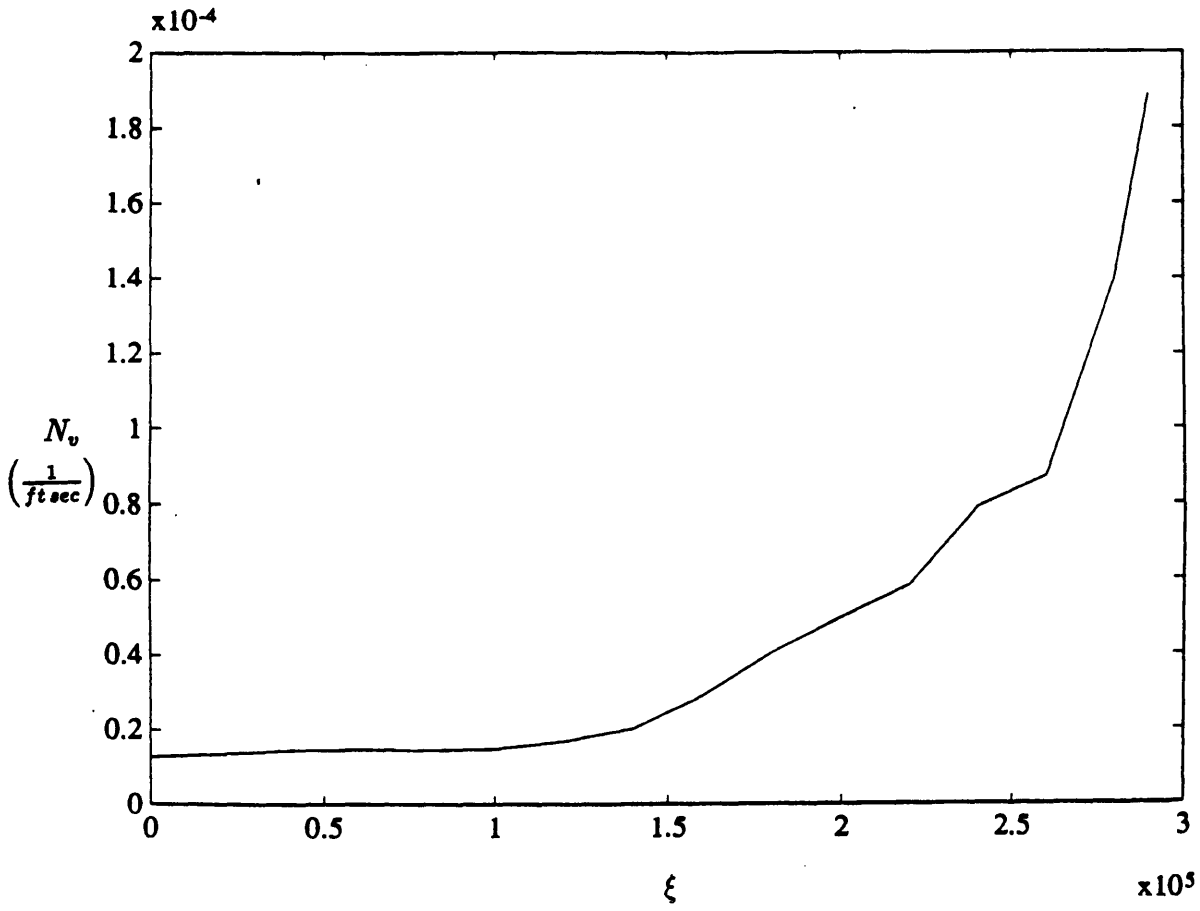

Figure 6-5: Directional Stability Derivative vs. Vehicle Lengths Along Trajectory

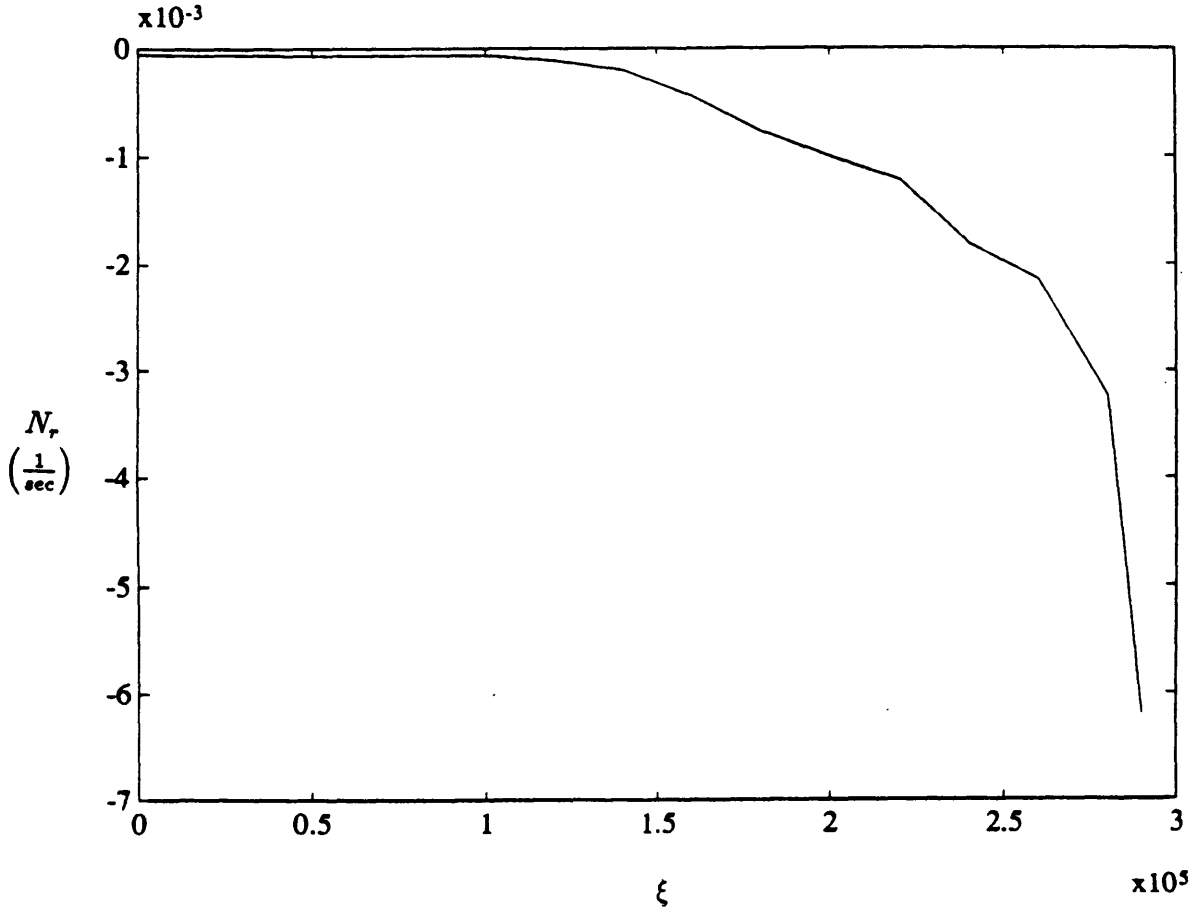

Figure 6-6: Yaw Damping Derivative vs. Vehicle Lengths Along Trajectory

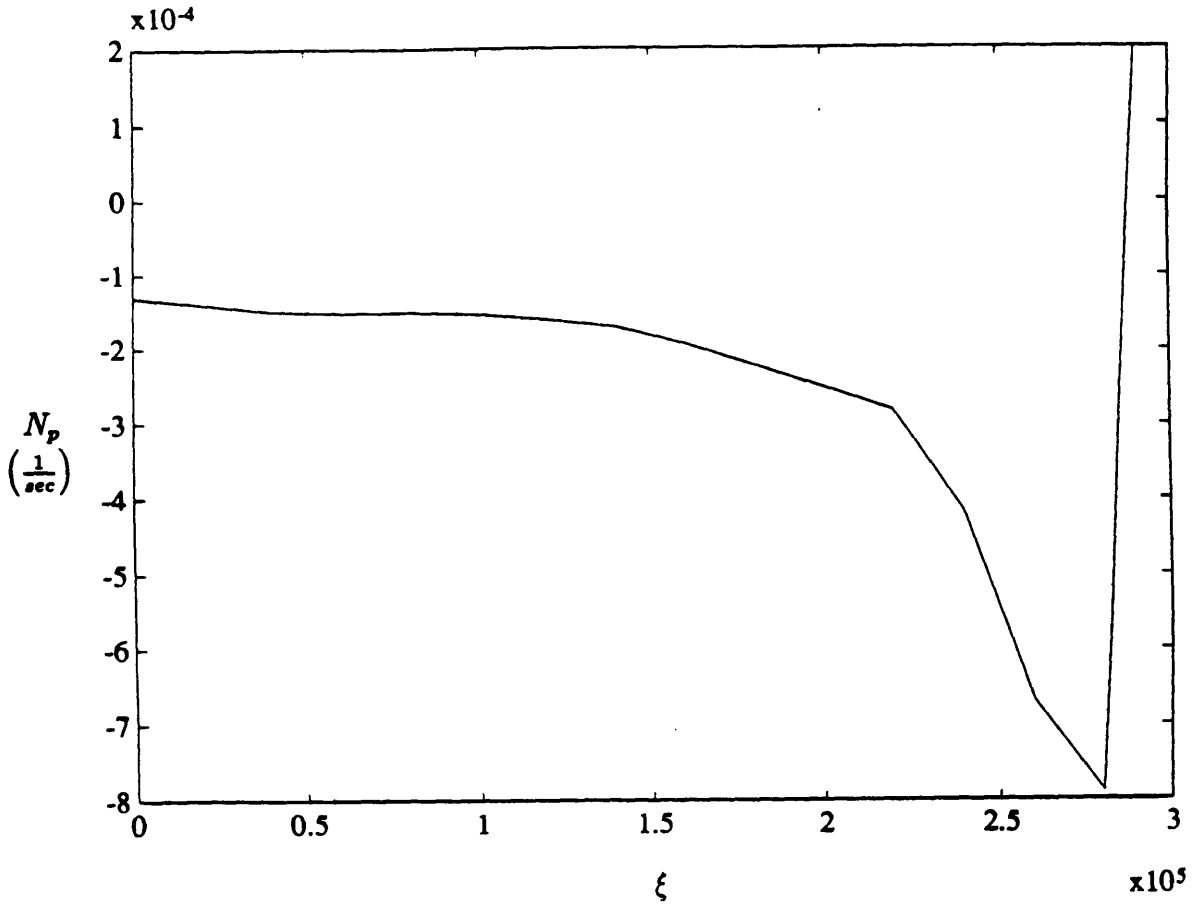

Figure 6-7: Yawing Moment Due to Roll Rate vs. Vehicle Lengths Along Trajectory

in the trajectory, the values of N_v are not much different from those of L_v, and a sideslip velocity will approximately cause equal rolling and yawing moments on the vehicle. However, as the GHAME vehicle progresses further into the atmosphere, the absolute value of N_v increases, and the directional stability term has a much greater effect on the vehicle than the dihederal term. In fact, with the exception of of L_v, all of the lateral-directional stability derivatives increase their effects on the vehicle as it travels further into the atmosphere. Since the stability derivatives represent aerodynamic tendencies of the vehicle, in all probability, the increased effects on the vehicle are due to the increase in air density further into the atmosphere.

The stability derivatives again with the exception of the dihederal term, do not exhibit abnormal behavior with regard to sign behavior at the hypersonic speeds encountered during reentry. The parameters remain as they would for conventional subsonic aircraft except for L_v. In conventional aircraft with positive dihederal angles, the definition of the standard coordinate system implies that the dihederal term is negative. If the aircraft sideslips to the right, the result is for the vehicle to roll right wing up. However, Fig.6-2 shows that the GHAME vehicle dihederal term is positive throughout the trajectory. If the GHAME vehicle sideslips to the right, it will experience a rolling moment causing the right wing to go down. If it is assumed that L_v is only affected by wing dihederal, then aerodynamically this makes no sense. However, since the GHAME vehicle has no wing dihederal, it is conceivable that the positive values of L_v are caused by the effects of the fuselage and tail.

The lateral-directional stability derivatives of the GHAME vehicle are employed in the next section to approximate solutions to reentry dynamics. Due to the fact that these parameters vary along the reentry trajectory, simple constant coefficient methods are not very useful, and GMS theory is employed. The sensitivity of the lateral-directional dynamics to each of these stability derivatives is considered in section 6.4.

6.4 GMS Solutions to Dynamics

Ramnath's GMS analysis outlined in Chapter 3 is utilized in this section to approximate the lateral-directional dynamics of the GHAME vehicle. The linearized lateral-directional equations of motion shown in Eq.6.7 are time-varying, and the asymptotic method is required to provide solutions to the system. As was the case with longitudinal dynamics, in order to apply GMS theory, it is convenient to express the linearized equations of motion in the form of a fourth order linear differential equation. This transformation is accomplished in exactly the same manner which was employed with the longitudinal equations of motion. First, it is assumed that the stability derivatives described in the previous section are of constant value through out the trajectory. Under such an assumption, the three independent variables of the lateral-directional equations of motion Δv, Δr, and $\Delta\phi$ have the same response. They are replaced by the generic variable y whose dynamics are described by the determinant of the main matrix in Eq.6.7. Following the same procedure and reasoning employed in transforming the longitudinal equations of motion, a dominant approximation to the lateral-directional motions is developed in the form desired. It is given by the fourth order linear time-varying differential equation

$$\frac{d^4y}{dt^4} + \omega_3(t)\frac{d^3y}{dt^3} + \omega_2(t)\frac{d^2y}{dt^2} + \omega_1(t)\frac{dy}{dt} + \omega_0(t)y = 0 \tag{6.11}$$

where

$$\omega_3(t) = -L_p - N_r - Y_v \tag{6.12}$$

$$\omega_2(t) = VN_v - L_rN_p + Y_vL_p + N_r(L_p + Y_v) \tag{6.13}$$

$$\omega_1(t) = Y_v(L_rN_P - N_rL_p) - gL_v + VN_pL_v - VL_pN_v \tag{6.14}$$

$$\omega_0(t) = g(L_vN_r - N_vL_r) \tag{6.15}$$

Solutions to this time-varying differential equation are approximated by the GMS method to determine the lateral-directional reentry behavior of the GHAME vehicle.

The fourth order GMS theory detailed in Chapter 3 approximates the solution

of a differential equation by first approximating the dynamics to each of the system's modes of motion. These approximations require that the characteristic roots associated with each of the GHAME vehicle's modes be determined along the entire trajectory. This is accomplished by solving the algebraic equation

$$s^4 + \omega_3 s^3 + \omega_2 s^2 + \omega_1 s + \omega_0 = 0 \tag{6.16}$$

where the coefficients are as defined in Eqs.6.12 through 6.15. Since, these coefficients vary with time, it is expected that the roots associated with the modes of motion will not remain stationary. The roots representing the lateral-directional motions of the GHAME vehicle are plotted in Fig.6-8 for up to 1657 seconds into the trajectory. It is clear that the GHAME vehicle possesses the three modes of motion which are typical of lateral-directional behavior in conventional aircraft. The dutch roll mode is represented by the complex conjugate pair of roots while the spiral divergence and roll convergence modes are identified by the two roots on the real axis. The root which remains in the left-half plane represents the roll convergence mode, while the other is the spiral divergence root. As the GHAME vehicle travel further into the atmosphere, the dutch roll mode experiences increase in both the frequency and damping terms. The changes in the frequency term are greater than those of the damping term which varies very little. Fig.6-8 shows that the roll convergence root initially starts close to the origin than travels away from it as time progresses. The spiral root generally remains in the same area. Figs.6-9 and 6-10 are plots of the roll convergence and spiral divergence roots versus time, and better show the way in which these roots vary along the trajectory.

The fourth order GMS equations shown in section 3.3 are now employed in order to approximate the characteristic motion associated with each of the GHAME vehicle's three lateral-directional modes of motion. Since the roll convergence and spiral divergence modes are each represented by a single real root, their respective dynamics

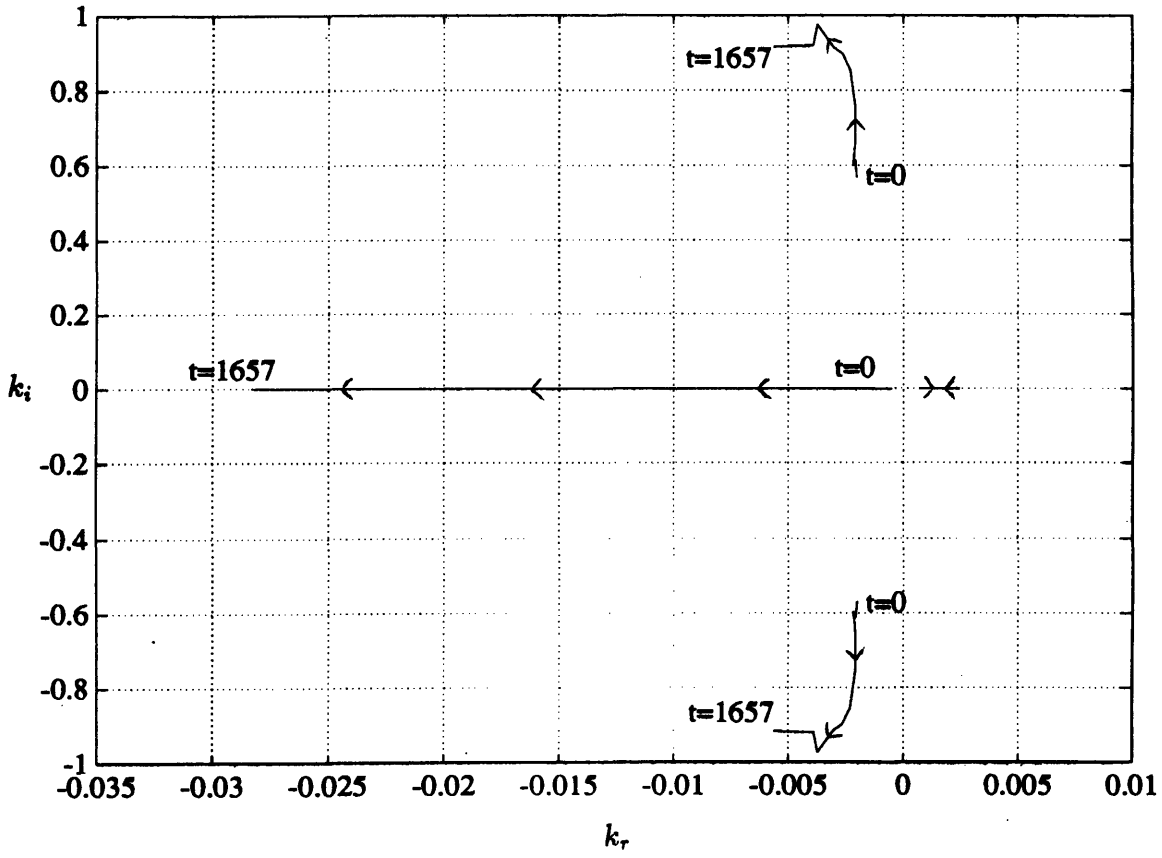

Figure 6-8: Lateral-Directional Roots Along Trajectory

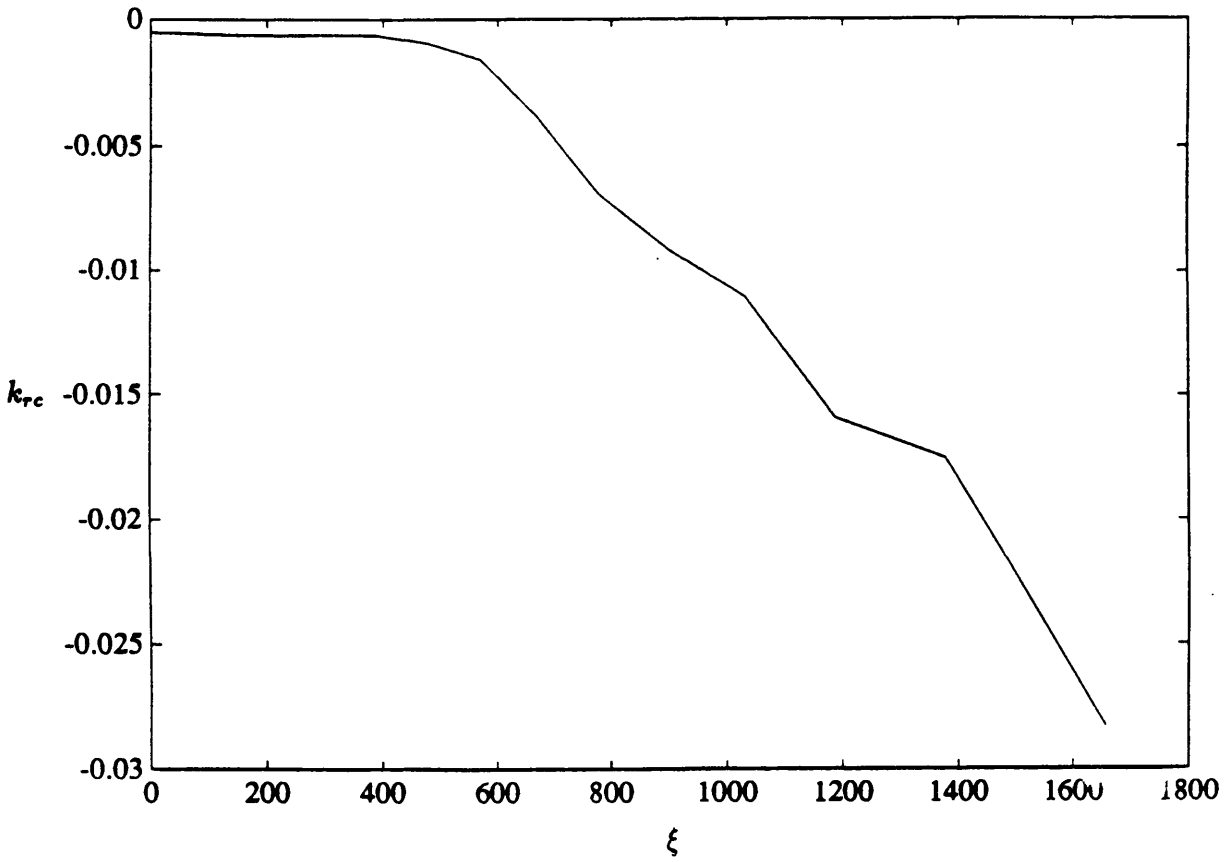

Figure 6-9: Roll Convergence Root vs. Time into Trajectory

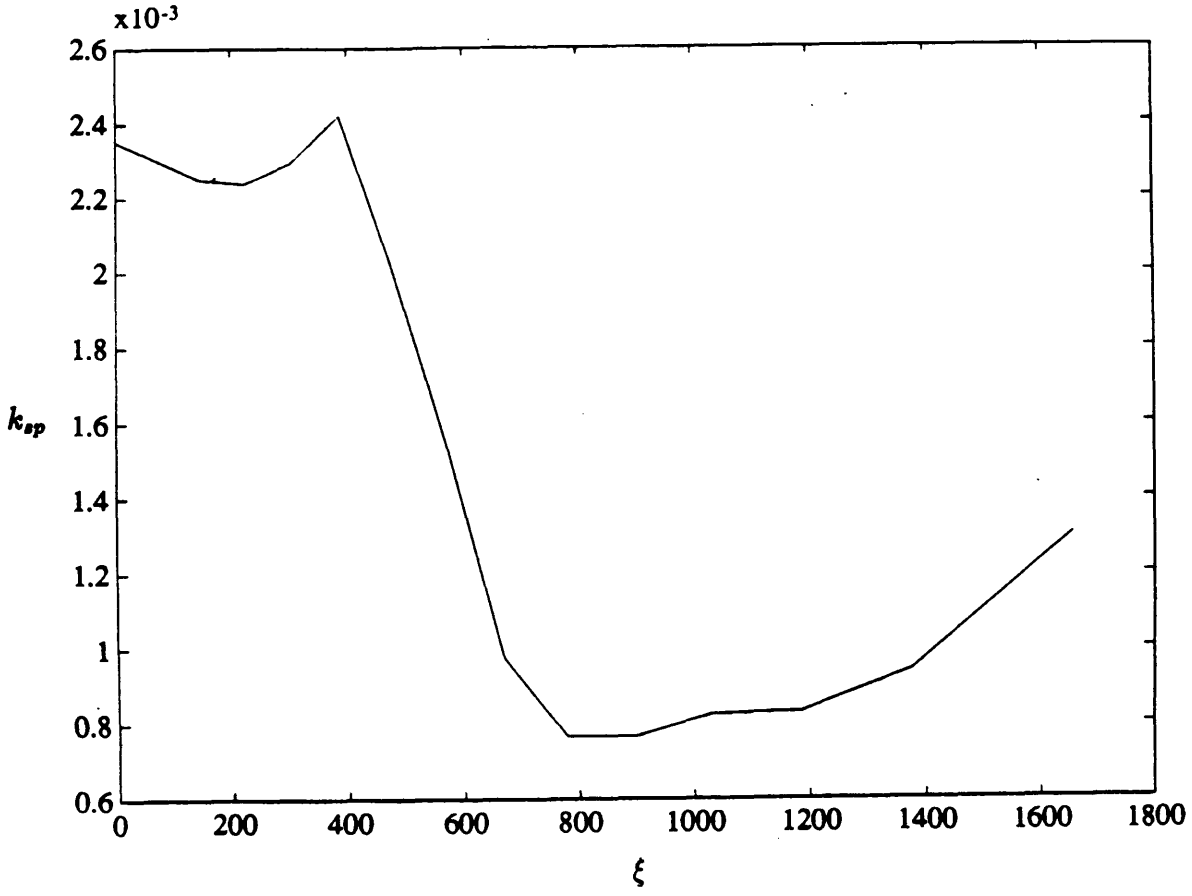

Figure 6-10: Spiral Divergence Root vs. Time into Trajectory

are predicted by the expressions

$$y_{rc}(t) = exp\left(\int_0^t k_{rc}(t)dt\right) \tag{6.17}$$

$$y_{sp}(t) = exp\left(\int_0^t k_{sp}(t)dt\right) \tag{6.18}$$

k_{rc} and k_{sp} are the roots of the roll convergence and spiral divergence modes respectively and are plotted in Figs.6-9 and 6-10. The characteristic dynamics of the remaining dutch roll mode are represented by a pair of complex conjugate roots as seen in Fig.6-8. If these roots are defined as $k_{dr} = k_{drr} + ik_{dri}$, then the dutch roll response is approximated by the equation

$$y_{dr}(t) = C_3 y_{dr1}(t) + C_4 y_{dr2}(t) \tag{6.19}$$

where C_3 and C_4 are arbitrary constants. y_{dr1} and y_{dr2} are given by

$$y_{dr1}(t) = exp\left(\int_0^t \left|\frac{\dot{k_{dr}}(t)}{2ik_{dri}(t)}\right| dt\right) exp\left(\int_0^t k_{drr}(t)dt\right) sin\left(\int_0^t k_{dri}(t)dt\right) \tag{6.20}$$

$$y_{dr2}(t) = exp\left(\int_0^t \left|\frac{\dot{k_{dr}}(t)}{2ik_{dri}(t)}\right| dt\right) exp\left(\int_0^t k_{drr}(t)dt\right) cos\left(\int_0^t k_{dri}(t)dt\right) \tag{6.21}$$

The roots of the GHAME vehicle's three modes along the Shuttle reentry trajectory are substituted into the above equations, and the characteristic motions of the lateral-directional behavior are predicted. The GMS approximations to the characteristic reentry dynamics associated with the roll convergence and spiral divergence modes are shown in Fig.6-11 and 6-12. Since the roll convergence roots remain in the left-half plane, it is expected that its response is stable. As seen in Fig.6-11, this is in fact the case. Similarly, the response of the spiral mode is unstable due to the fact that its roots remain in the right-half of the complex plane through out the entire reentry trajectory. Also, the dynamics of the spiral mode diverges faster than the roll mode converges. The characteristic motions of the dutch roll mode during reentry are shown in Figs.6-13 and 6-14. The first of these figures represents the sine wave component

of the dutch roll motions. The cosine component, y_{dr2}, is shown in Fig.6-14. Both plots show that the dutch roll reentry dynamics are damped oscillations with high frequency and little damping. There is little change in either as the GHAME vehicle progresses along the trajectory.

The responses shown in Figs.6-11 through 6-14 are approximations to the characteristic motions associated with each of the GHAME vehicle's three lateral-directional modes. In order to predict the complete lateral-directional behavior during reentry, the approximations to each of the modes are combined in a linear fashion. The full GMS approximation to the solution of Eq.6.11 is given by

$$y(t) = C_1 y_{rc}(t) + C_2 y_{sp}(t) + C_3 y_{dr1}(t) + C_4 y_{dr2}(t) \tag{6.22}$$

where C_1, C_2,C_3, and C_4 are arbitrary constants dependent on initial conditions of the original differential equation. Using this linear combination of the characteristic modal motions, the lateral-directional reentry behavior of the GHAME vehicle is predicted for two different sets of initial conditions. In order to assess the accuracy of the GMS approximations, numerical solutions are also obtained for both sets of initial conditions. Fig.6-15 shows both GMS and numerical approximations to the reentry lateral-directional dynamics for the initial conditions $y'''(0) = 1$, $y''(0) = 0$, $y'(0) = 0$, and $y(0) = 0$. The GMS and numerical solutions for the initial conditions $y'''(0) = 0$, $y''(0) = 0$, $y'(0) = 1$, and $y(0) = 0$ are plotted in Fig.6-16. It can be seen for both sets of initial conditions that the GMS approximations are virtually indistinguishable from the numerical solutions. Since the characteristic motion associated with the spiral divergence mode is unstable, the full lateral-directional behavior of the GHAME vehicle during reentry is also unstable. The first set of initial conditions produces a response containing enough of the dutch roll motions to exhibit some oscillatory behavior. The dynamics for the second set of initial conditions contain very little of the dutch roll motions and therefore produces a response which appears to be non-oscillatory.

In this section, the lateral-directional dynamics of the GHAME vehicle along

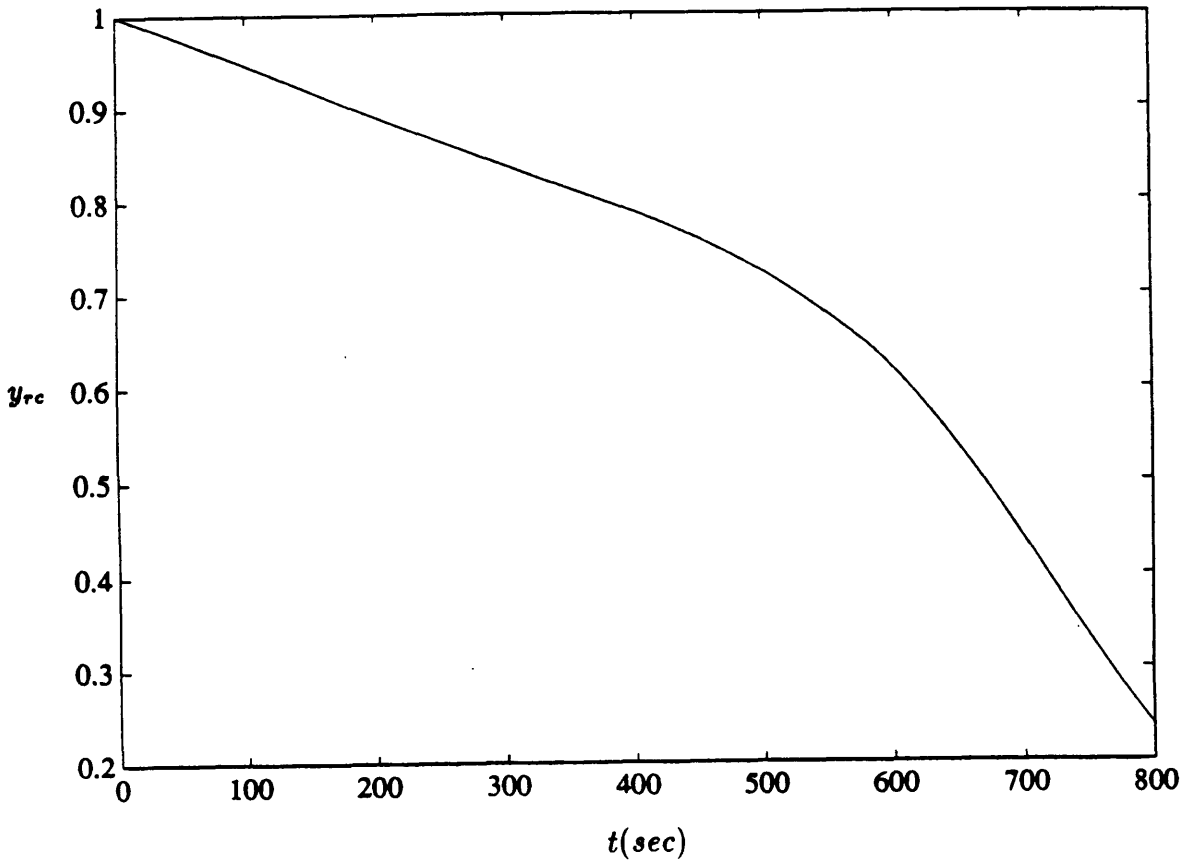

Figure 6-11: GMS Solution to Roll Convergence Dynamics

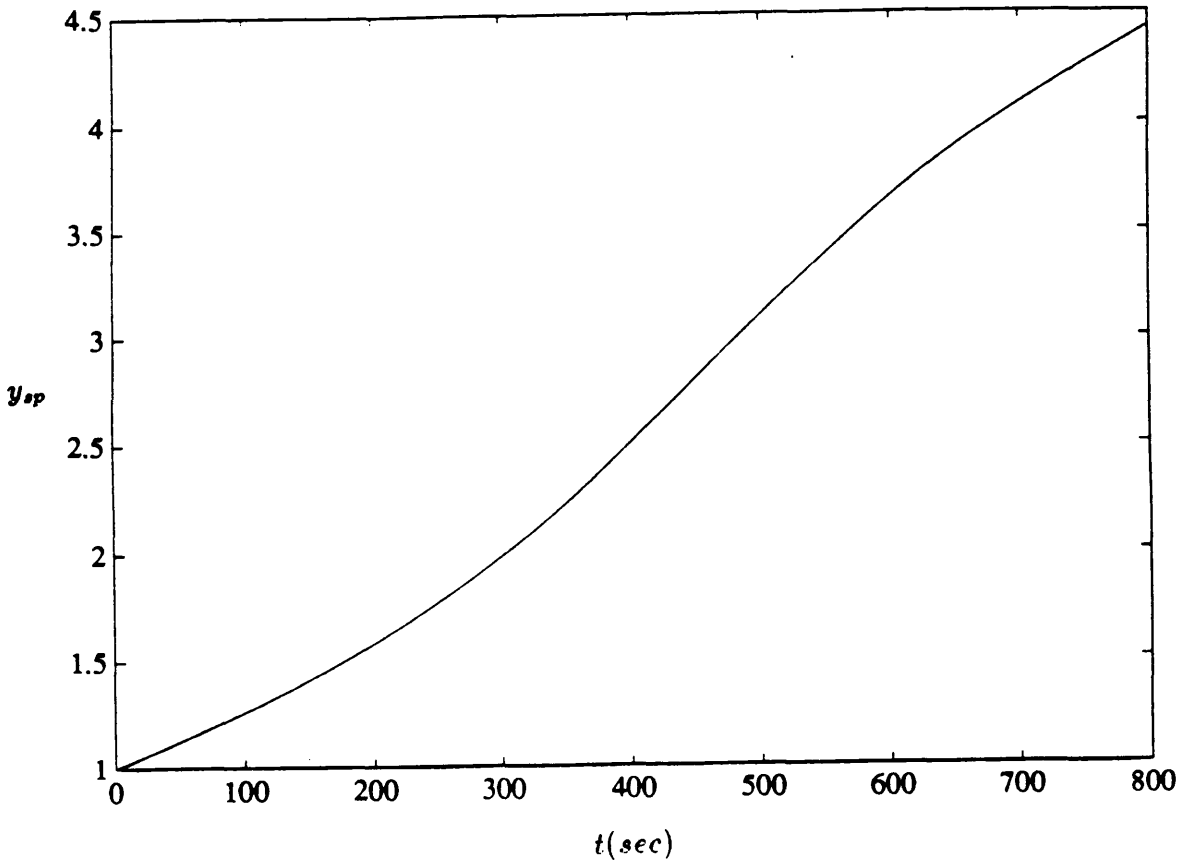

Figure 6-12: GMS Solution to Spiral Divergence Dynamics

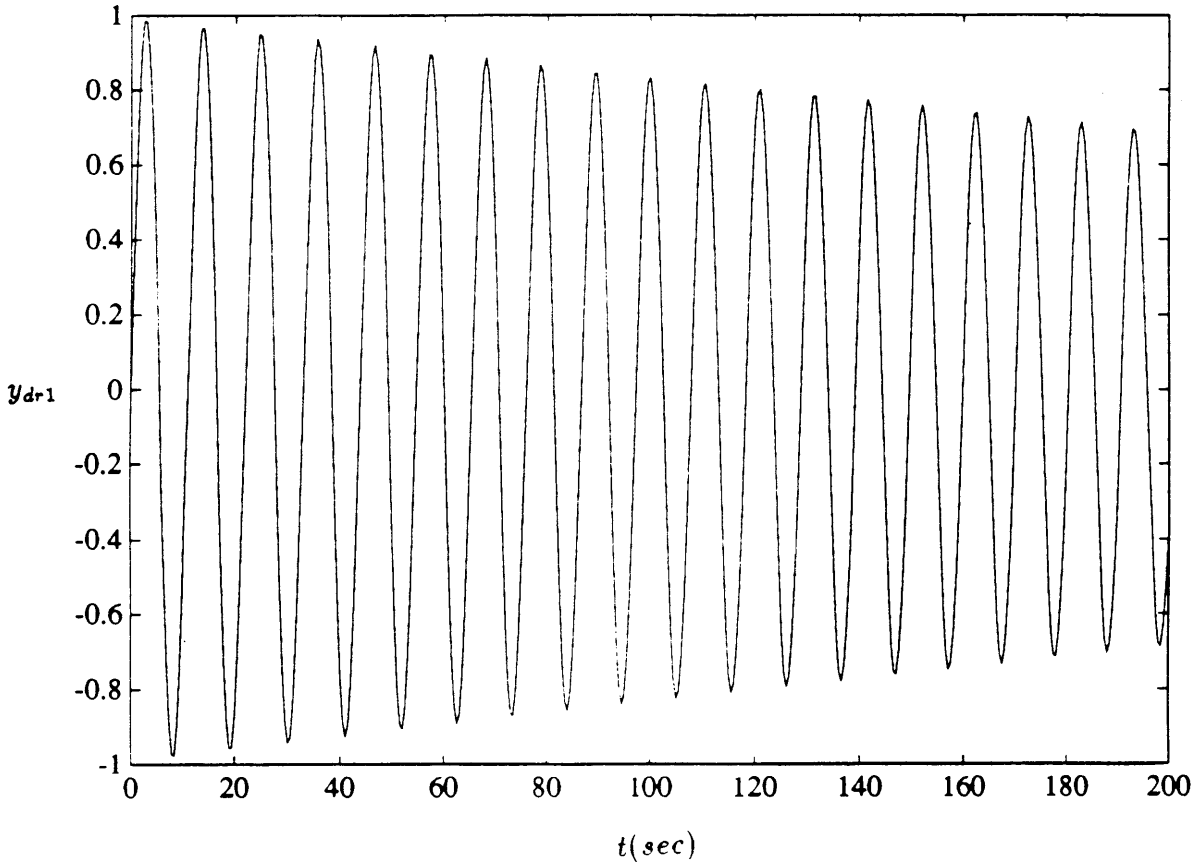

Figure 6-13: GMS Solution to Sine-like Dutch Roll Dynamics

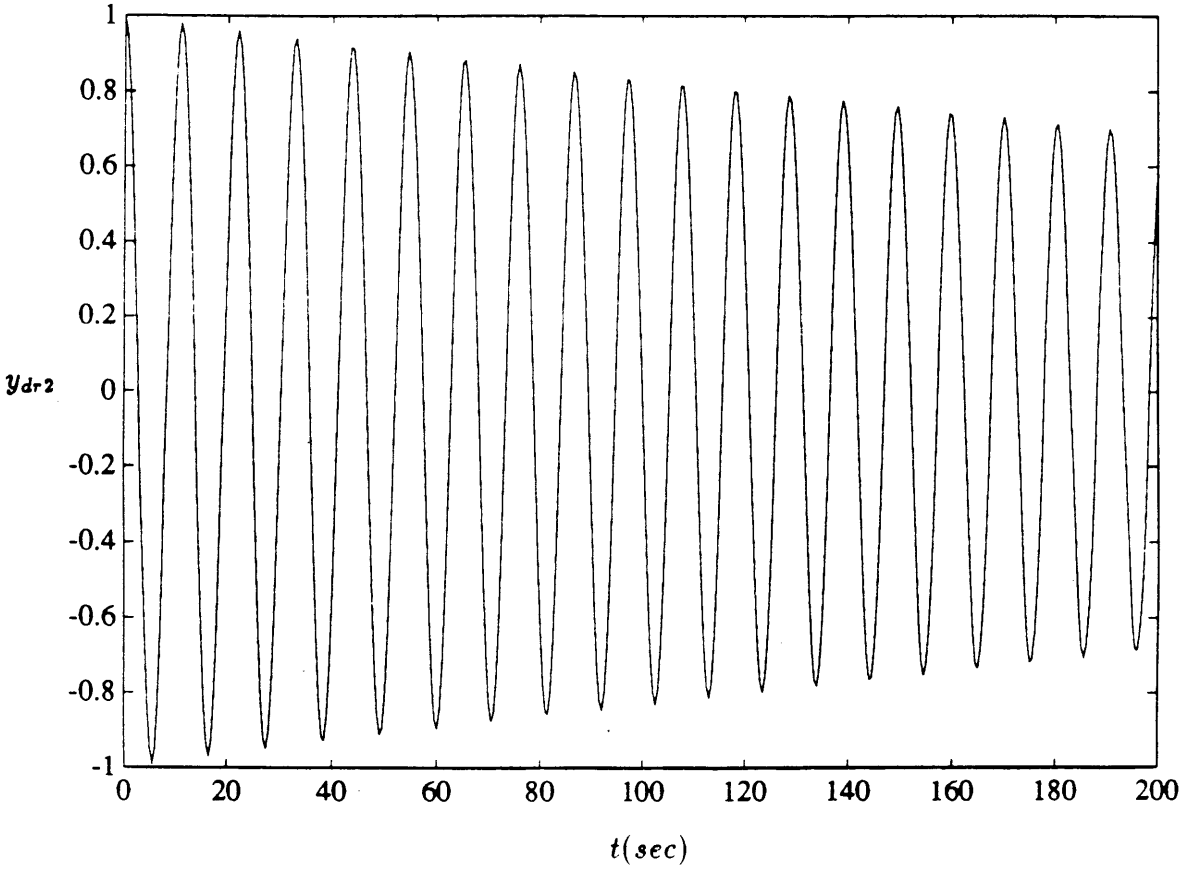

Figure 6-14: GMS Solution to Cosine-like Dutch Roll Dynamics

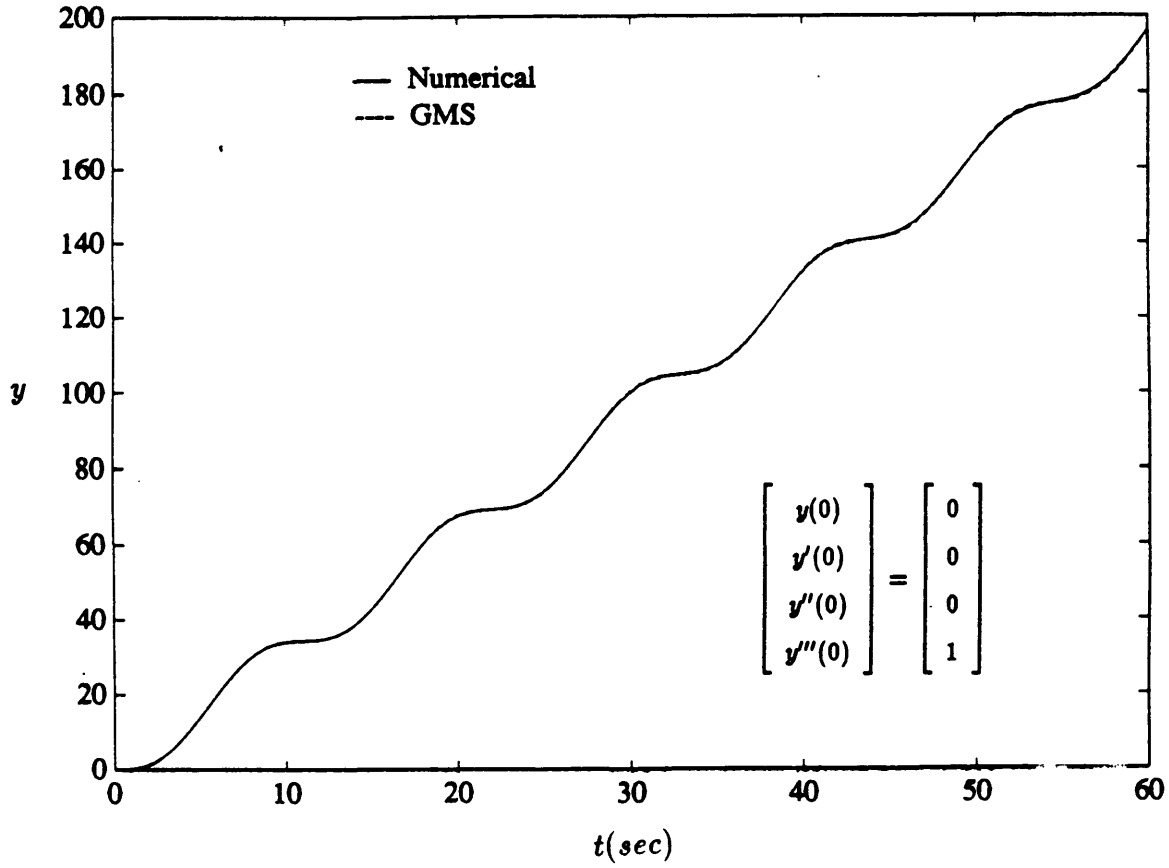

Figure 6-15: GMS Solution to Lateral-Directional Reentry Dynamics

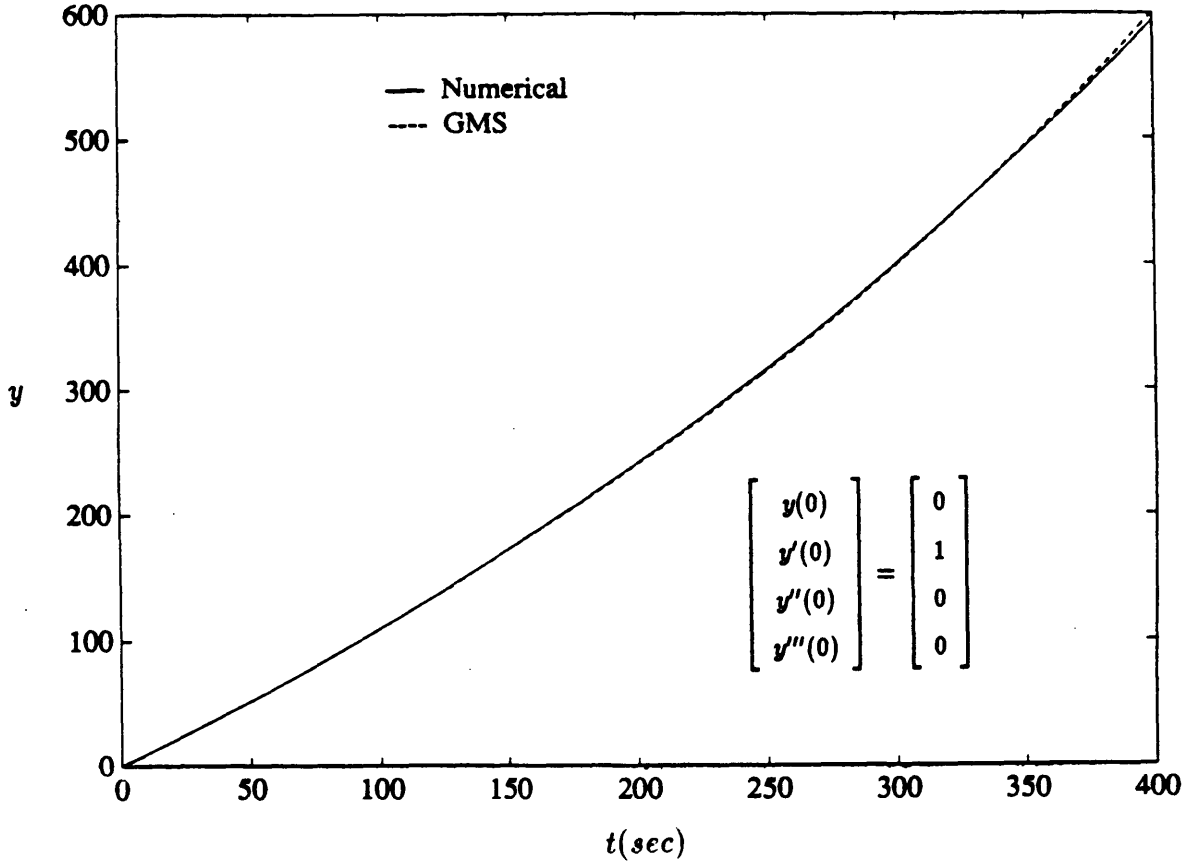

Figure 6-16: GMS Solution to Lateral-Directional Reentry Dynamics

the Space Shuttle reentry trajectory were predicted by employing fourth order GMS approximations. The GMS solutions were indistinguishable from numerical solutions, and once again proved themselves to be accurate. The lateral-directional reentry behavior of the GHAME vehicle was shown to be unstable due to the instability of the characteristic motion associated with the spiral divergence mode. Since the lateral-directional variable y is a dominant approximation to the actual variables Δv, Δr and $\Delta \phi$, these parameters should possess the same unstable behavior found in the above analysis.

6.5 Sensitivity Analysis

In this section, the sensitivity of the GHAME vehicle's lateral-directional reentry dynamics to the stability derivatives detailed in section 3.3 is studied. The effects of changing these stability derivatives on the dynamics of the vehicle are determined by employing the GMS approximations to the motions associated with each of the lateral-directional modes. Once again, due to the analytical forms of these GMS approximations, it is possible to conduct a sensitivity analysis by partial differentiation with respect to the stability derivatives. As noted in section 4.4, partial differentiation does not provide a true sensitivity analysis due to the fact that the stability derivatives themselves are functions of time. In order to determine the exact sensitivity of the dynamics to these parameters, variational calculus is necessary. However, partial differentiation is justified by Ramnath's asymptotic sensitivity theory and is employed in this study.

As with the approximation of the actual lateral-directional dynamics, the sensitivity of vehicle motions to the stability derivatives is developed by first considering the motions associated with each of the modes. The sensitivity of the characteristic modal motions is determined by partially differentiating Eqs.6.17 through 6.21 with respect to the stability derivatives. For example, the sensitivity of the roll convergence and spiral divergence motions to the directional stability derivative is given by partially differentiating Eqs.6.17 and 6.18 with respect to N_v. After, shifting the

differentiation inside the integral, this lead to

$$\frac{\partial y_{rc}}{\partial N_v} = exp\left(\int_0^t k_{rc}dt\right)\left(\int_0^t \frac{\partial k_{rc}}{\partial N_v}dt\right) \tag{6.23}$$

$$\frac{\partial y_{sp}}{\partial N_v} = exp\left(\int_0^t k_{sp}dt\right)\left(\int_0^t \frac{\partial k_{sp}}{\partial N_v}dt\right) \tag{6.24}$$

In order to determine the sensitivity of the dutch roll motions, only the fast GMS solution is considered. The slow solution has little effect on the approximation, and for the purposes of simplicity, it is disregarded. The sensitivity of the sine-like and cosine-like dutch roll motions to the directional stability term is determined by differentiating the fast GMS solution contained in Eqs.6.20 and 6.21. Again, after shifting the differentiation inside the integral, this results in

$$\begin{aligned}\frac{\partial y_{dr1}}{\partial N_v} &= \left(\int_0^t \frac{\partial k_{drr}}{\partial N_v}dt\right) exp\left(\int_0^t k_{drr}dt\right) sin\left(\int_0^t k_{dri}dt\right) + \\ &\left(\int_0^t \frac{\partial k_{dri}}{\partial N_v}dt\right) exp\left(\int_0^t k_{drr}dt\right) cos\left(\int_0^t k_{dri}dt\right)\end{aligned} \tag{6.25}$$

$$\begin{aligned}\frac{\partial y_{dr2}}{\partial N_v} &= \left(\int_0^t \frac{\partial k_{drr}}{\partial N_v}dt\right) exp\left(\int_0^t k_{drr}dt\right) cos\left(\int_0^t k_{dri}dt\right) - \\ &\left(\int_0^t \frac{\partial k_{dri}}{\partial N_v}dt\right) exp\left(\int_0^t k_{drr}dt\right) sin\left(\int_0^t k_{dri}dt\right)\end{aligned} \tag{6.26}$$

The differentiation can be accomplished in the same manner for the other stability derivatives, and their sensitivities can be obtained simply by replacing N_v with the parameter of choice in the above equations. In Eqs 6.23 through 6.26, the partial derivatives $\frac{\partial k_{rc}}{\partial N_v}$, $\frac{\partial k_{sp}}{\partial N_v}$, $\frac{\partial k_{drr}}{\partial N_v}$, and $\frac{\partial k_{dri}}{\partial N_v}$ still need to be determined before the sensitivity of each characteristic motion is obtained. It is known that the coefficients of the algebraic equation which determine the mode roots are functions of the stability derivatives as defined by Eq.6.12 through 6.15. Also, the roots can be explicitly written as functions of the coefficients. Therefore, in order to obtain partial derivatives of the roots with respect to the stability derivative, the chain rule is employed. Since the process relating the roots of Eq.6.22 to its coefficients is rather tedious, the details

of the complete differentiation are left for Appendix B. The results of the chain rule differentiation and root information is substituted into the above equations to complete the analysis. The sensitivities of the GHAME vehicle's lateral-directional reentry modal motions with respect to the seven stability derivatives are shown in Figs.6-17 through 6-44. The results of the dutch roll mode are separated into the sensitivities of the sine and cosine components.

In order to obtain the sensitivity of the full lateral-directional reentry dynamics, a linear combination is employed once more. Without considering the dependence of initial and boundary conditions on the parameter, differentiating the linear GMS approximation to the full dynamics given in Eq.6.22 leads to

$$\frac{\partial y}{\partial N_v} = C_1 \frac{\partial y_{rc}}{\partial N_v} + C_2 \frac{\partial y_{sp}}{\partial N_v} + C_3 \frac{\partial y_{dr1}}{\partial N_v} + C_4 \frac{\partial y_{dr2}}{\partial N_v} \tag{6.27}$$

where C_1, C_2, C_3, and C_4 are constants previously determined by the initial conditions of the original differential equation. Justification for this procedure is based on Ramnath's work on GMS sensitivity theory. It is evident from section 6.4 that the full lateral-directional response of the GHAME vehicle is very much dependent on the initial conditions. The initial conditions determine the amount of influence that each of the modes of motion has on the full response. Since initial conditions can be chosen arbitrarily and the presence of each mode can vary, it is meaningless to study the sensitivity of the GHAME vehicle lateral-directional dynamics for a specific set of initial conditions. Much more insight is gained by considering the sensitivities of each mode of motion which are combined to obtain the full sensitivity.

It is clear from studying Figs.6-17 through 6-44 that the sensitivities of the modal motions associated with respect to each of the stability derivatives exhibit similar patterns of behavior. First, all of the stability derivatives have the most influence on the spiral divergence mode. A change in any of the seven stability derivatives will have a greater effect on the dynamics of the spiral mode than on either of the roll convergence or dutch roll modes. The roll convergence dynamics are almost as sensitive as the spiral divergence motions, however, are not quite as affected by variations

in the stability derivatives. Variations in any stability derivative has the least effect on the motions associated with the dutch roll mode. Its sensitivity is several orders of magnitude less than the sensitivities of the other two modes. Therefore, lateral-directional responses which contain relatively greater portions of the spiral divergence mode are more sensitive to changes in the stability derivatives than responses which may contain relatively greater portions of either the roll convergence or dutch roll modes.

Although variations in any of the seven stability derivatives will affect the spiral mode more than the other two, each of the stability derivatives does not affect a particular motion in the same manner. It is evident from Figs.6-17 through 6-44 that each of the modal motions is more sensitive to the directional derivative, N_v than any of the other stability derivatives. The roll convergence, spiral divergence, and dutch roll motions are each more affected by changes in N_v than any of the other six stability derivatives. An equal change in the dihederal term, L_v has almost as much affect, however, the other derivatives have sensitivities which are several orders of magnitude less than the sensitivity with respect to the directional derivative. This behavior of the GHAME vehicle is similar to that of a conventional aircraft whose lateral-directional motions are also most sensitive to N_v and L_v. Since the directional stability term is very much a function of the vertical tail size of the aircraft, the GHAME vehicle vertical tail size has great implications on its reentry lateral-directional dynamics. Of the other stability derivatives, the plots reveal that L_p, Y_v, and N_p have the least effect on the dynamics. Particularly, the sensitivity of each modal motion to L_p remains relatively very small for up to approximately 500 seconds into the trajectory. Compared to the sensitivities of modal motions to N_v and L_v, variations in L_p, Y_v, and N_p have virtually no effect on the lateral-directional reentry dynamics of the GHAME vehicle.

It is evident from the plots in Figs.6-17 through 6-44 that the sensitivities of the characteristic spiral divergence motion with respect to all the stability derivatives grow unbounded. This is to be expected since the actual spiral mode dynamics are unstable. The sensitivities of the roll convergence and dutch roll modes both grow

rapidly at approximately 600 seconds into the trajectory. The time histories of the roll convergence and dutch roll sensitivity variations are exhibited for the specific values of the vehicle parameters and trajectory flown in this investigation. As seen in Appendix B, this is due to the nature of the partial differentiation which renders the sensitivities proportional to the time integrals of various parameters. A possible explanation is that the increasing behavior of these integrals forces the sensitivities of the roll convergence and dutch roll motions to exhibit rapidly increasing behavior before the convergence of the true dynamics can take effect. However, the sensitivities of roll convergence and dutch roll motions with respect to the derivatives, L_p, L_v, and N_p all have an instant which their values become zero before they experience the rapid increase and subsequent convergence. The sensitivities of the roll convergence and dutch roll motions with respect to L_v and N_p are zero at approximately 600 seconds into the shuttle trajectory. The sensitivity of the motions to L_p is zero at approximately 500 seconds into the trajectory. Although the effects of changing L_p and N_p on the lateral-directional reentry dynamics are minimal, there are moments in the trajectory where such variations will have absolutely no effect on roll convergence and dutch roll motions. This is significant for the stability derivative L_v which has relatively great effect on the dynamics throughout the trajectory except for this particular section where it becomes zero before increasing rapidly and then converging..

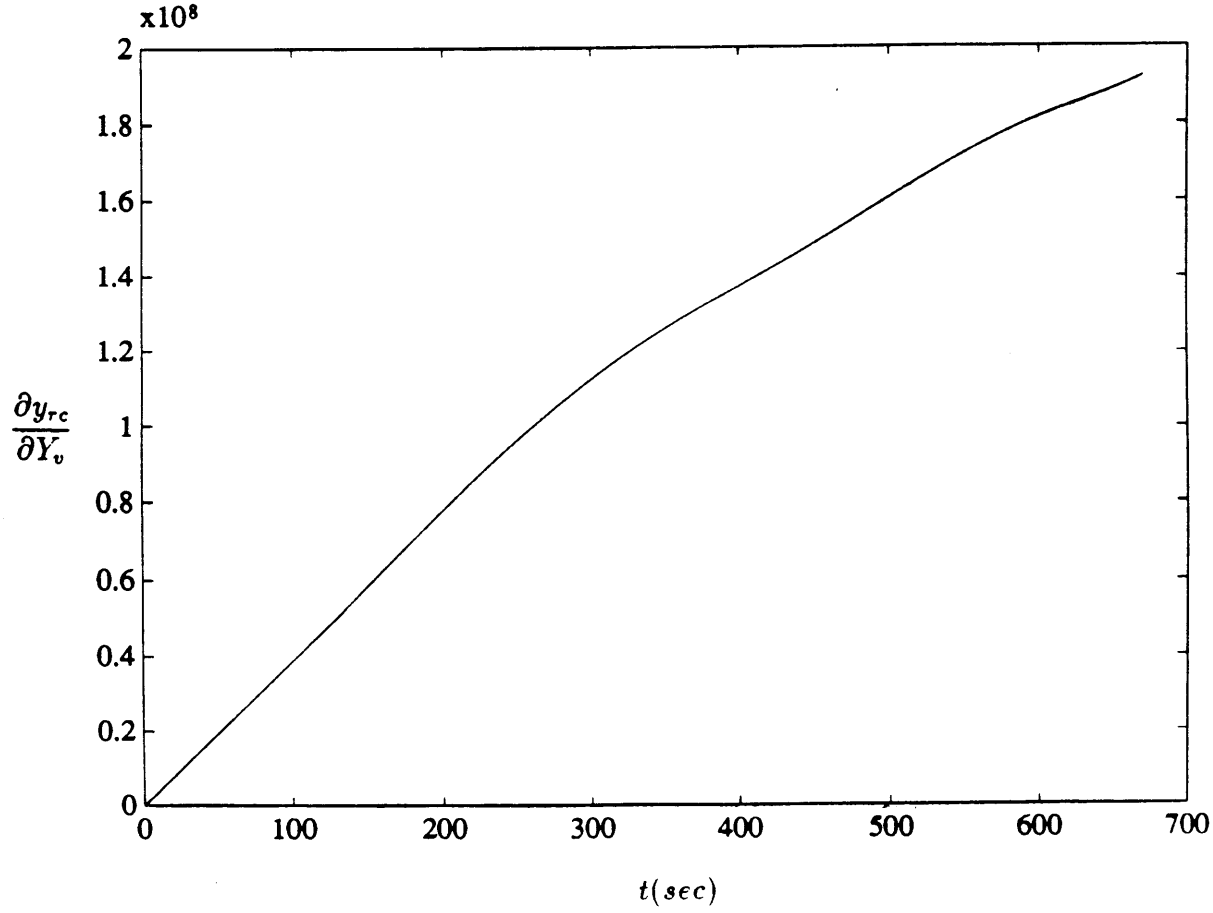

Figure 6-17: Sensitivity of Roll Convergence Dynamics to Y_v

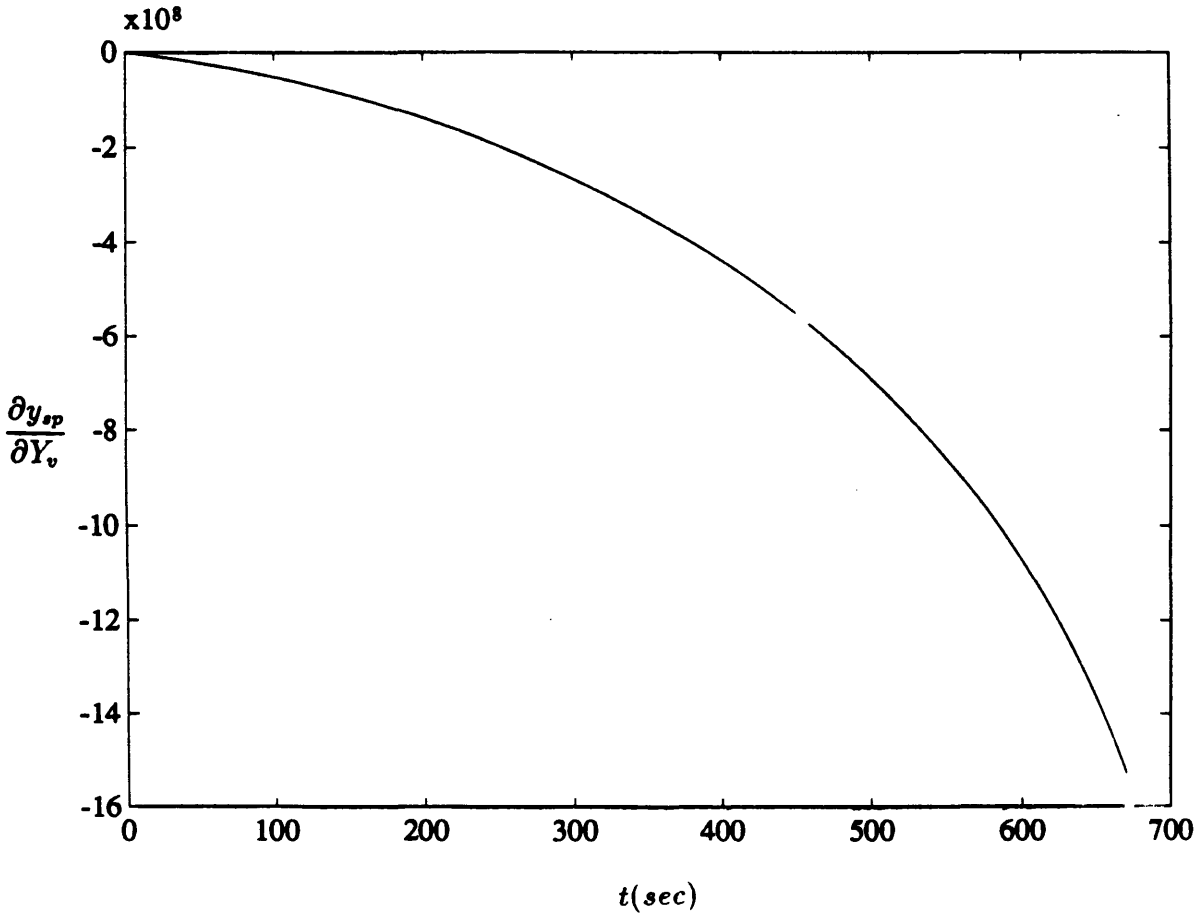

Figure 6-18: Sensitivity of Spiral Divergence Dynamics to Y_v

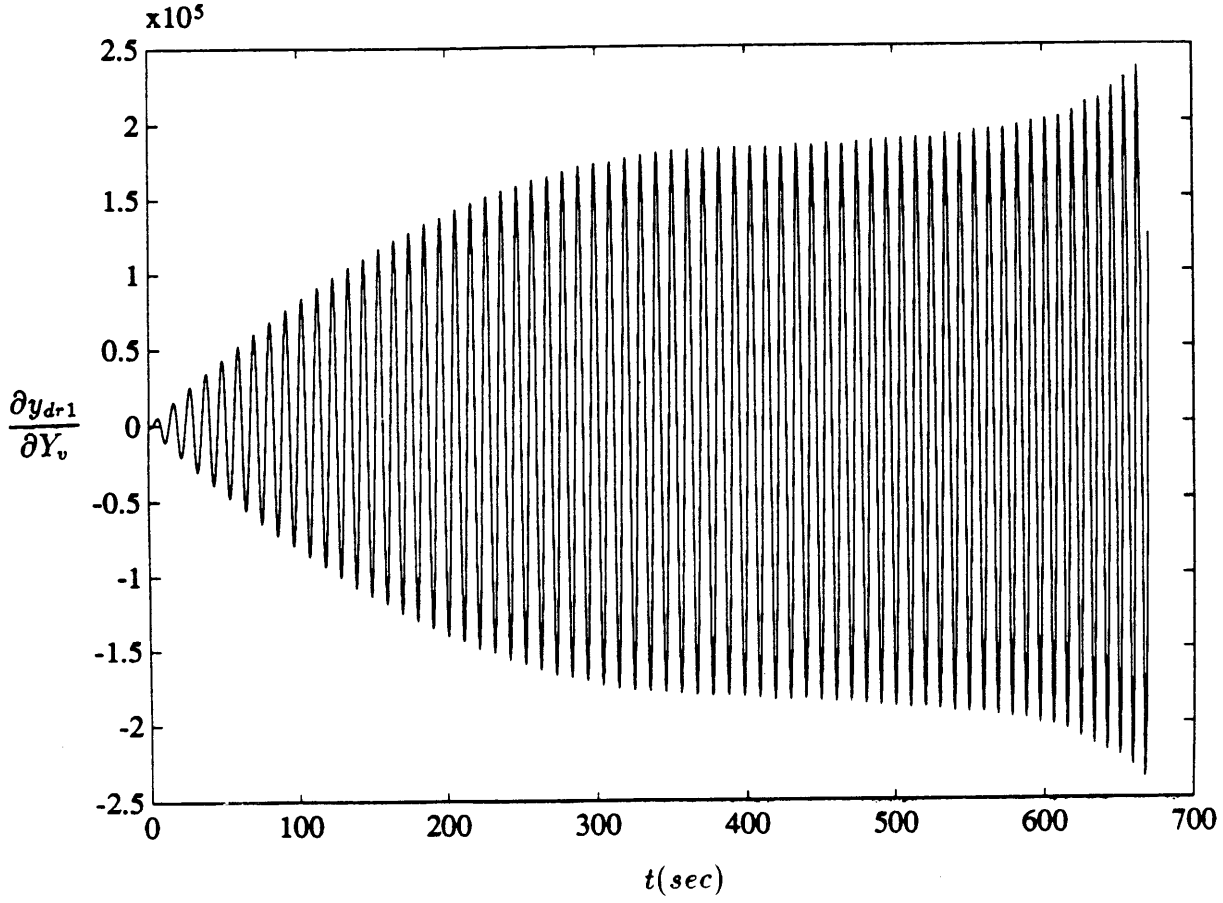

Figure 6-19: Sensitivity of Sine-like Dutch Roll Dynamics to Y_v

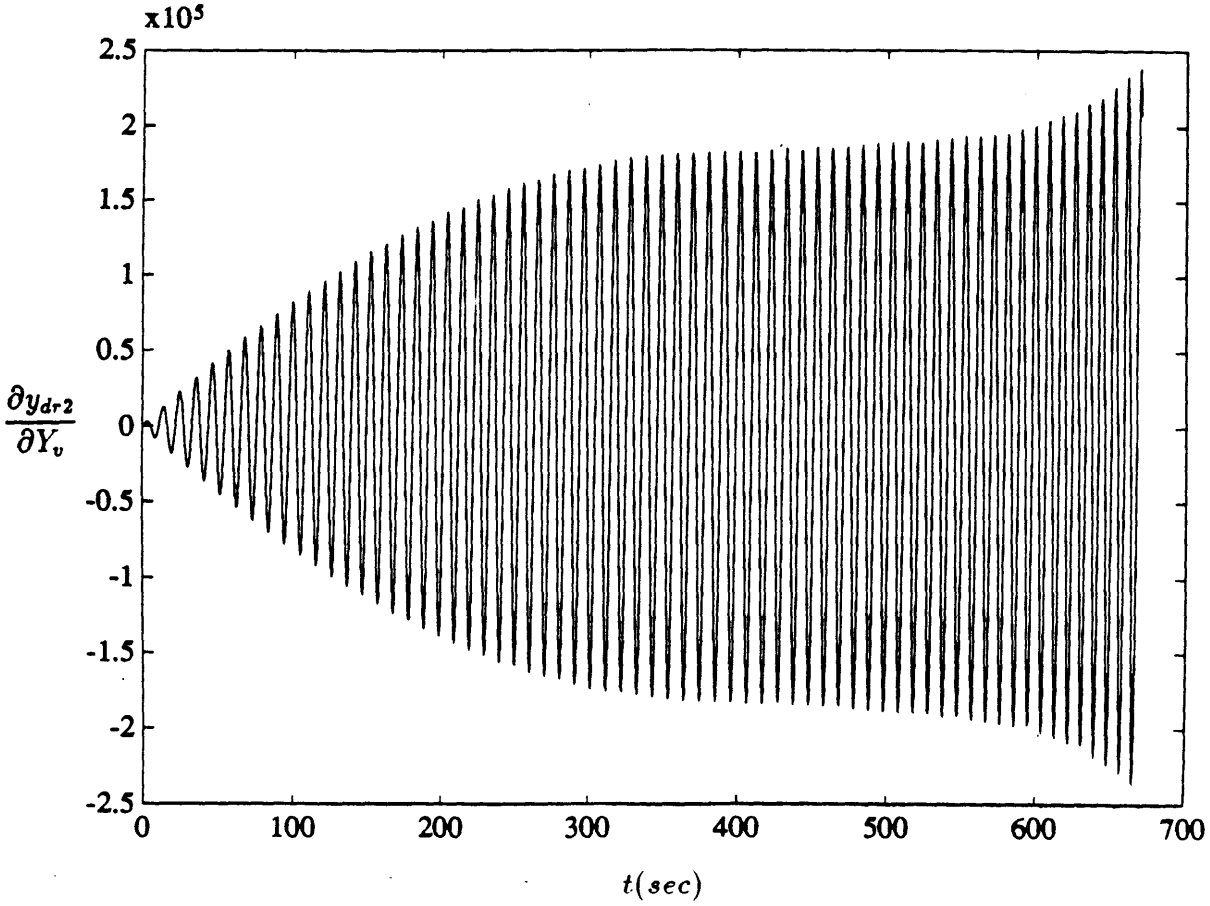

Figure 6-20: Sensitivity of Cosine-like Dutch Roll Dynamics to Y_v

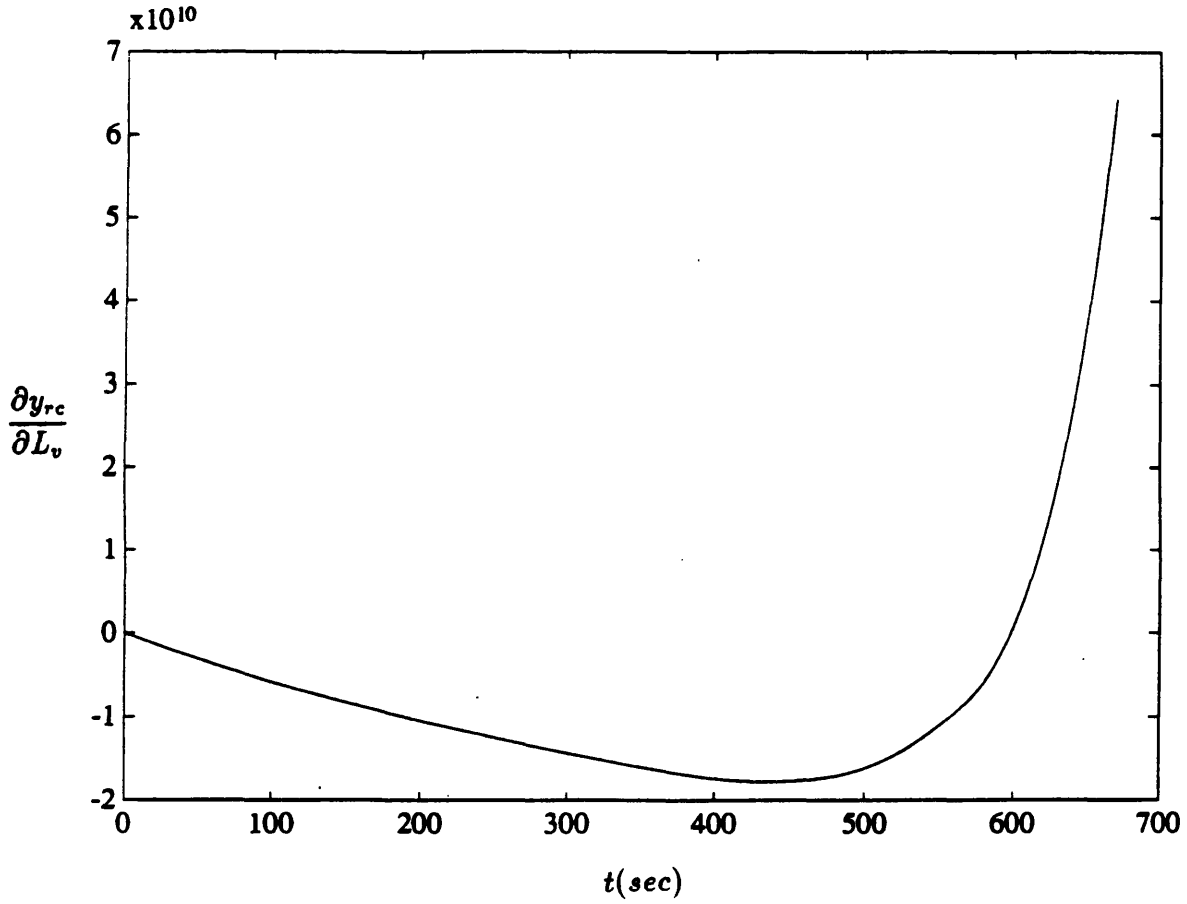

Figure 6-21: Sensitivity of Roll Convergence Dynamics to L_v

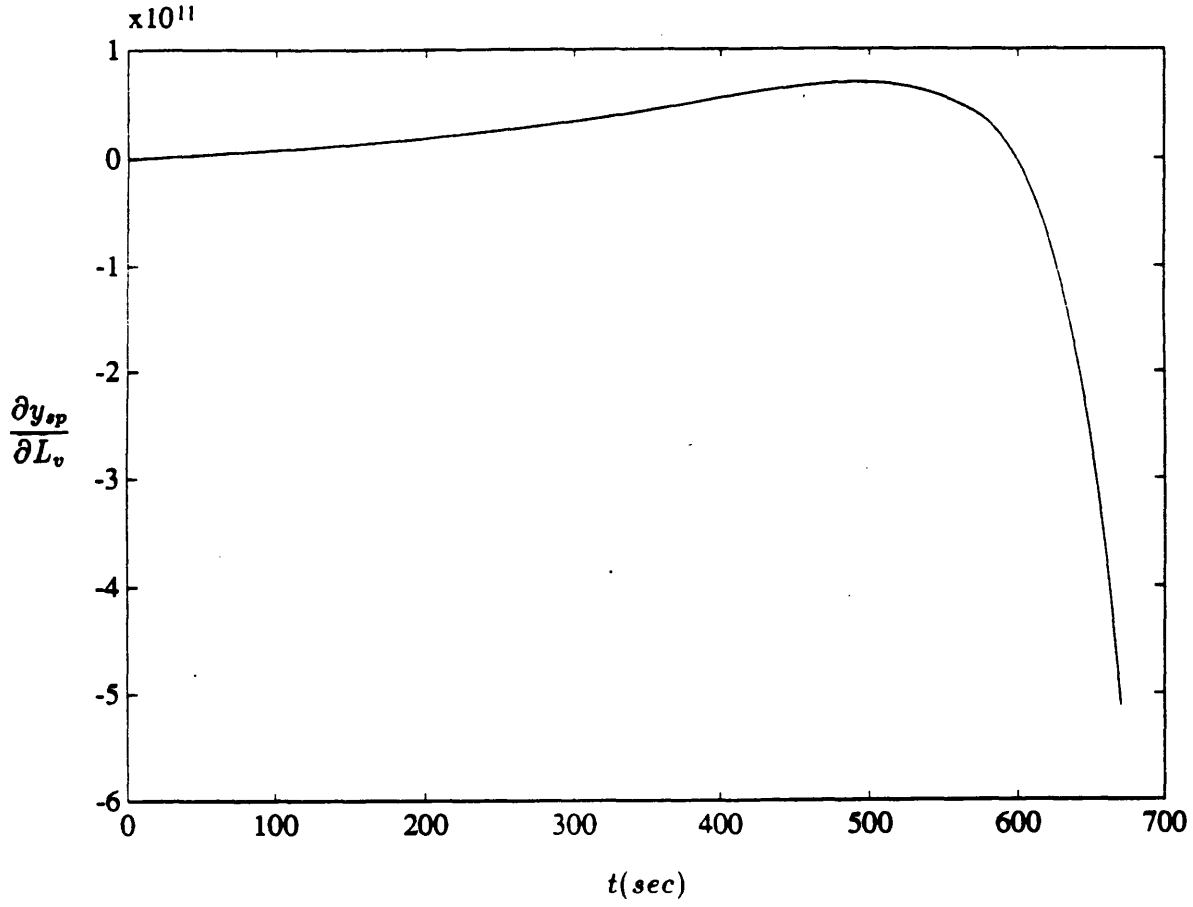

Figure 6-22: Sensitivity of Spiral Divergence Dynamics to L_v

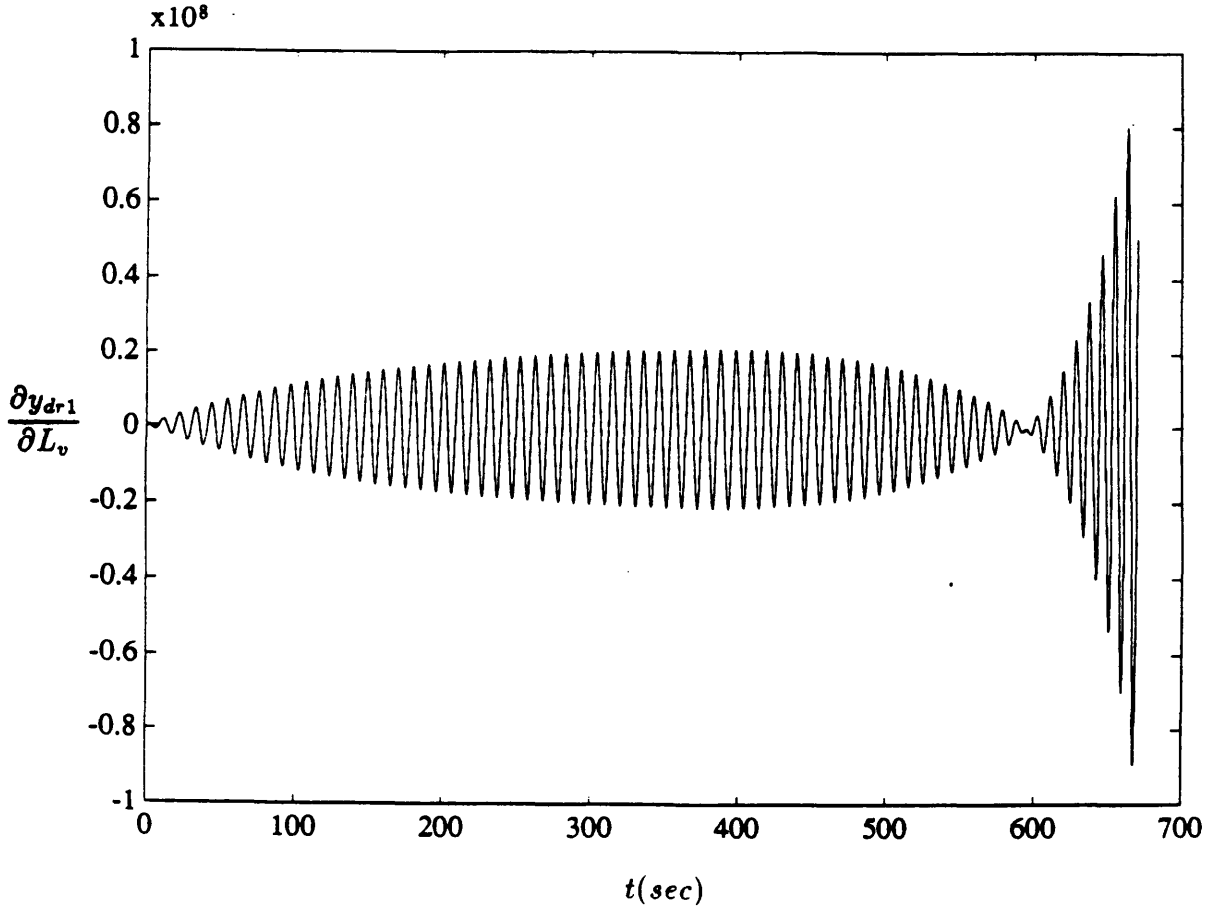

Figure 6-23: Sensitivity of Sine-like Dutch Roll Dynamics to L_v

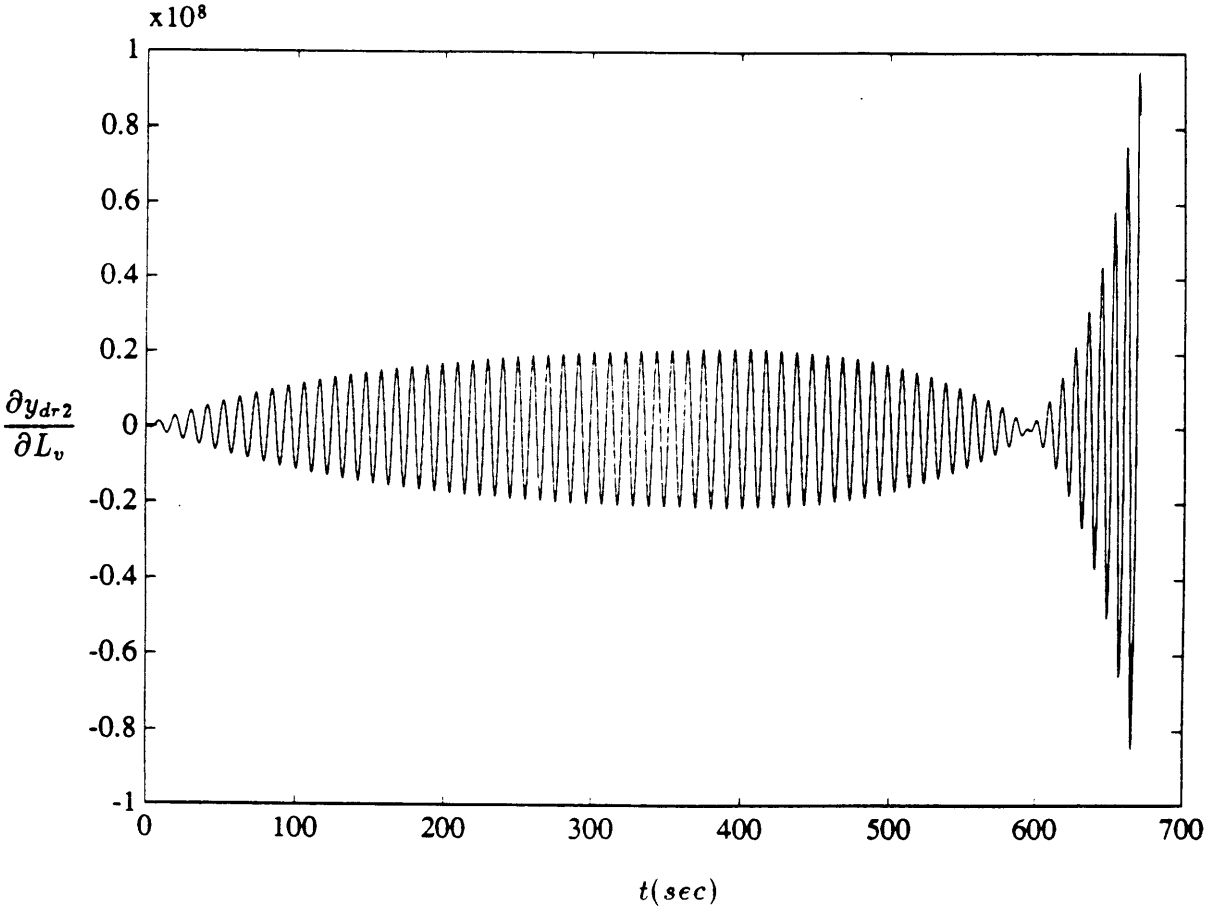

Figure 6-24: Sensitivity of Cosine-like Dutch Roll Dynamics to L_v

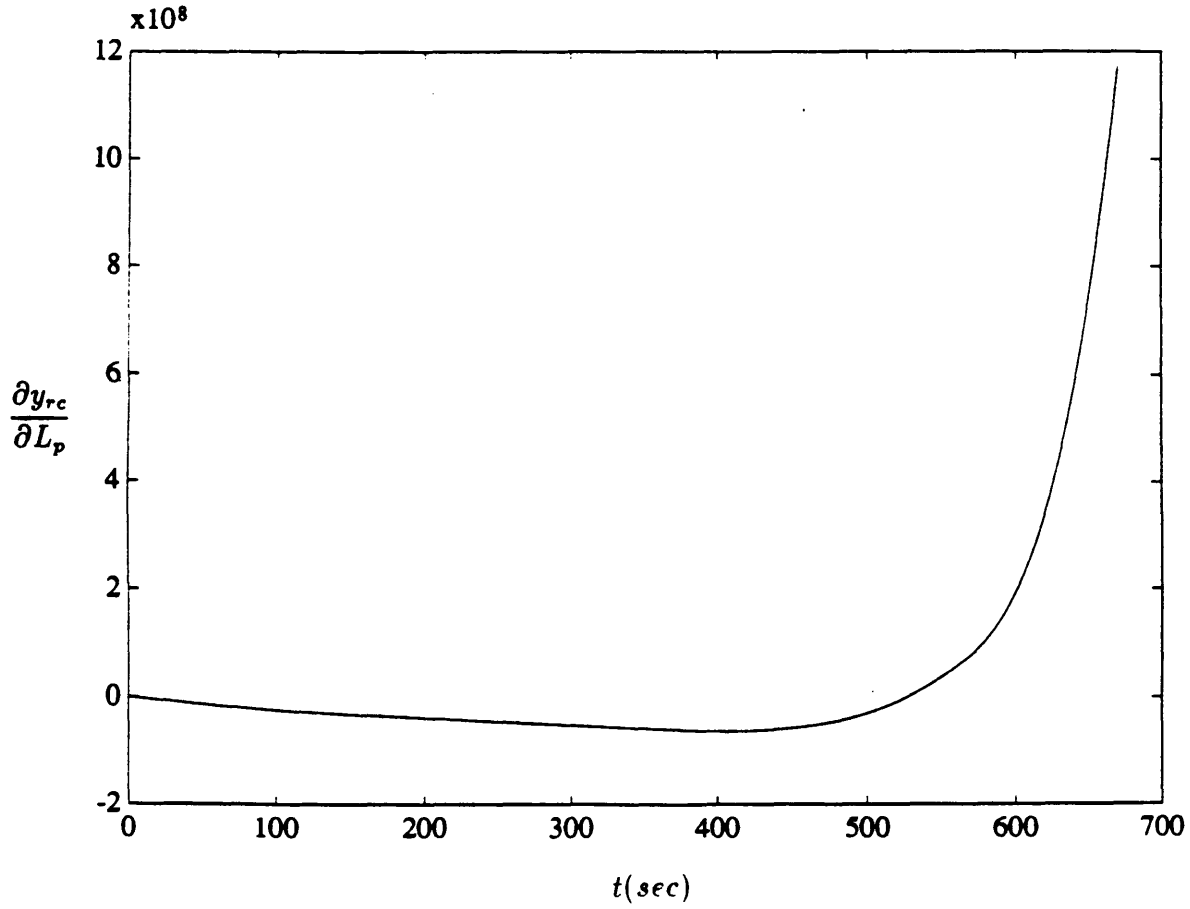

Figure 6-25: Sensitivity of Roll Convergence Dynamics to L_p

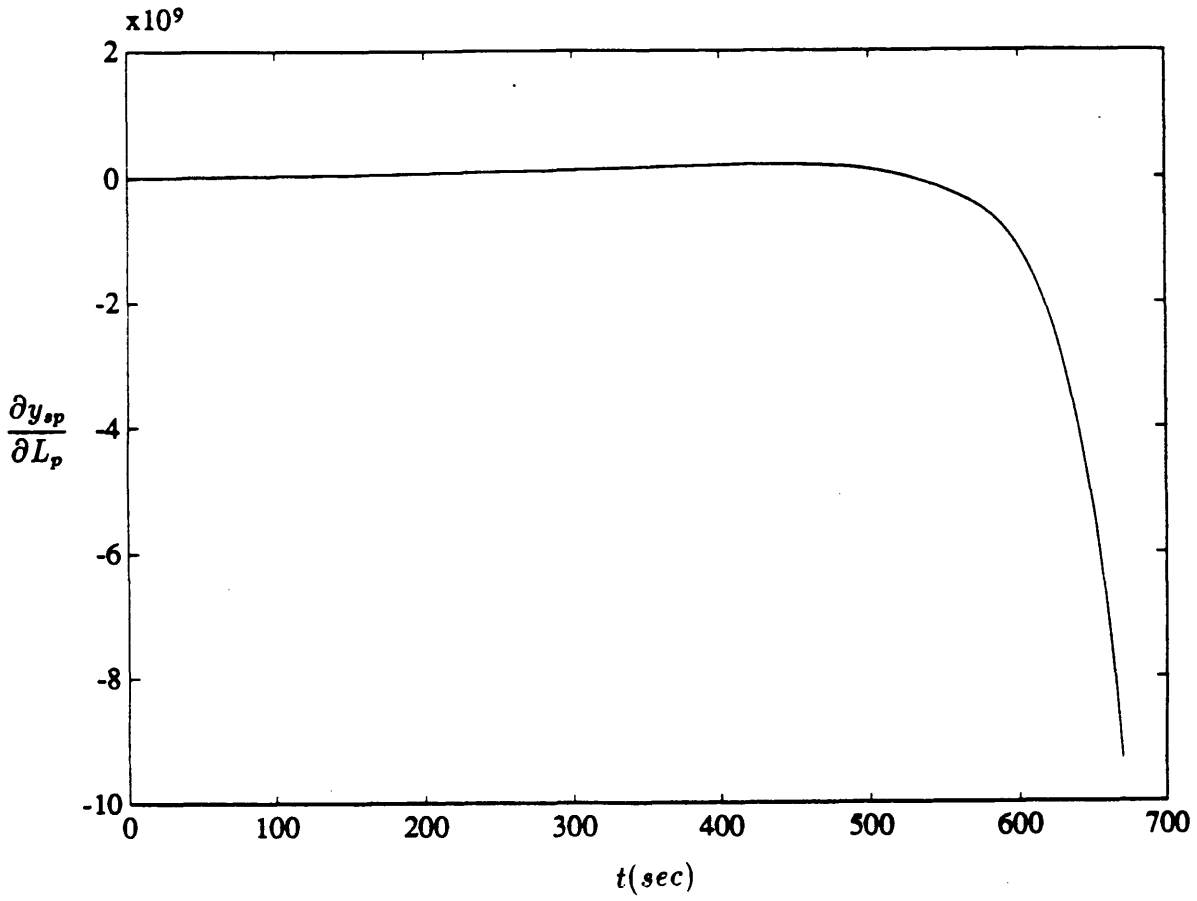

Figure 6-26: Sensitivity of Spiral Divergence Dynamics to L_p

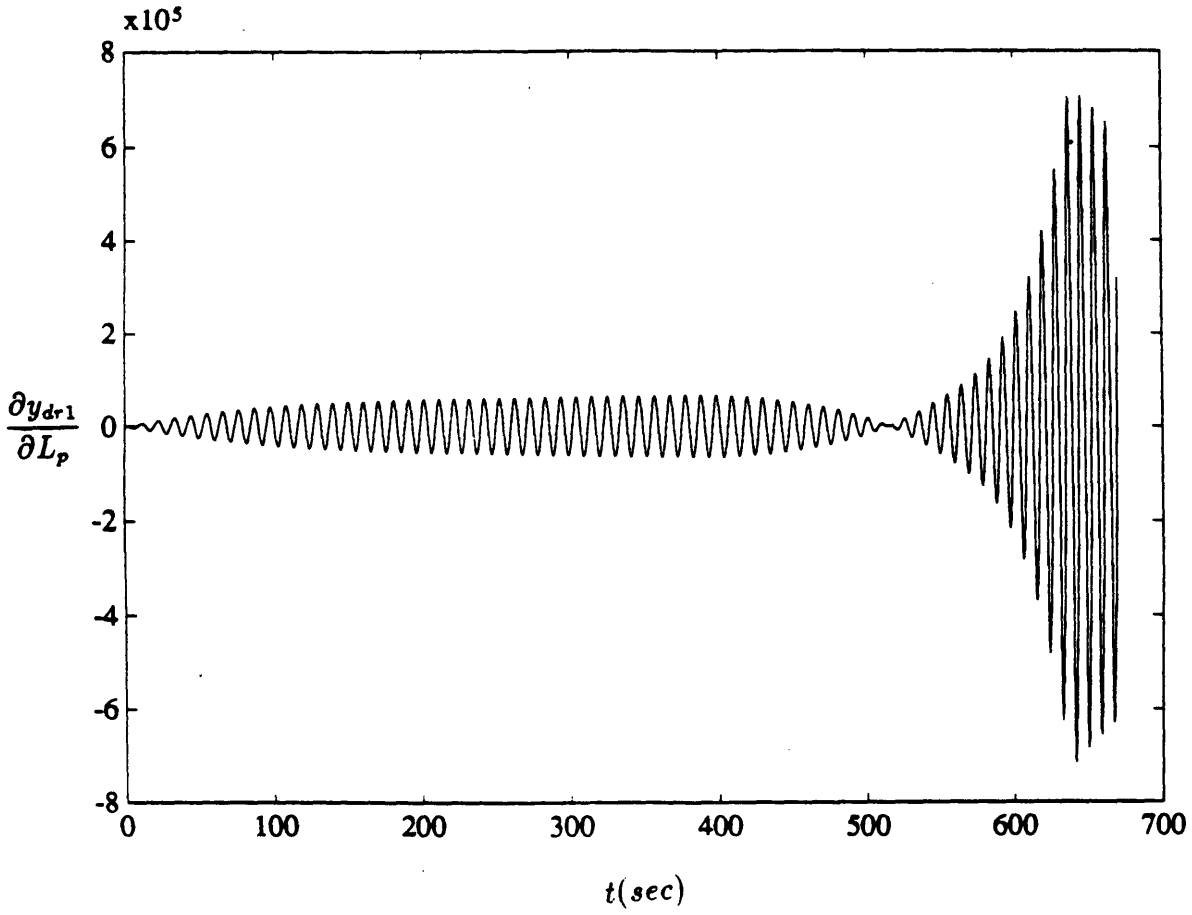

Figure 6-27: Sensitivity of Sine-like Dutch Roll Dynamics to L_p

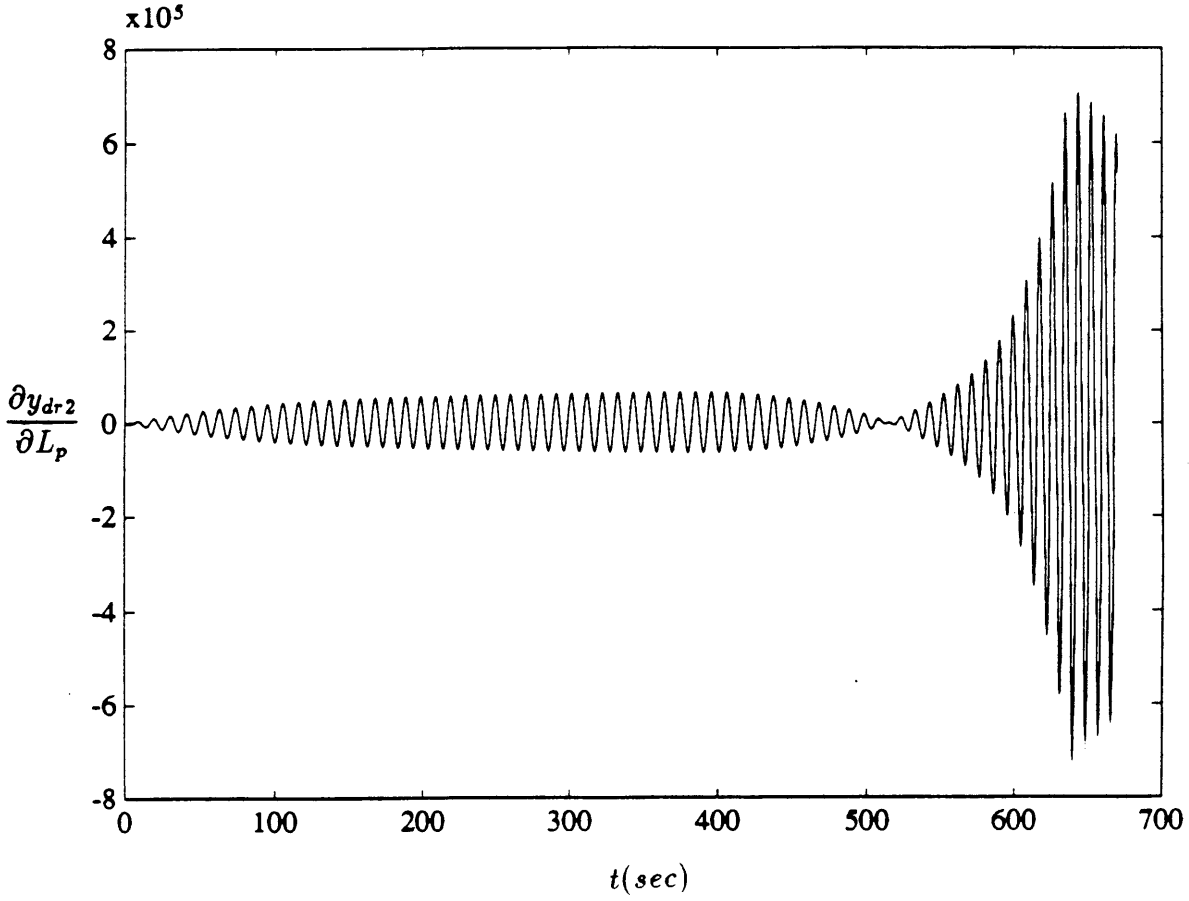

Figure 6-28: Sensitivity of Cosine-like Dutch Roll Dynamics to L_p

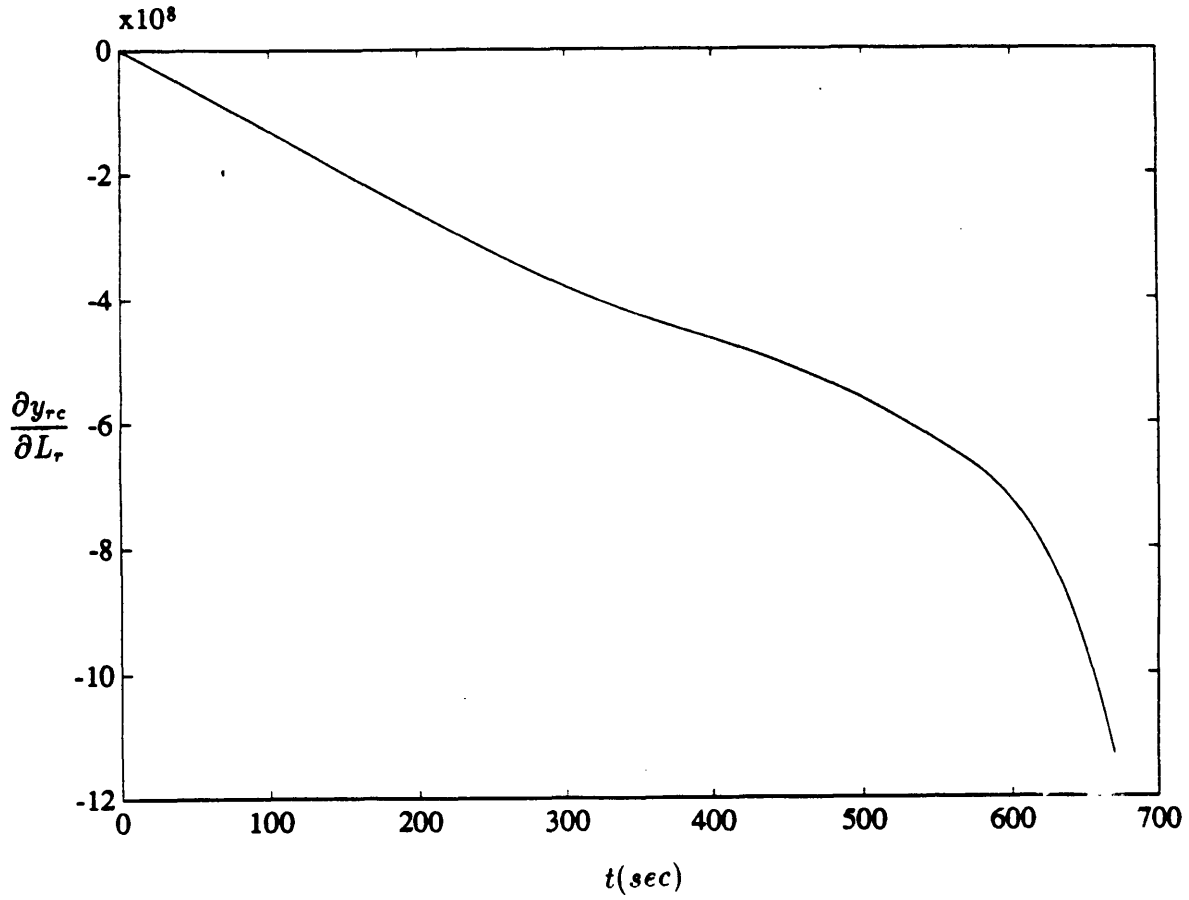

Figure 6-29: Sensitivity of Roll Convergence Dynamics to L_r

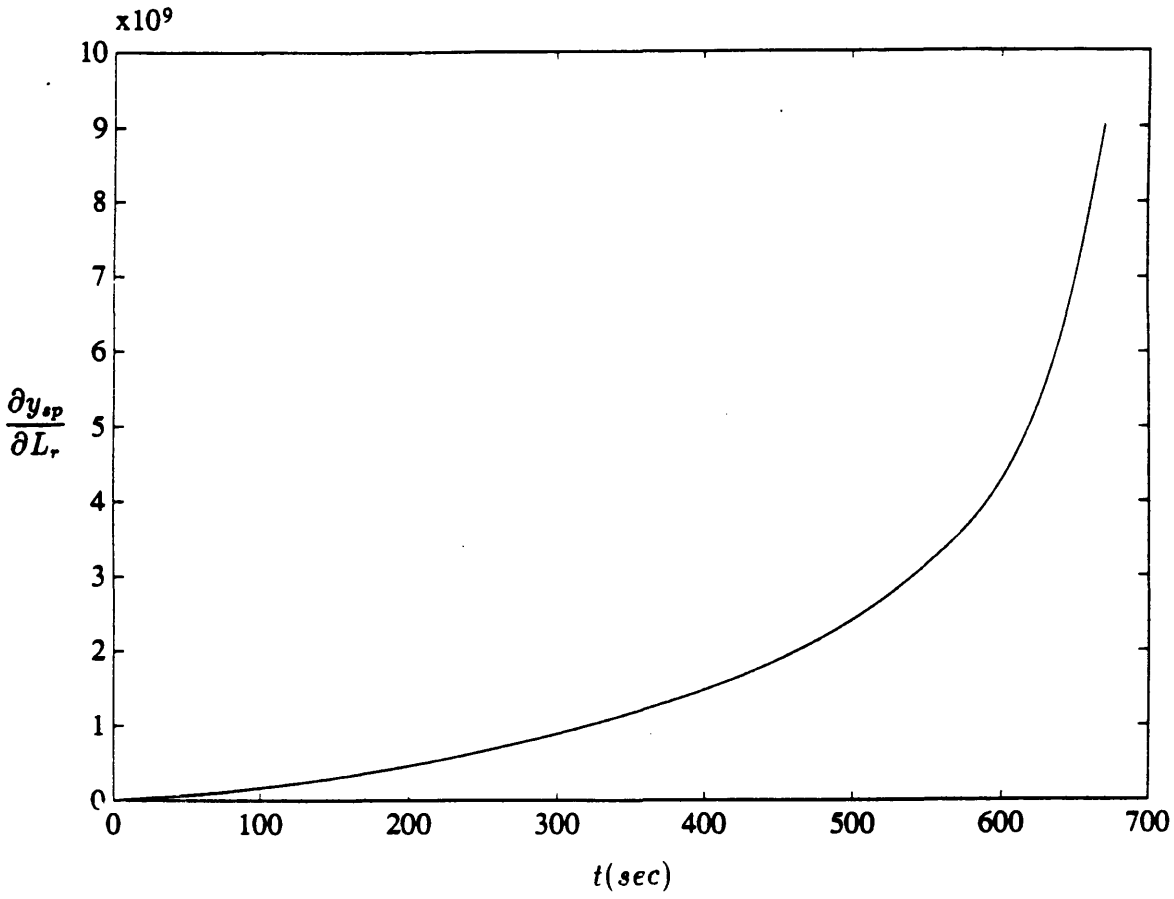

Figure 6-30: Sensitivity of Spiral Divergence Dynamics to L_r

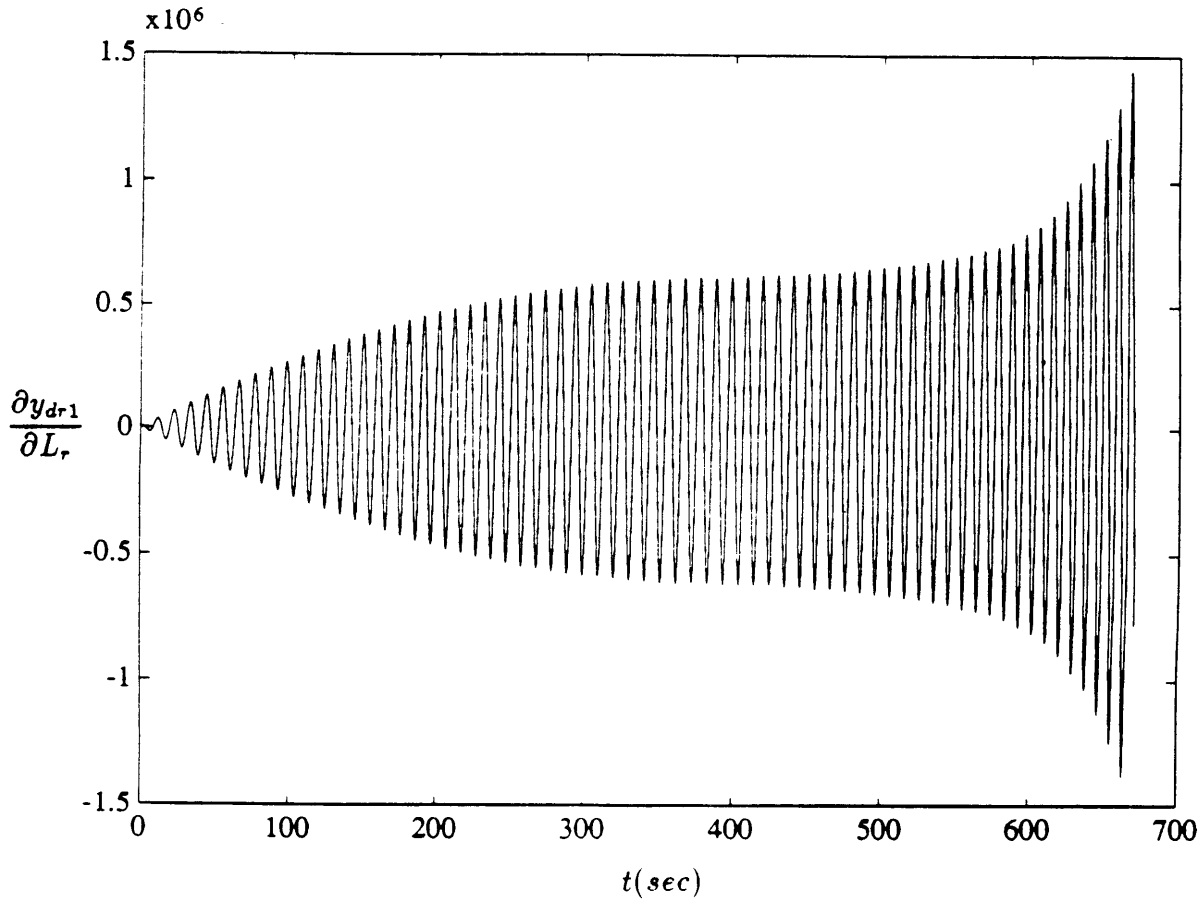

Figure 6-31: Sensitivity of Sine-like Dutch Roll Dynamics to L_r

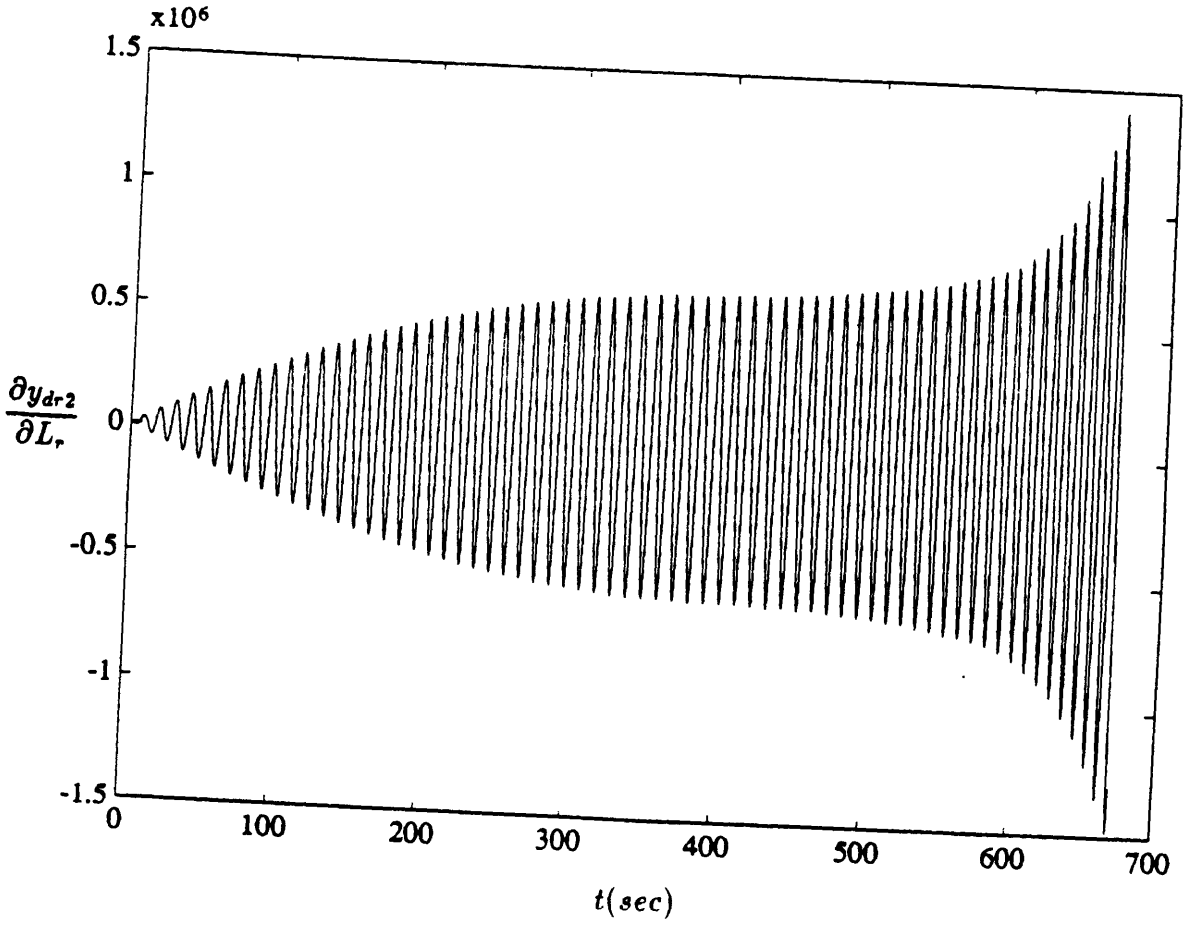

Figure 6-32: Sensitivity of Cosine-like Dutch Roll Dynamics to L_r

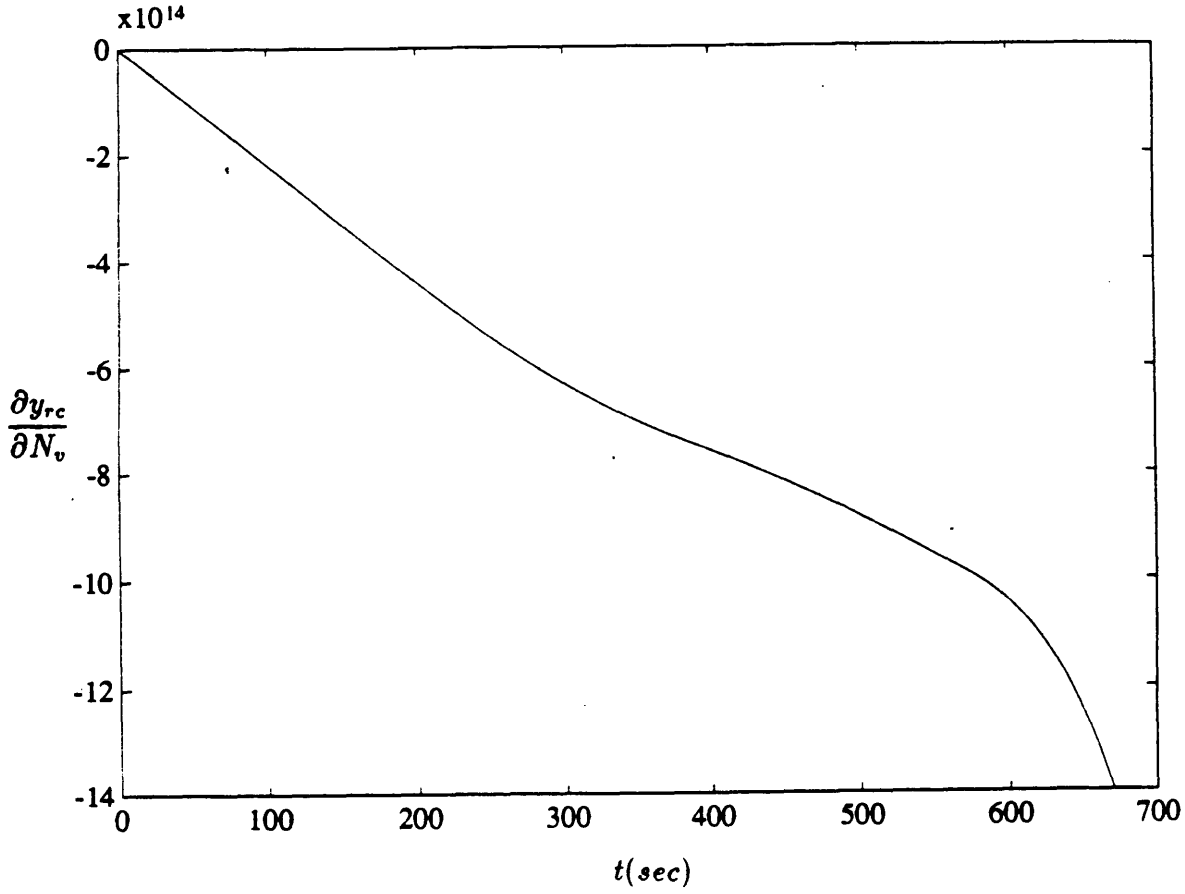

Figure 6-33: Sensitivity of Roll Convergence Dynamics to N_v

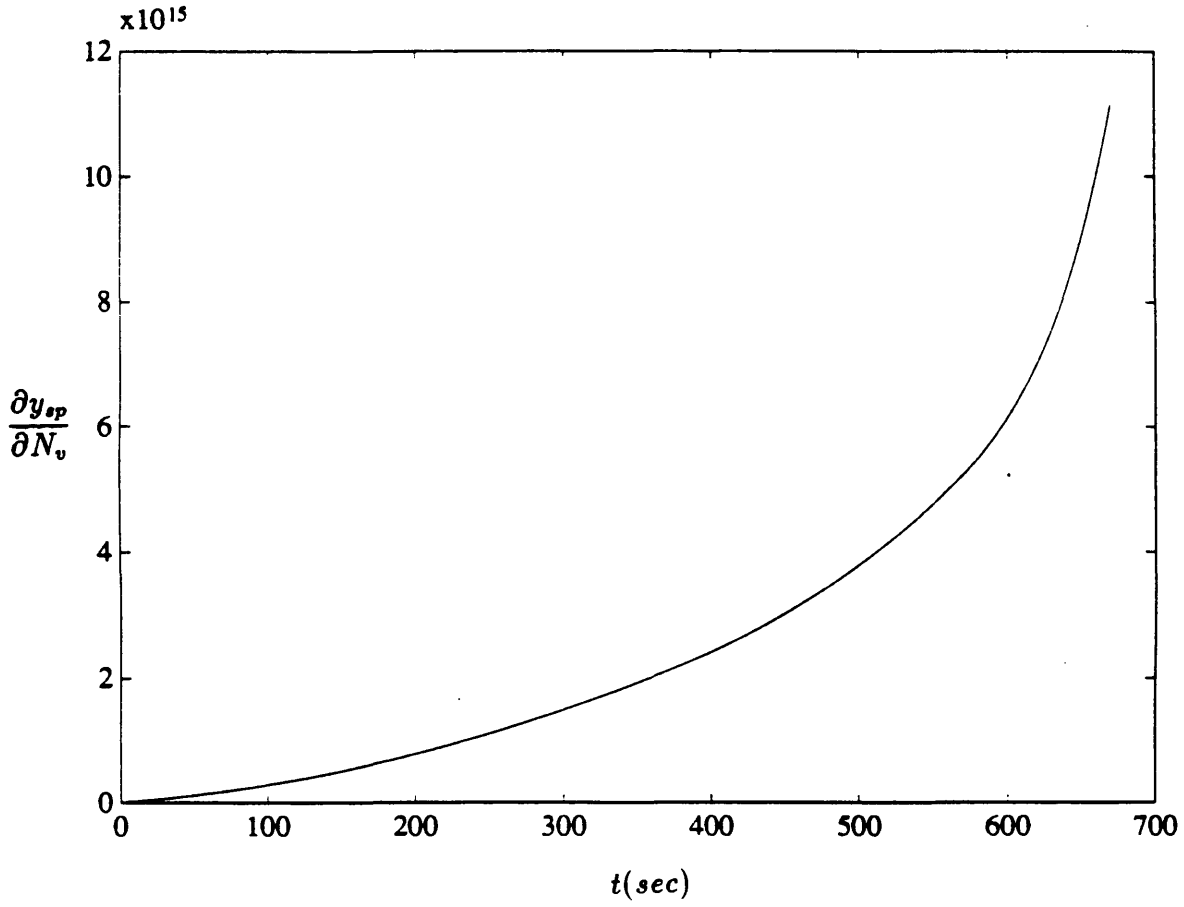

Figure 6-34: Sensitivity of Spiral Divergence Dynamics to N_v

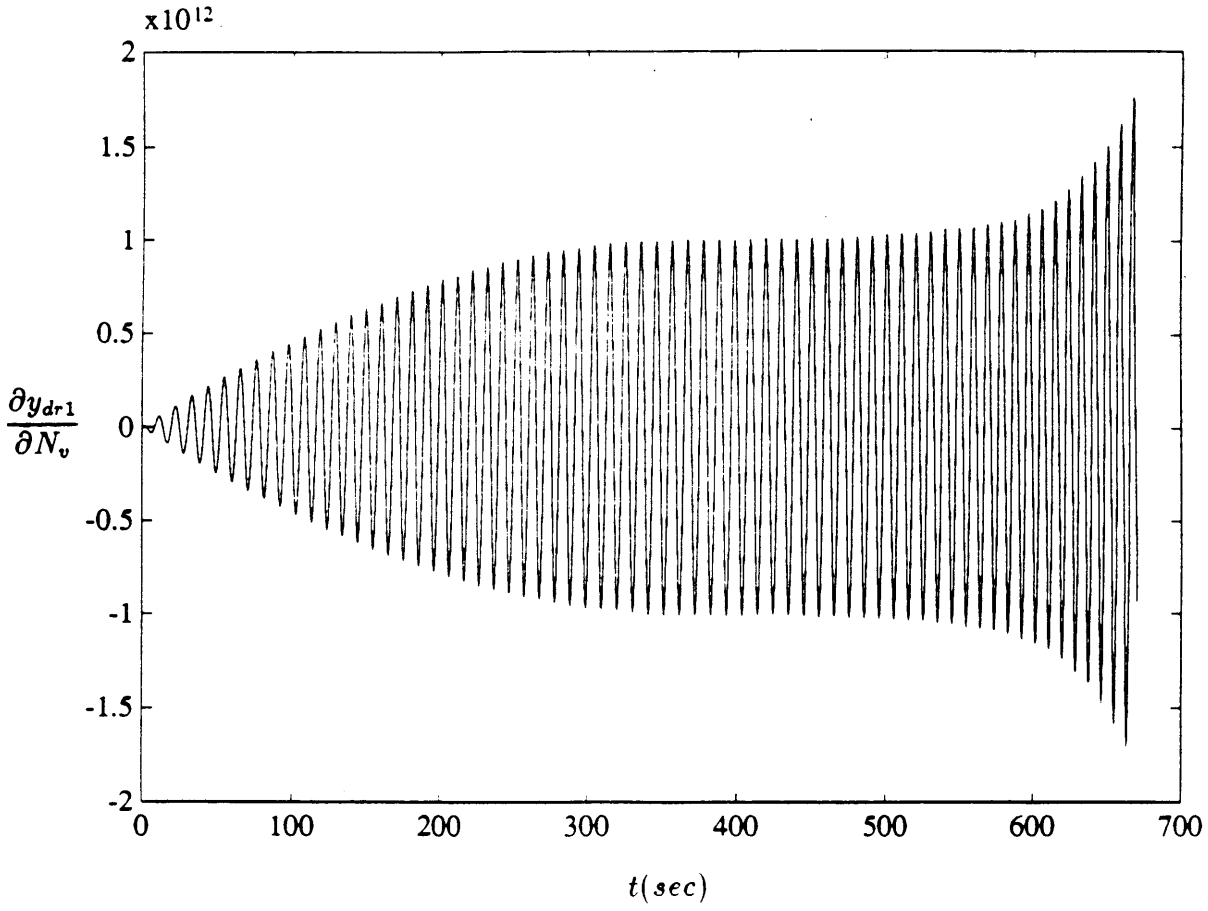

Figure 6-35: Sensitivity of Sine-like Dutch Roll Dynamics to N_v

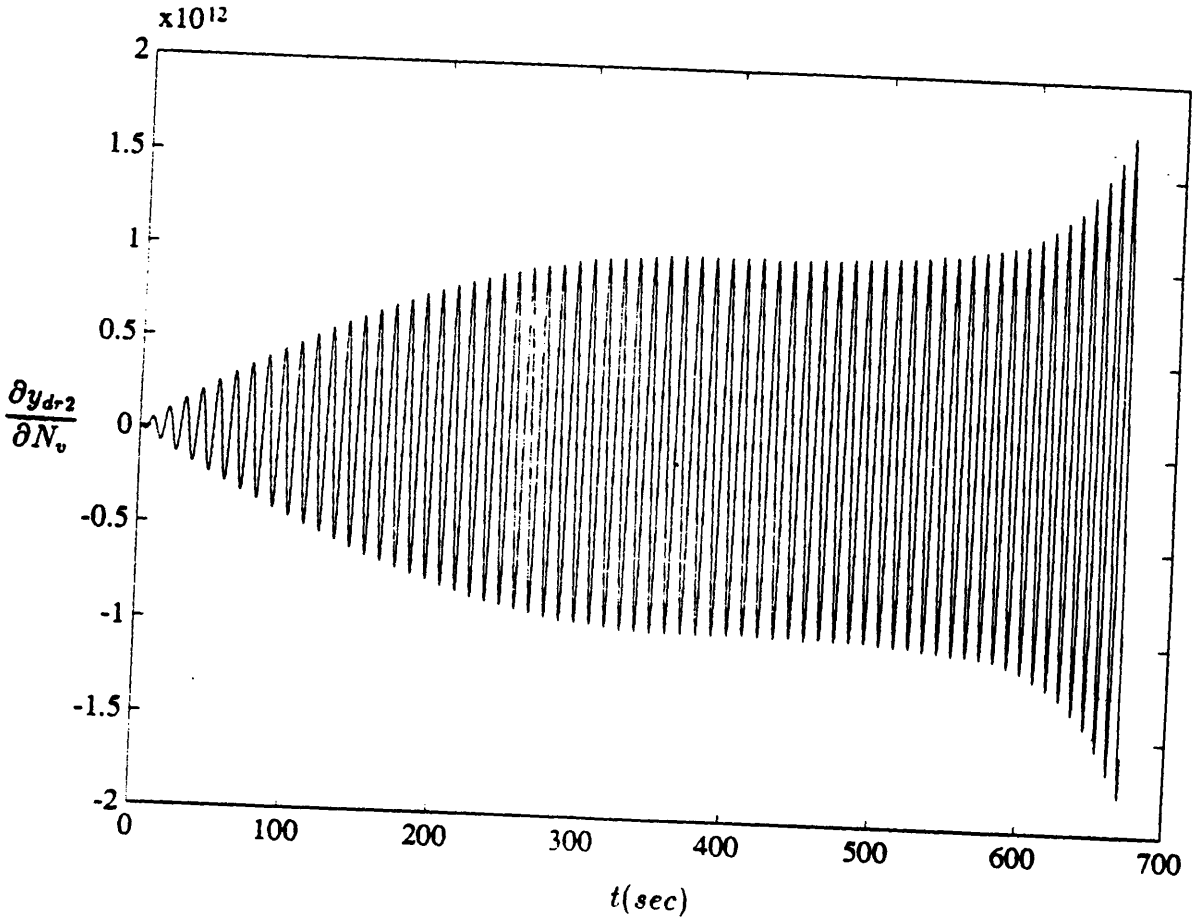

Figure 6-36: Sensitivity of Cosine-like Dutch Roll Dynamics to N_v

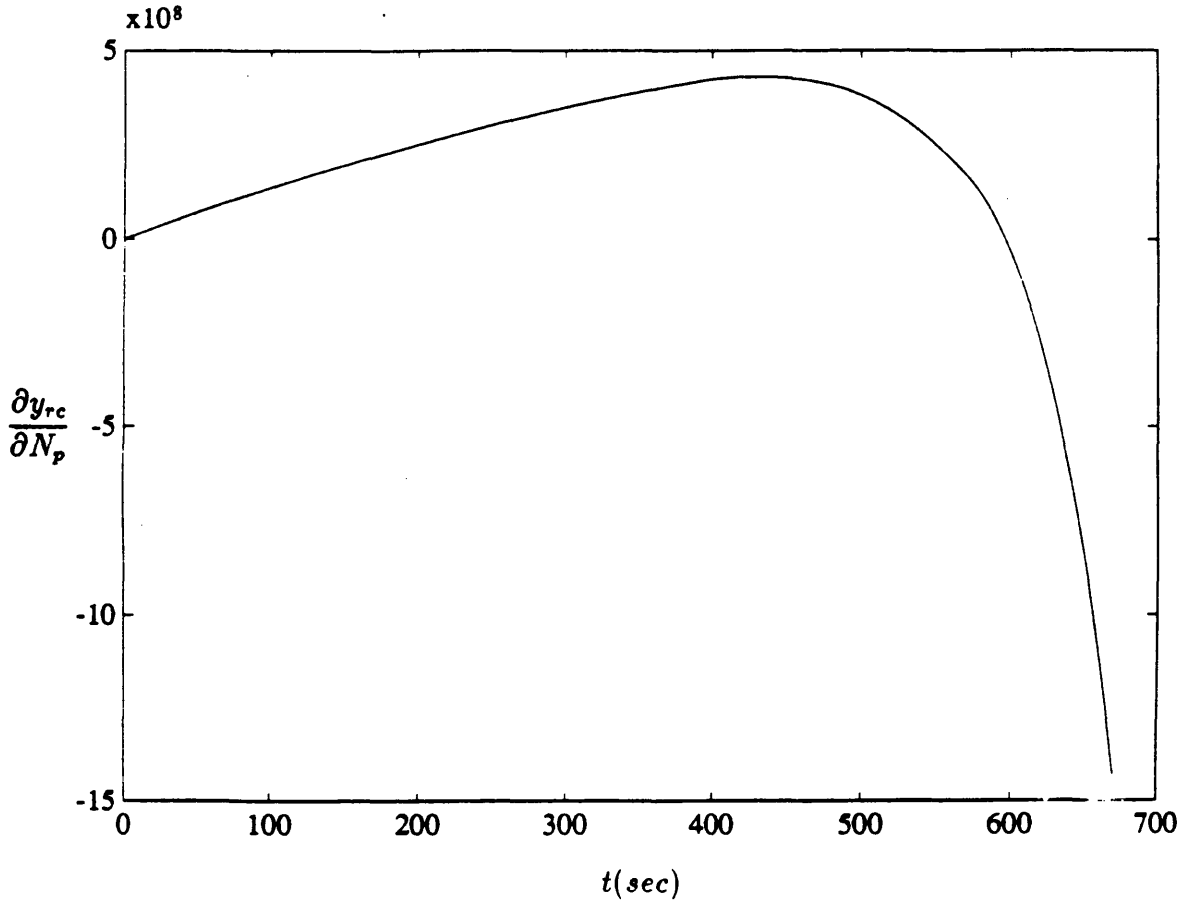

Figure 6-37: Sensitivity of Roll Convergence Dynamics to N_p

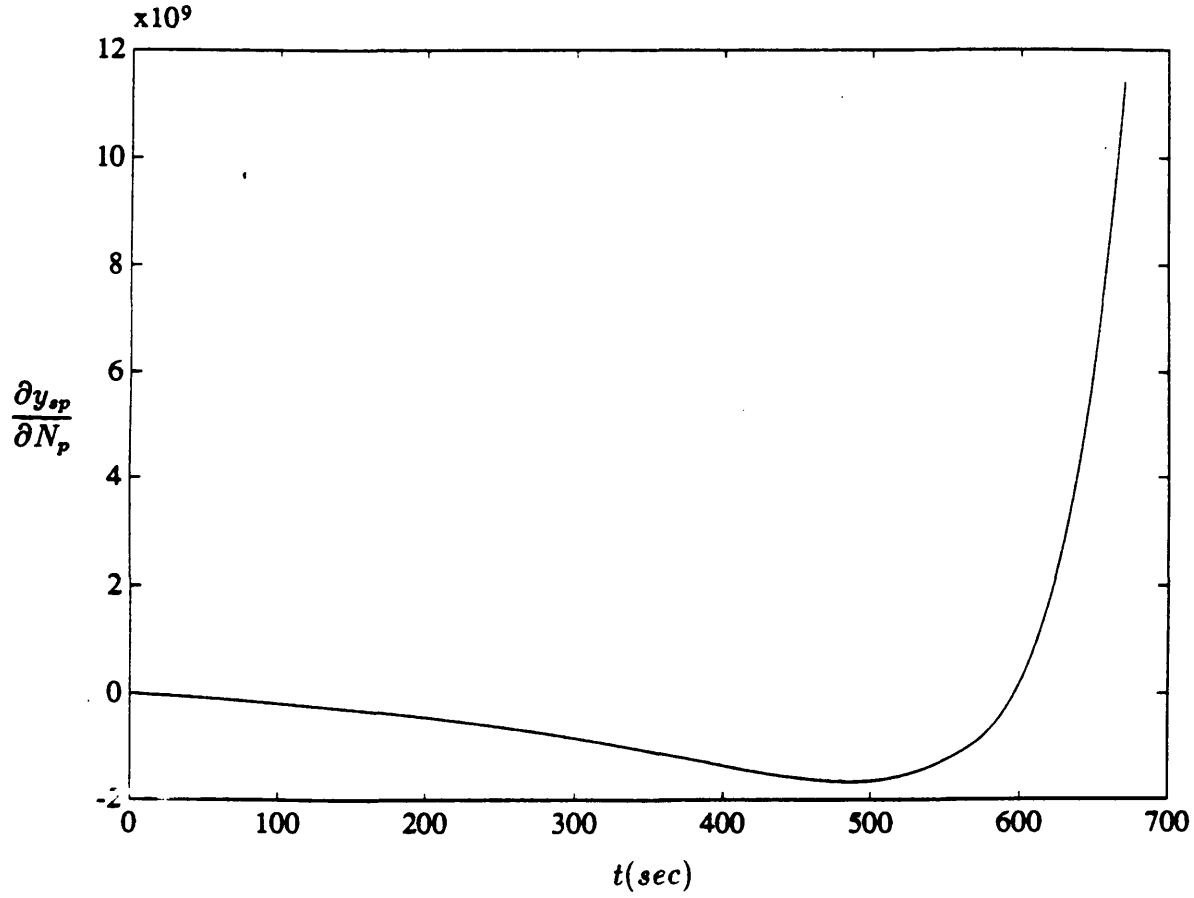

Figure 6-38: Sensitivity of Spiral Divergence Dynamics to N_p

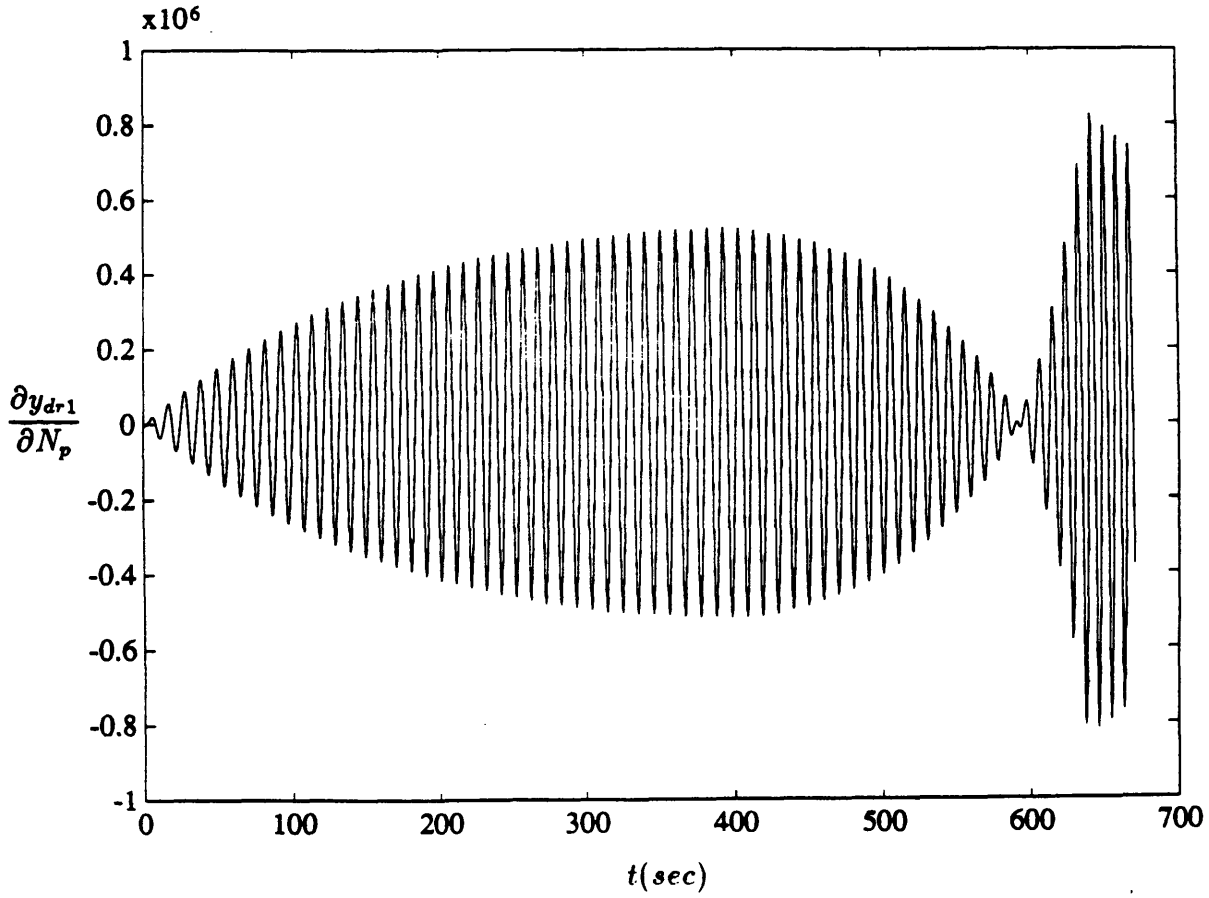

Figure 6-39: Sensitivity of Sine-like Dutch Roll Dynamics to N_p

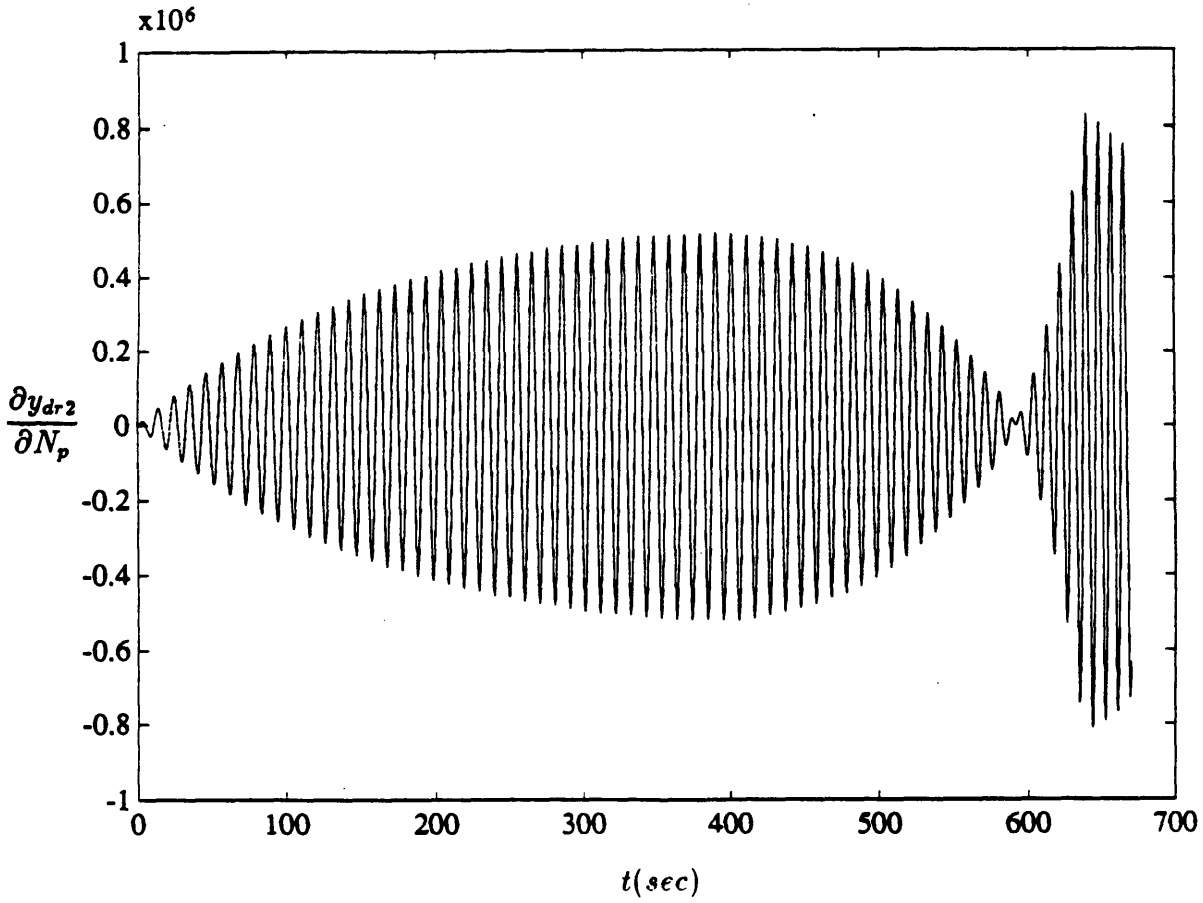

Figure 6-40: Sensitivity of Cosine-like Dutch Roll Dynamics to N_p

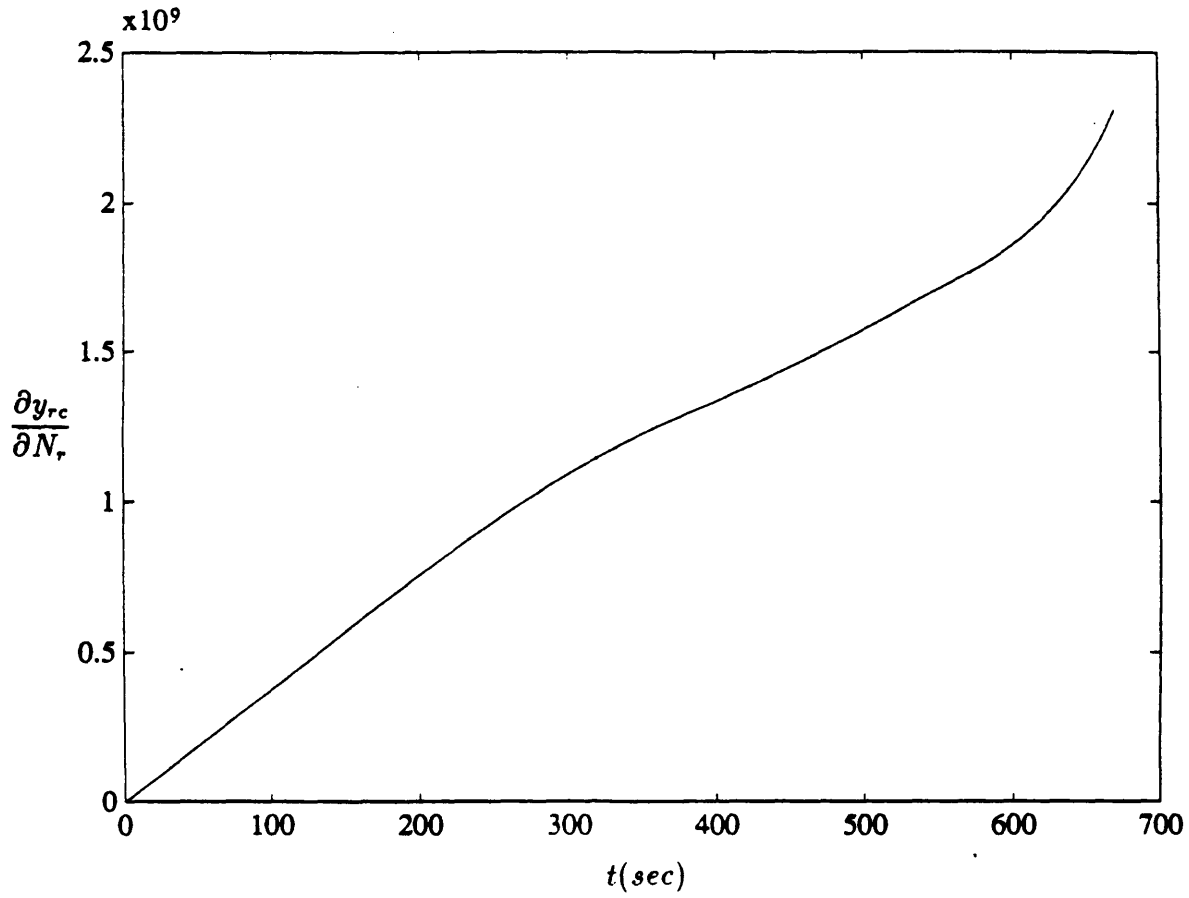

Figure 6-41: Sensitivity of Roll Convergence Dynamics to N_r

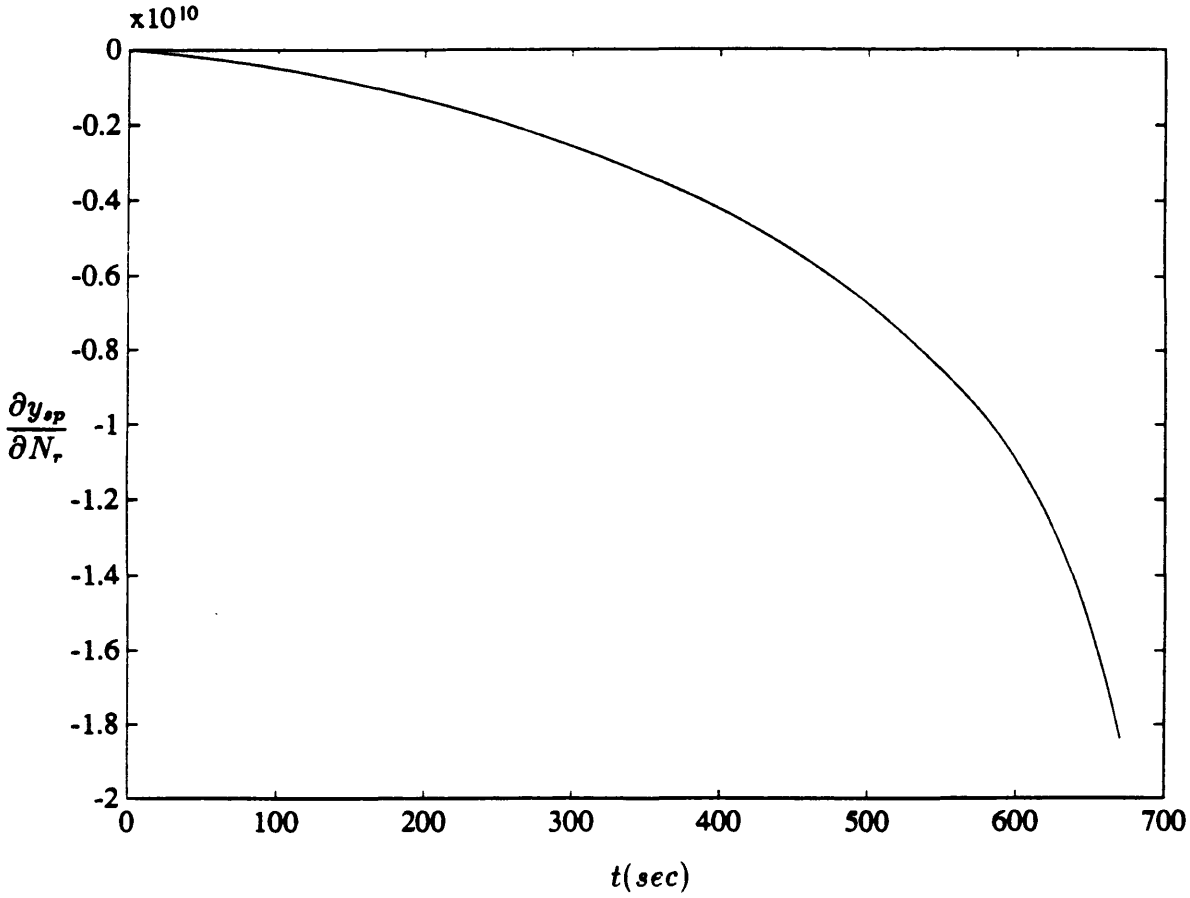

Figure 6-42: Sensitivity of Spiral Divergence Dynamics to N_r

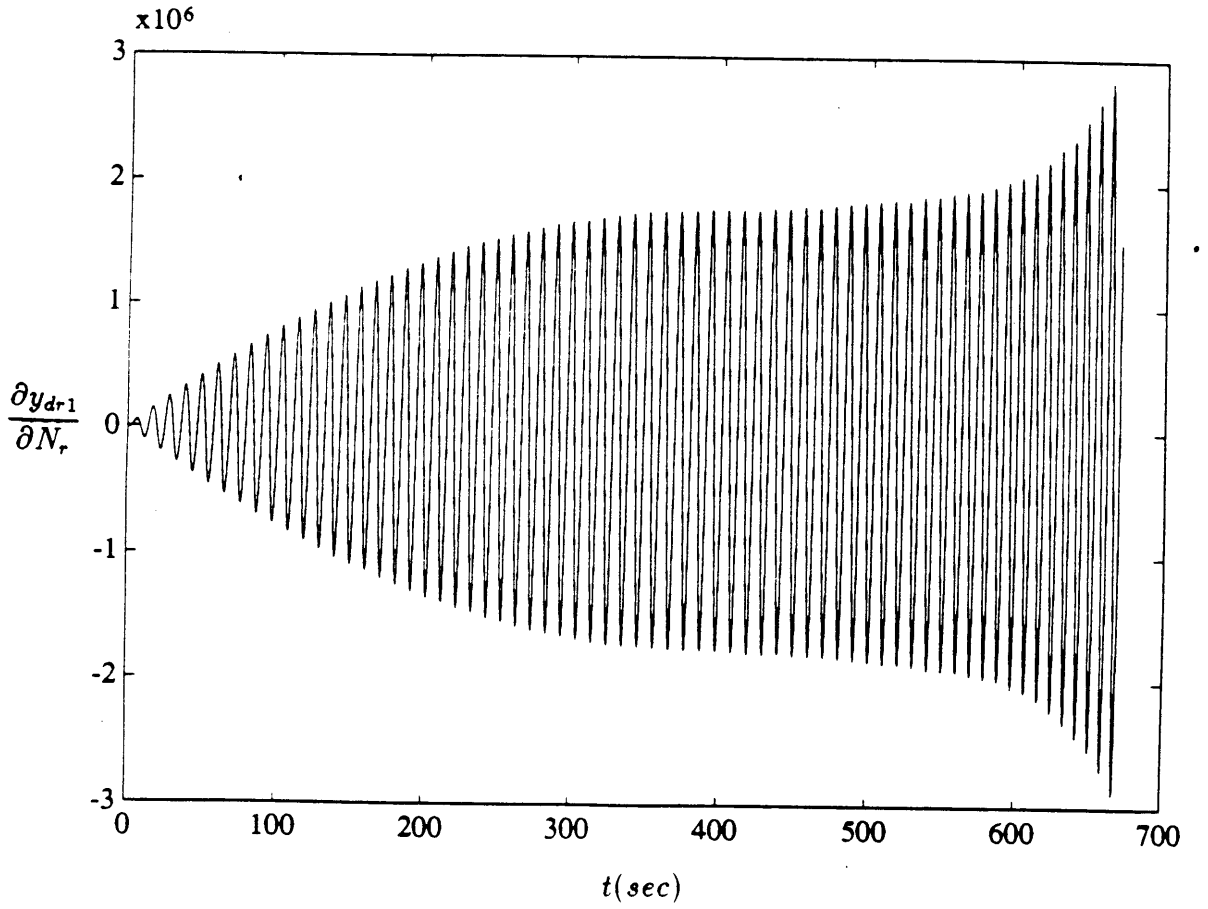

Figure 6-43: Sensitivity of Sine-like Dutch Roll Dynamics to N_r

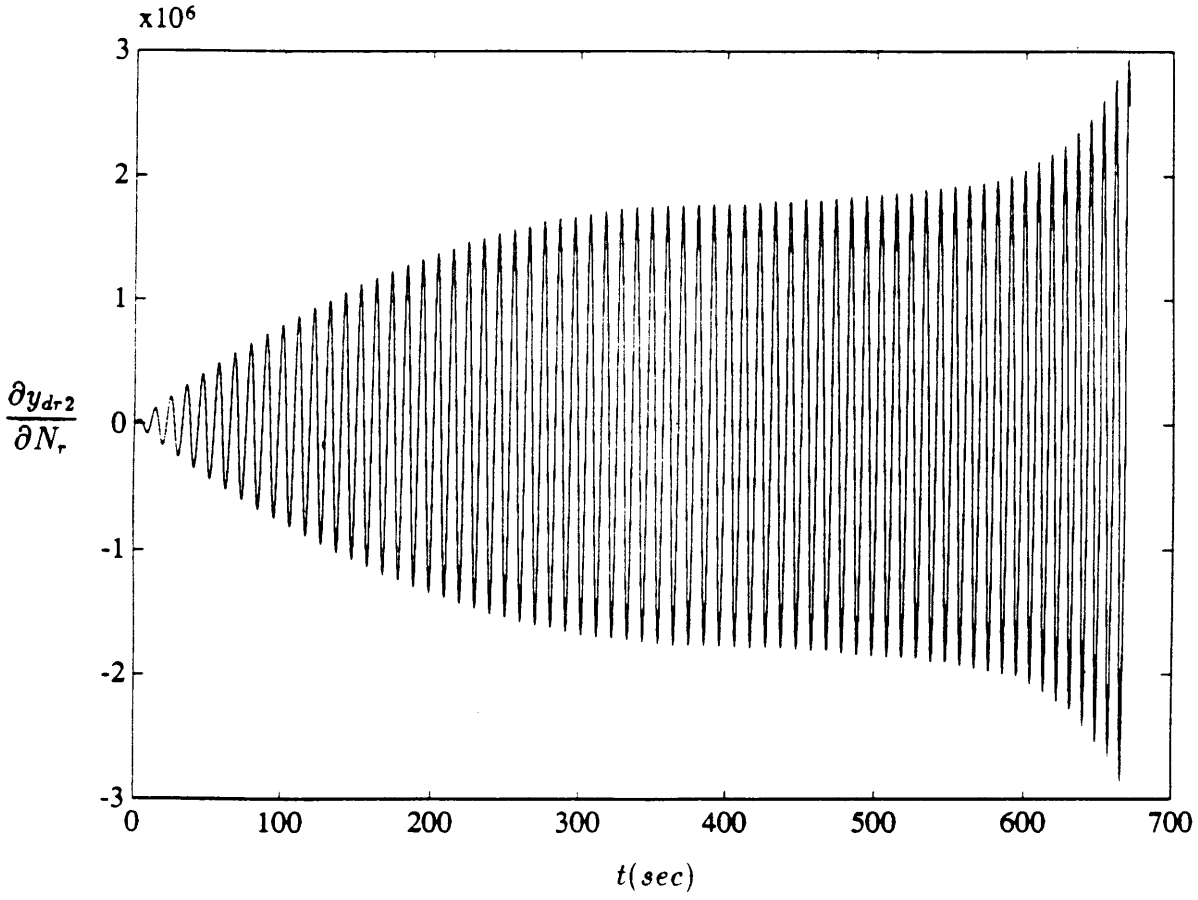

Figure 6-44: Sensitivity of Cosine-like Dutch Roll Dynamics to N_r

Chapter 7

Handling Qualities

7.1 Overview

The issue of handling qualities with regard to the GHAME vehicle is considered in this chapter. First, the handling qualities of the GHAME vehicle during reentry along the optimal Space Shuttle trajectory are determined. This is accomplished by comparing the reentry values of certain vehicle parameters with specifications designed to differentiate levels of handling qualities. The specifications are taken from a set of military standards for flying qualities of piloted vehicles. Also, GMS theory is employed to briefly consider the handling qualities of a generic second order time-varving system. By comparing the responses of systems with differing characteristic root behavior, general conclusions are drawn regarding the relationship between system root movement and handling qualities.

7.2 GHAME Vehicle Reentry Handling Qualities

The handling qualities of the GHAME vehicle during reentry along the Shuttle trajectory are studied in this section. The level of handling quality is determined by comparing GHAME vehicle reentry parameters to a set of military specifications. These specifications are taken from 'Military Specification: Flying Qualities of Piloted Airplanes'[13] which contains the handling quality requirements of all United

States military aircraft. For the purposes of this military document, the GHAME vehicle is classified as Class III aircraft which is described as a large, heavy, low-to-medium maneuverability aircraft. Also, the optimal Shuttle reentry trajectory is assumed to be of flight phase category B. This part of a mission is described as a phase normally accomplished using gradual maneuvers without precision tracking although accurate flight path control may be required.

The specifications to meet flying quality requirements are presented such that the handling qualities are separated into three levels. Level 1 represents flying qualities which are clearly adequate for accomplishing a particular flight phase. If the handling qualities allow the completion of a flight phase but only after a significant increase in pilot workload, then they are Level 2. Finally, Level 3 flying qualities represent dynamics which allow the vehicle to be controlled safely but only with excessive pilot workload. In terms of a well known subjective rating system, Level 1 corresponds to Cooper-Harper ratings of 1 through 3, while Level 2 represents Cooper-Harper ratings of 4 through 6. A Cooper-Harper rating between 6 and 9 corresponds to handling quality Level 3.[13, 14] Requirements necessary to be classified into one of these levels are made on each of the longitudinal and lateral-directional modes. As seen in Chapter 5, the behavior of the GHAME vehicle phugoid mode during reentry is quite abnormal, and it is not considered in this section. The handling quality requirements for a Class III vehicle in the Category B flight phase are shown in Tables 7.1 through 7.3.[13]

The damping ratios and the natural frequencies of the dutch roll and short period modes of the GHAME vehicle during reentry are calculated from their respective characteristic roots shown in Figs.5-8 and 6-8. Since, the roots of these modes vary along the reentry trajectory, the damping ratios and natural frequencies are functions of time. If the roots are defined as $k = k_r + ik_i$, then the damping ratio and natural frequency are given by

$$\zeta = -k_r/(k_r^2 + k_i^2)^{\frac{1}{2}} \tag{7.1}$$

$$\omega_n = (k_r^2 + k_i^2)^{\frac{1}{2}} \tag{7.2}$$

	Min. ζ	Max. ζ
Level 1	0.30	2.00
Level 2	0.20	2.00
Level 3	0.15	–

Table 7.1: Short Period Requirements for Handling Qualities

	Min. ζ	Min. $\zeta\omega_n$	Min. ω_n
Level 1	0.08	0.15	0.40
Level 2	0.02	0.10	0.40
Level 3	0	–	0.40

Table 7.2: Dutch Roll Requirements for Handling Qualities

	Roll Convergence Max. time constant	Spiral Divergence Min. time to double amplitude
Level 1	1.4 sec.	20.0 sec.
Level 2	3.0 sec.	8.0 sec.
Level 3	10.0 sec.	4.0 sec.

Table 7.3: Roll Convergence and Spiral Divergence Requirements for Handling Qualities

The natural frequency of the short period mode is plotted against its damping ratio in Fig.7-1. Likewise, Fig.7-2 shows the dutch roll natural frequency plotted against its damping ratio. It is interesting to note that except scaling,the behavior seen in these two plots is quite similar. This is to be expected since the behavior of the roots seen in Figs.5-8 and 6-8 also exhibit similar behaviors.

The information shown in Figs.7-1 and 7-2 is compared to the handling quality requirements of Tables 7-1 through 7-3 to determine whether the short period and dutch roll modes of the GHAME vehicle insure adequate handling qualities during reentry. Upon analysis, it is clear that the short period behavior is quite inadequate in terms of handling qualities. It is not until the vehicle is at the end of the trajectory that the short period damping ratio satisfies minimum Level 3 requirements. The dutch roll reentry behavior also has poor implications on the handling qualities of the GHAME vehicle. Fig.7-2 shows although dutch roll natural frequency by itself satisfies Level 1 requirements, ζ and $\zeta\omega_n$ only satisfy Level 3 specifications. Therefore, dutch roll behavior induces a handling quality rating of Level 3 during reentry. It is obvious that neither of the GHAME vehicle's two oscillatory modes induce adequate handling qualities in the aircraft during reentry. At Level 3, the dutch roll behavior allows the vehicle to be controlled safely, but only after excessive workload on the pilot. The short period reentry behavior does not even qualify for Level 3 status and renders the GHAME vehicle uncontrollable during reentry along the Shuttle trajectory.

The handling quality specifications for the roll convergence and spiral divergence modes are expressed in terms of time parameters concerning the amplitude of their respective responses. The roll convergence requirement is placed on the time constant which is defined as the time required for the amplitude of a response to decay to $exp(-1)$ times its original value. From the characteristic response shown in Fig.6-11, the time constant of the GHAME vehicle's roll convergence mode is approximately 750 seconds. This does not even satisfy the handling qualities requirements for Level 3. The roll convergence behavior of the GHAME vehicle also renders it uncontrollable during reentry. The spiral divergence mode, however, does exhibit favorable behavior

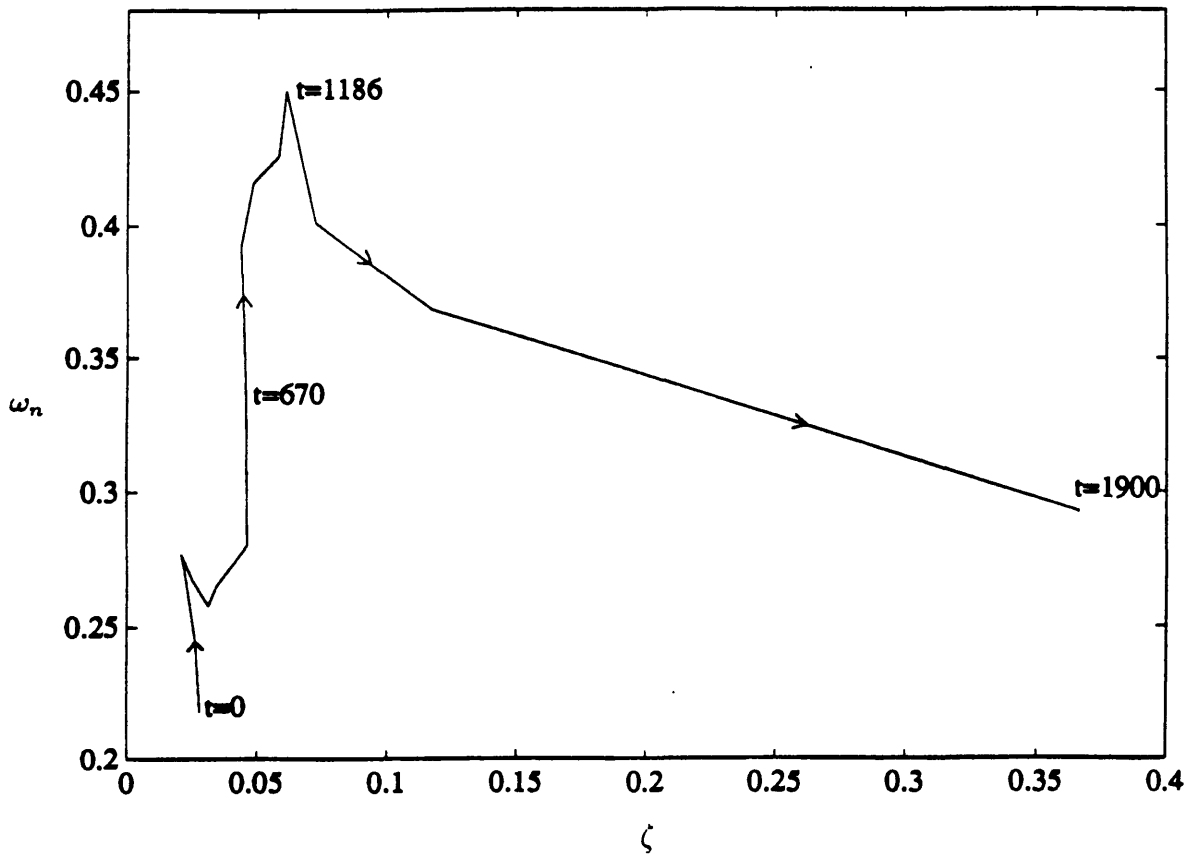

Figure 7-1: Short Period Natural Frequency vs. Damping Ratio Along Trajectory

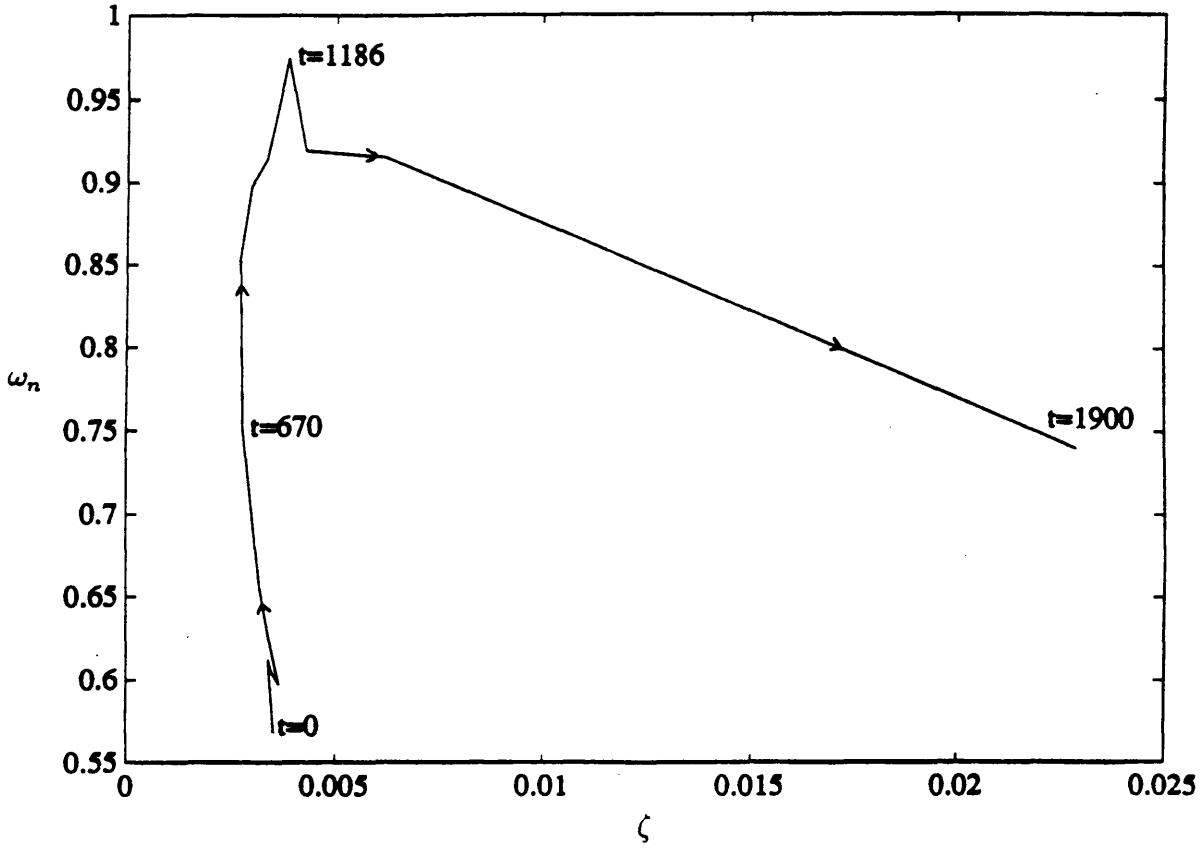

Figure 7-2: Dutch Roll Natural Frequency vs. Damping Ratio Along Trajectory

with regard to handling qualities. Fig.6-12 shows that the time for the spiral divergence characteristic response to double its amplitude is approximately 300 seconds. This clearly satisfies the Level 1 handling qualities requirement detailed in Table 7-3. Although the spiral divergence behavior is favorable to handling qualities, the other three modes only represent handling quality ratings of Level 3 or poorer. The GHAME vehicle is clearly uncontrollable during reentry along the Shuttle trajectory.

7.3 Handling Qualities of a Generic Second Order System

In this section, the handling qualities and of a generic time-varying second order system is studied in order to determine the general effects of varying characteristic root behaviors. The responses of the systems are approximated using the second order GMS solutions developed in section 3.2. A generic time-varying second order system can be expressed by the equation

$$\ddot{y} + \omega_1(t)\dot{y} + \omega_0(t)y = 0 \tag{7.3}$$

The response of this system is then governed by the roots of the algebraic equation

$$s^2 + \omega_1 s + \omega_0 = 0 \tag{7.4}$$

If the system is autonomous, then the two coefficient of Eq.7.3 are constant and the response is described by a pair of roots which remain fixed with time. However, if the coefficients ω_1 and ω_0 vary with time, than the characteristic roots do not remain stationary. The path and speed of the characteristic roots in the complex plane are determined by the nature of the two coefficients. The effects of simple variations in the path and speed of the roots on the response and handling qualities is examined in this section. In order to accomplish this, systems having the same characteristic roots at the initial and final time are considered. The path and speed at which the

roots get from the initial point to the final point are varied and the their responses are compared.

In order to gain insight with regards to handling qualities, the initial and final points of the characteristic roots for the systems to be considered are chosen such that they represent two different levels of handling quality ratings. If the characteristic roots are a pair of complex conjugates in the form $k = k_r \pm k_i$, then they are set such that

$$k_r(0) = -.054 \qquad k_i(0) = .8984 \tag{7.5}$$

$$k_r(T) = -.225 \qquad k_i(T) = 1.483 \tag{7.6}$$

where T is the total time the roots of the system take to travel from the initial point to their final position. It follows from Eq.7.1 and 7.2 that

$$\omega_n(0) = .9\ rads/sec \qquad \zeta(0) = .06 \tag{7.7}$$

$$\omega_n(T) = 1.5\ rads/sec \qquad \zeta(T) = .15 \tag{7.8}$$

If it is assumed that the generic second order system represents a dutch roll mode, then upon comparing the above natural frequency and damping ratio values to Table 7-2, the initial point is of Level 2 handling qualities. Similarly, the system exhibits Level 1 handling qualities at the final time. The roots are now allowed to move from the Level 2 point to the Level 1 point in varying ways. The responses of these differing root behaviors are compared to each other as well as to those of two constant systems where the roots remain fixed at the Level 1 and Level 2 points.

Initially, only systems with roots moving from the Level 2 point to the Level 1 point in a straight line with constant speed are considered. The straight line root trajectory of these systems is shown in Fig.7-3. The total time allowed for the roots to travel from initial to final point is varied in order to determine how the speed of root movement affects the response. The specifications of the systems considered as well as the two constant systems are shown in Table 7.4. The solutions to the systems in Table 7.4 are approximated using second order GMS theory and are plotted in

	Root Trajectory	Initial Root Position	Final Root Position	Total Trajectory Time, T	Root Speed
Case 1	–	Level 1	Level 1	–	–
Case 2	–	Level 2	Level 2	–	–
Case 3	Straight Line	Level 2	Level 1	800 sec.	Const.
Case 4	Straight Line	Level 2	Level 1	250 sec.	Const.
Case 5	Straight Line	Level 2	Level 1	125 sec.	Const.
Case 6	Straight Line	Level 2	Level 1	50 sec.	Const.
Case 7	Straight Line	Level 2	Level 1	25 sec.	Const.
Case 8	Straight Line	Level 2	Level 1	5 sec.	Const.
Case 9	Straight Line	Level 2	Level 1	1 sec.	Const.

Table 7.4: Straight Root Trajectory Systems

Figs.7-4 through 7-6. It is evident from Fig.7-4 that as the root speed between initial and final points increases, the frequency and the settling time of the response both decrease. As the speed of the roots is increased further, Fig. 7-5 shows that the responses of the systems approach the solution to the constant system with roots fixed at the Level 1 point. Conversely, as the speed of the roots is decreased greatly, the responses of the systems approach the Level 2 constant system as seen in Fig.7-6. In general, as the speed of the roots increases from slow to fast, the behavior of the response changes from exhibiting similar behavior to the solution of the system with fixed roots at the initial point to the solution of the system with roots constant at the final point. This implies that if a second order time-varying system possesses characteristic roots which travel in a straight line at constant speed, then the handling qualities of the system fall in between the behavior of the systems with fixed roots at the initial and final positions. No matter how fast or slow the roots travel between the two points shown in Fig.7-3, the resulting behavior never exceeds the handling quality ratings of Case 1 and 2.

Three different systems are now considered whose characteristic roots do not necessarily travel between the initial and final points in a straight line or with constant speed. The specifications of these three systems are shown in Table 7.5. The acceleration of the roots along the straight line trajectory of Case 10 is detailed in Fig.7-7.

	Root Trajectory	Initial Root Position	Final Root Position	Total Trajectory Time, T	Root Speed
Case 10	Straight Line	Level 2	Level 1	50 sec.	Accel.
Case 11	See Fig.7-8	Level 2	Level 1	50 sec.	Const.
Case 12	See Fig.7-8	Level 2	Level 1	50 sec.	Const.

Table 7.5: Miscellaneous Systems

The response of this accelerating system is compared to the Case 5 response in Fig.7-8 because they initially share the same root velocity. The non-straight line trajectories of Case 11 and 12 are shown in Figs. 7-9. These two curved trajectory systems are compared to the Case 6 system due to the fact that they possess equal trajectory times. Their responses are shown in Fig.7-10.

Fig.7-8 shows that the response of the Case 10 system initially mirrors the response of Case 5, but later exhibits greater frequency and damping. Upon examination of the second order GMS approximations detailed in Chapter 2, this behavior becomes clear. Initially, the roots of both systems travel with the same velocity along the same path, and therefore, they experience the same response. Later, when the roots of the Case 10 system have accelerated to greater speed, they experience smaller values of k_r and greater values of k_i than those of the Case 5 system. Hence, the response exhibits higher frequency and greater damping. It is evident that even if the roots are allowed to accelerate or decelerate along the straight line trajectory, the responses of such systems still falls in between the behavior exhibited by the Case 1 and 2 constant systems.

The responses of the two systems with the curved root trajectories shown in Fig.7-9 also behave as would be expected from the nature of the GMS approximations. Although they possess equal trajectory time, Fig.7-9 shows that the characteristic roots of the Case 11 system experience greater values of k_i and smaller values of k_r than those of the Case 6 system. Hence, the Case 11 response exhibits higher frequency, but less damping than the Case 6 response. Similar arguments can be employed to explain the response of the Case 12 system which exhibits smaller frequency and

greater damping than the Case 6 response. It is concluded upon examination of the GMS equations that no matter what the speed of the characteristic roots, as long as their path does not stray beyond the rectangular boundaries defined by their initial and final points, the resulting handling qualities behavior falls in between those of the constant systems with roots fixed at initial and final points.

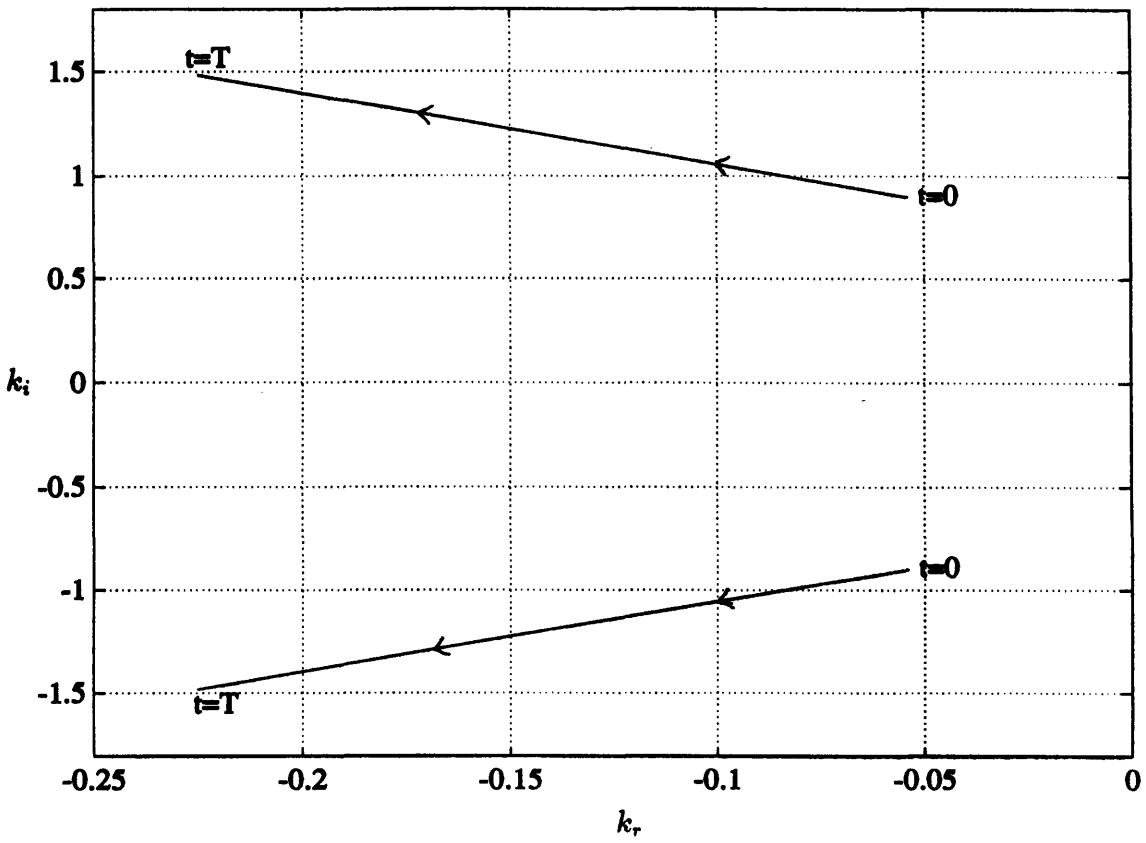

Figure 7-3: Straight Line Root Trajectory

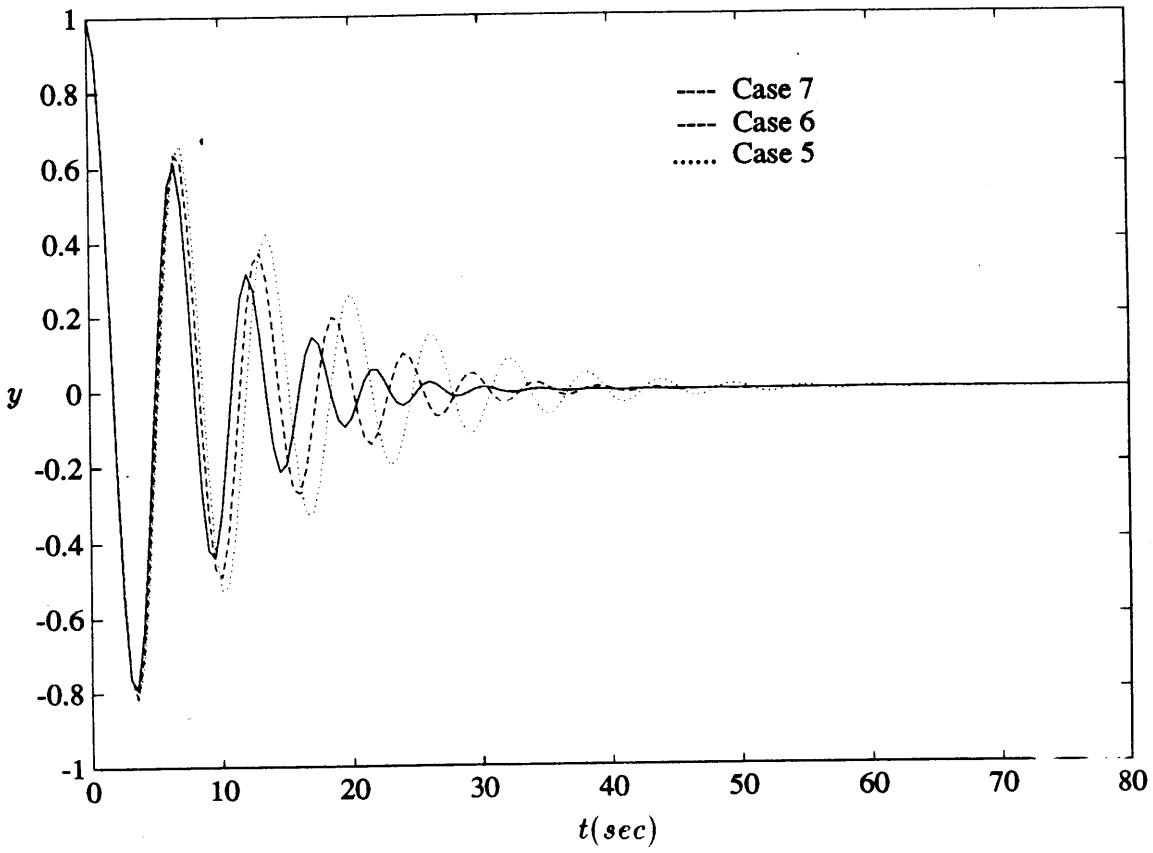

Figure 7-4: GMS Solutions to Cases 5,6,7

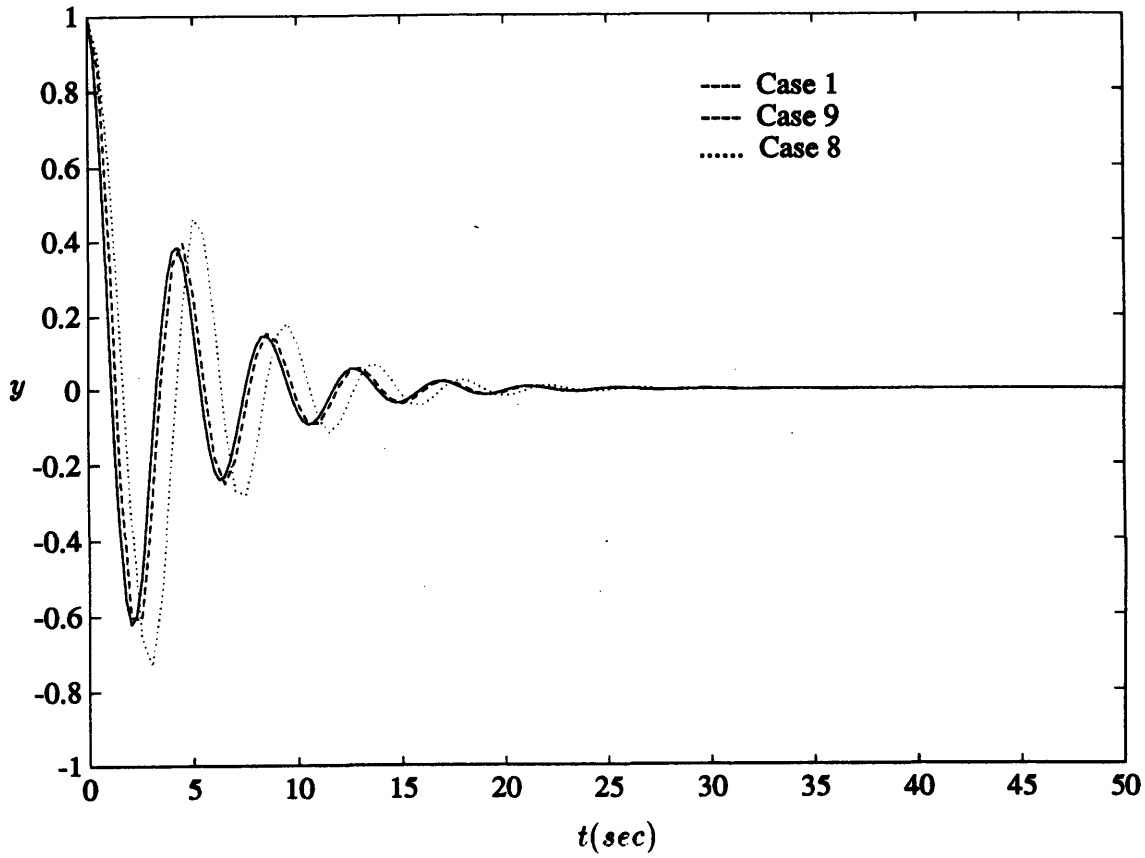

Figure 7-5: GMS Solutions to Cases 1,8,9

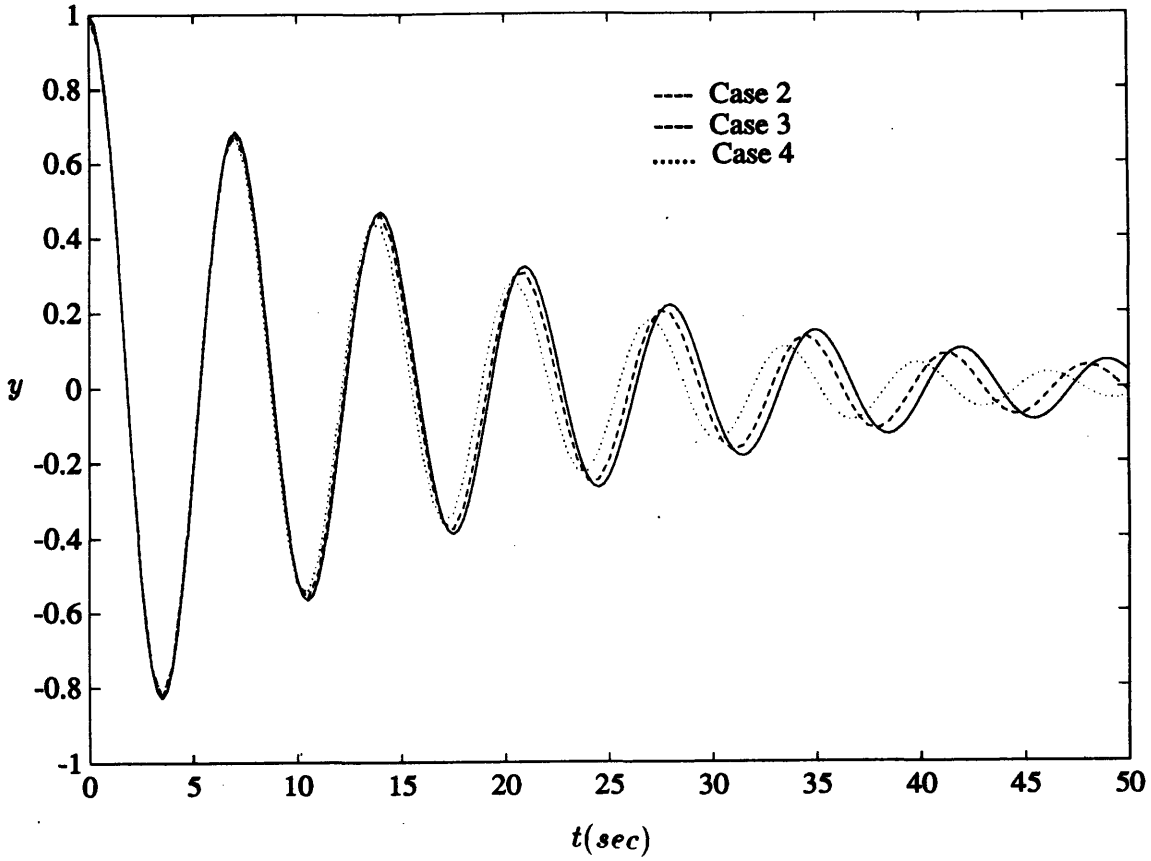

Figure 7-6: GMS Solutions to Cases 2,3,4

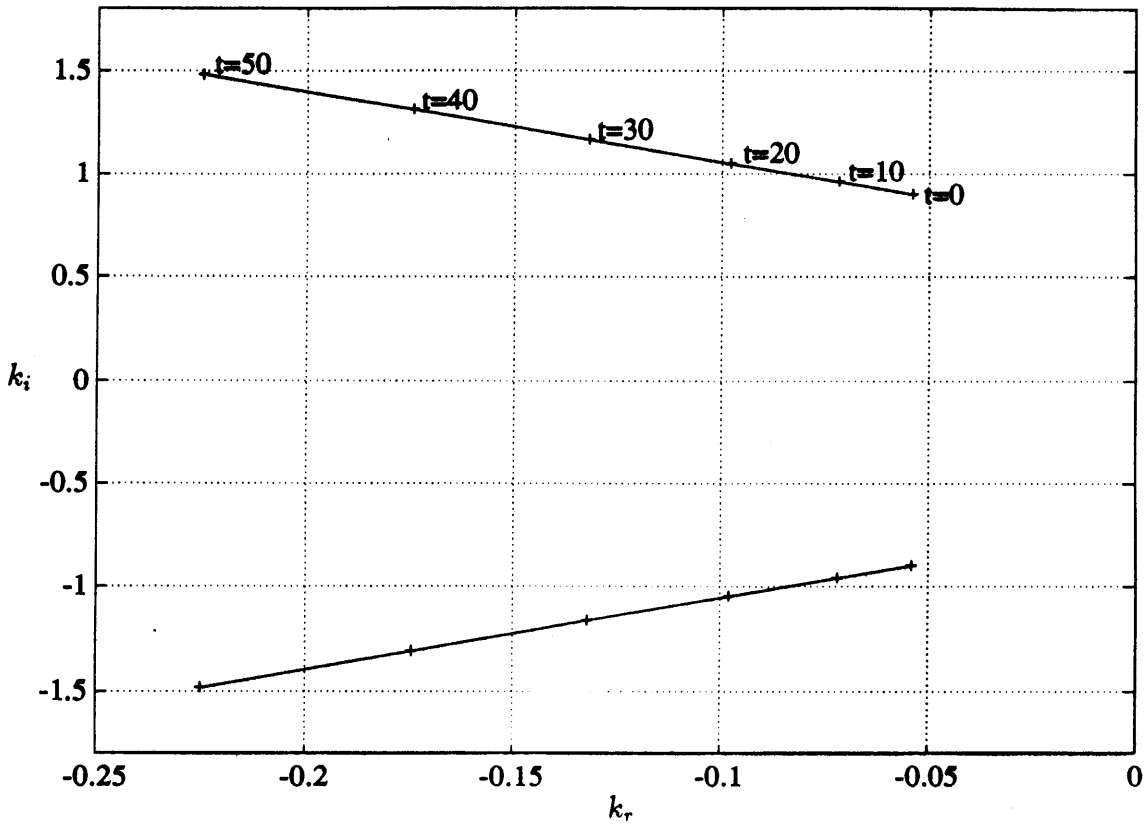

Figure 7-7: Straight Line Root Trajectory of Accelerating System

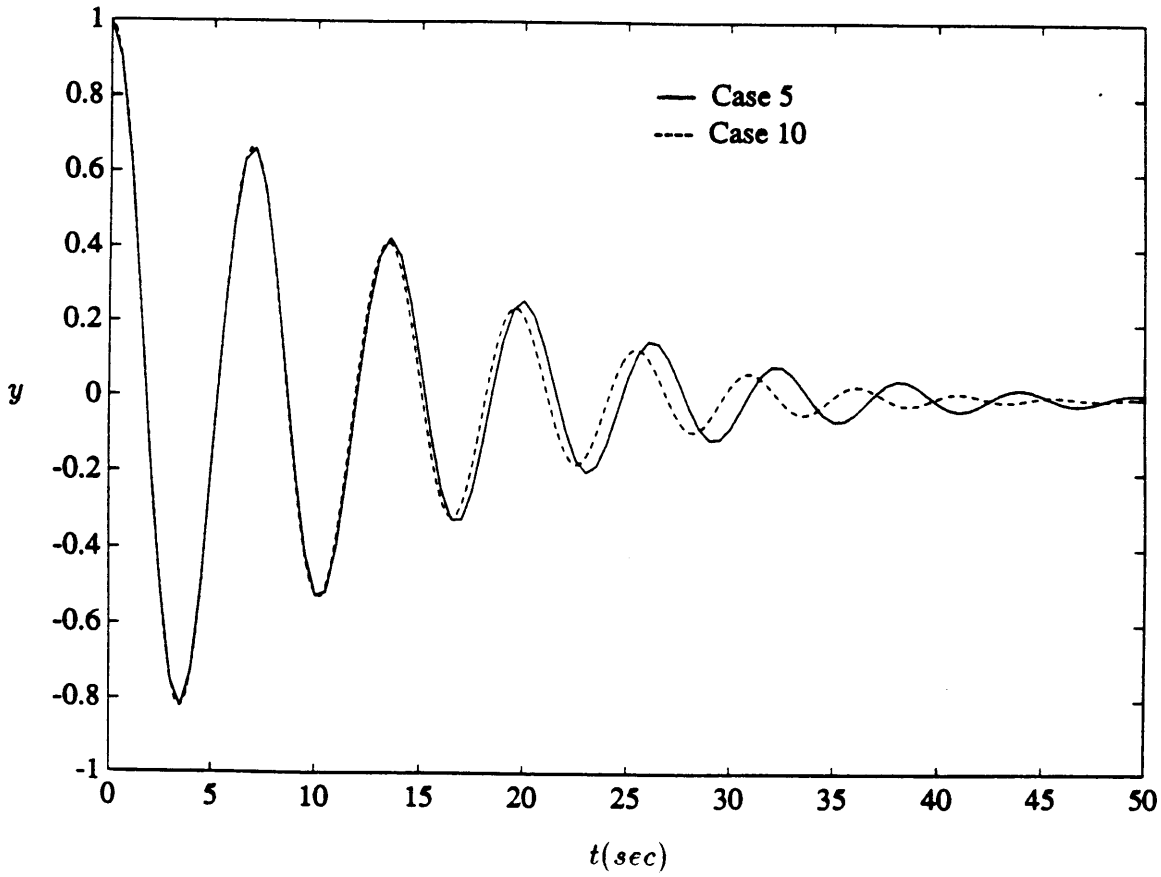

Figure 7-8: GMS Solutions to Cases 5,10

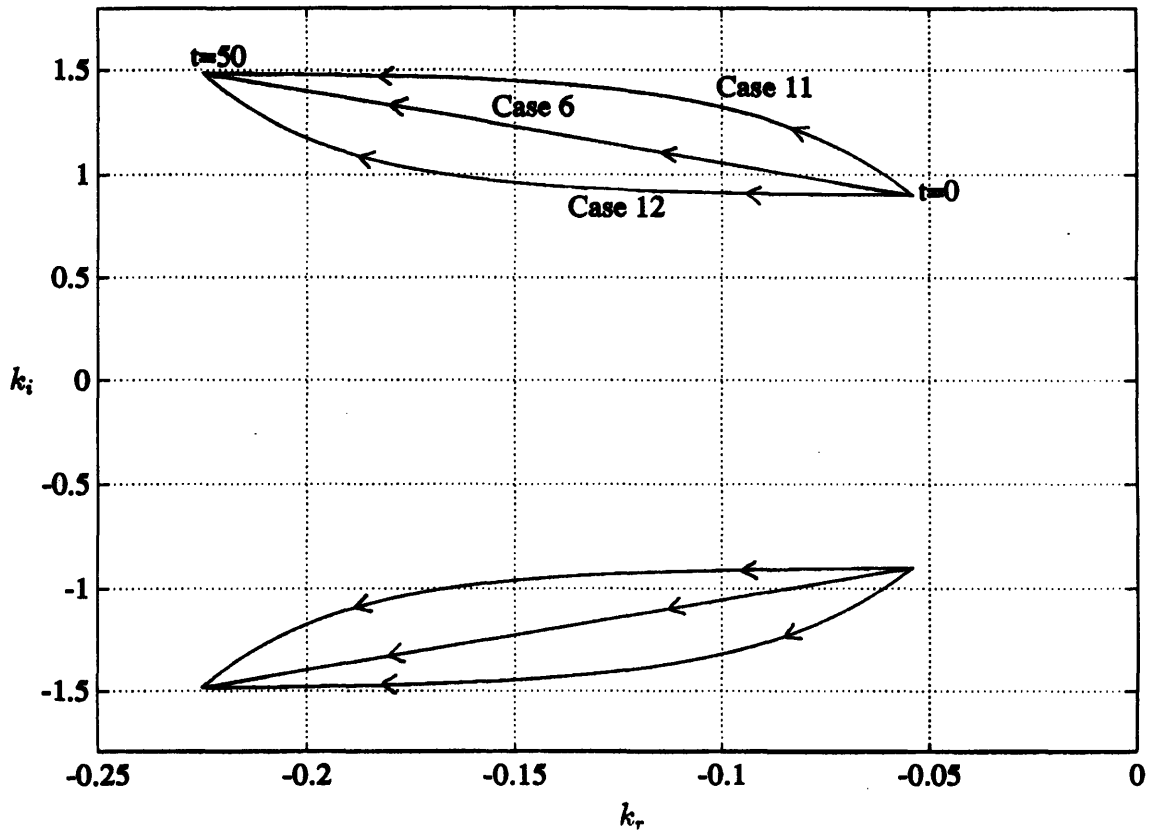

Figure 7-9: Non-Straight Line Root Trajectories of Cases 11,12

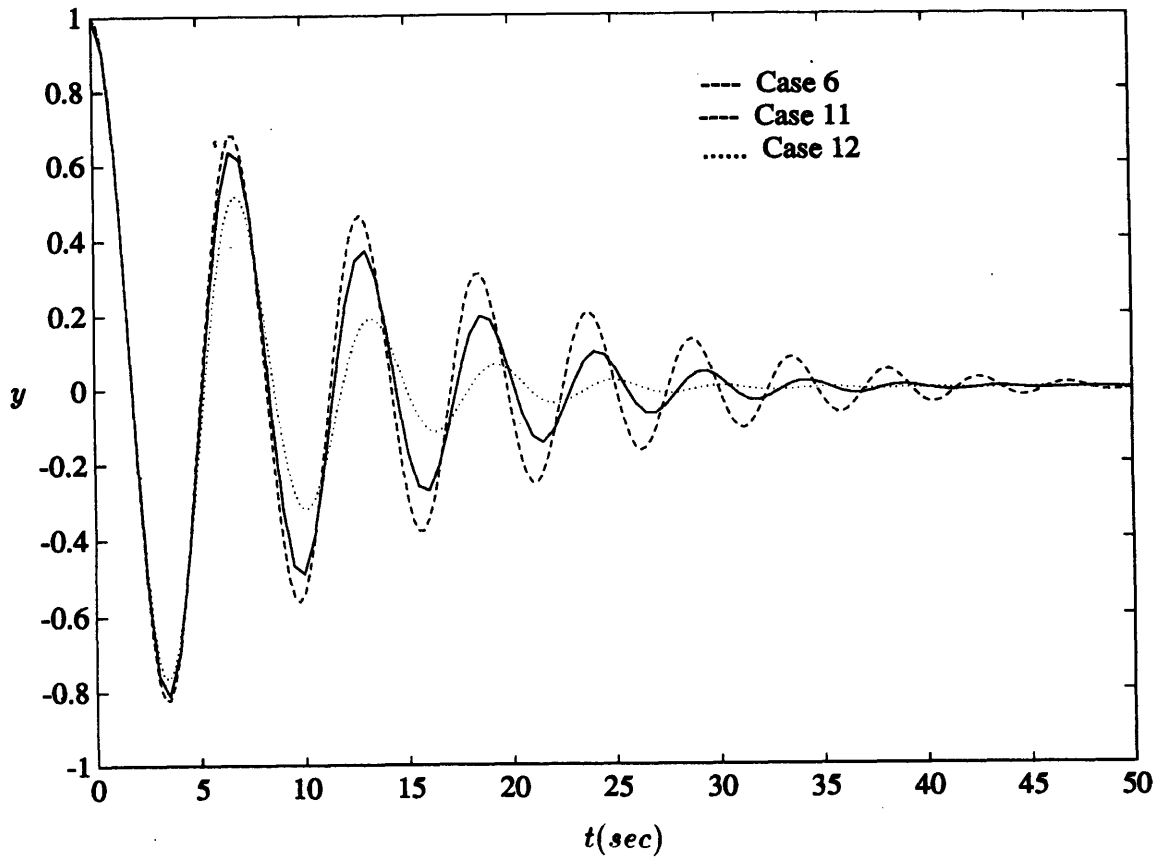

Figure 7-10: GMS Solutions to Cases 6,11,12

Chapter 8

Summary and Conclusions

8.1 Summary and Conclusions

In this work, the reentry dynamics and handling qualities of the Generic Hypersonic Aerodynamic Model Example vehicle were examined along a Space Shuttle optimal trajectory. The analysis of both the longitudinal and lateral-directional reentry motions was conducted through asymptotic approximations provided by Generalized Multiple Scales theory developed by Ramnath.

The reentry angle-of-attack perturbations of the vehicle were predicted by applying second order GMS solutions to the linear differential equation developed by Vinh and Laitone. GMS approximations showed that the dynamics of the GHAME vehicle angle-of-attack perturbations along the Shuttle optimal trajectory behave as damped oscillations with increasing frequency. Comparison with numerical integration approximations showed the GMS solutions to be of considerable accuracy. The fast part of the GMS solution predicted the frequency variations of the true dynamics extremely well while the amplitude changes were incorporated by the slow solution. The GMS approximations to the angle-of-attack perturbations were also compared with constant coefficient solutions applied after freezing the system at its initial point. Although such 'frozen' approximations are employed often in engineering analysis, it was shown that such methods totally misrepresent the angle-of-attack perturbations after only half a cycle of the dynamics.

The sensitivity of the angle-of-attack perturbations to the aerodynamic coefficients C_{L_α}, C_{m_α}, and C_{m_q} was studied through partial differentiation of the GMS solutions. It was seen that the sensitivity of the dynamics to these three parameters oscillate with the same frequency behavior of the actual dynamics. Changes in the three aerodynamic coefficients have the greatest effect on angle-of-attack perturbations at approximately 50,000 to 60,000 vehicle lengths into the reentry trajectory. The parameter C_{m_α} was shown to have much greater influence on the second order longitudinal dynamics than either of the other two parameters. GHAME vehicle angle-of-attack perturbations were found to be 2000 times more sensitive to variations in C_{m_α} than to C_{m_q} and 500 times more sensitive than to changes in C_{L_α}. Finally, the second order longitudinal dynamics was investigated using a stability criterion. The dynamics were shown to be closest to instability at approximately the same time that the vehicle was most sensitive to changes in the aerodynamic coefficients.

The full fourth order longitudinal dynamics of the GHAME vehicle along the Shuttle reentry trajectory were examined after deriving a fourth order time-varying differential equation from the linearized equations of motion. The longitudinal stability derivatives were estimated along the reentry trajectory for use in the fourth order GMS approximations. It was seen that the stability derivatives of the GHAME vehicle exhibit the same behavior as those of conventional aircraft with regards to sign convention. The angle-of-attack stability term, M_α remained negative throughout the entire trajectory to insure static stability of the longitudinal dynamics. It was also seen that values of the derivative M_v were extremely small as desired for design purposes. M_V was found to be statically most destablizing at approximately 60,000 vehicle lengths into the trajectory. Since the parameter remained negative throughout the entire reentry, it had no negative effects on the dynamic stability. The stability derivatives were employed to determine the characteristic roots associated with each of the longitudinal modes of motion. The characteristic roots of the phugoid mode were found to contain several 'turning' points where the roots changed from being complex to real pairs. Such a behavior represents deep mathematical difficulties was considered beyond the current scope to predict phugoid mode motions.

GMS solutions to the short period mode showed its reentry behavior to be one of damped oscillations. Unlike the angle-of-attack perturbations, there were no frequency variations of significance. Also, the GMS fast solution to short period motions were virtually identical with the full GMS approximation. Once again, the GMS approximation was compared to numerical solutions in order to determine accuracy. Although the asymptotic approximations slightly over shot the amplitude of short period dynamics, they were still of considerable accuracy. Due to the behavior of the phugoid mode roots, a complete analysis of the full GHAME vehicle fourth order longitudinal dynamics could not be accomplished with GMS theory. However, the accuracy of the asymptotic method was again demonstrated in predicting the reentry short period behavior of the vehicle.

In order to study the lateral-directional reentry dynamics of the GHAME vehicle, once again, a fourth order time-varying linear differential equation was derived form the equation of motions. The lateral-directional stability derivatives were estimated along the reentry trajectory employing the equations in Appendix A. With the exception of the dihederal derivative L_v, the lateral-directional stability derivatives of the GHAME vehicle exhibited the same sign behavior as those of conventional aircraft. Since, the GHAME vehicle has no dihederal in the main wings, the values of L_v were relatively small. Again with the exception of L_v, all of the derivatives increased their effect on the vehicle dynamics as the GHAME vehicle progressed further into the atmosphere.

The characteristic roots associated with each of the vehicles modes of motion were found and the GMS approximations were employed to predict the dynamics associated with each of these modes. The the roll convergence mode was found to be stable, while the spiral divergence mode exhibited unstable behavior. The characteristic motions of the dutch roll mode were shown to be damped oscillations with little damping and virtually no variations in the frequency. Once again, there was little difference between the GMS fast solution and the full GMS approximations to dutch roll motions. The asymptotic solutions to each of the mode dynamics were linearly combined for two sets of different initial conditions to obtain approximations

to the complete lateral-directional reentry motions. Due to the instability of the spiral divergence mode, the full lateral-directional dynamics were found to be unstable regardless of the initial conditions. Once again comparisons between the GMS solutions and numerical solutions showed the asymptotic approximations to be of great accuracy.

The sensitivity of the reentry lateral-directional dynamics to each of the stability derivatives was determined through partial differentiation of the the GMS approximations to each of the mode motions. Spiral mode dynamics were found to be most sensitive to changes in any of the stability derivatives. Roll convergence motions were almost as sensitive, however, effects of variations in the stability derivatives were several orders of magnitude less for dutch roll dynamics than either of the other two modes. Reentry lateral-directional dynamics which contain proportionally greater amounts of the spiral divergence mode will experience greater sensitivity to the stability derivatives. Also, it was seen that the directional derivative N_v has the most effect on all modal motions. Changes in N_v affected the roll convergence, spiral divergence, and dutch roll dynamics more than any of the other derivatives. The sensitivity of motions to L_v were comparable to those of N_v, however, effects of changing the other stability derivatives on the dynamics were orders of magnitude less. Especially the parameter L_p which remained relatively very small for a significant part of the trajectory. The sensitivities of spiral mode motions with respect to the different stability derivatives grew unbounded due to the behavior of the actual dynamics. The roll convergence and dutch roll sensitivities exhibited rapidly increasing behavior at approximately 500 seconds into the trajectory. It was seen that the sensitivity of roll convergence and dutch roll motions to the derivatives L_p, L_v, and N_P became zero shortly before this rapid increase and subsequent convergence.

Finally, the handling qualities of the GHAME vehicle along the Shuttle trajectory were examined by comparing reentry parameters with a set of flying quality specifications. It was found that the short period handling qualities do not qualify for Level 3 status, and render the GHAME vehicle uncontrollable. The dutch roll mode exhibited handling qualities of Level 3 which represents controllable behavior but only after

excessive workload on the flight crew. The GMS approximation to the roll convergence motion was employed to determine that the time constant of its response also did not meet Level 3 specifications. Only the spiral divergence reentry behavior was found to represent satisfactory handling qualities. In general, the handling qualities of the GHAME vehicle along the Shuttle reentry trajectory were found to be clearly inadequate.

The way in which variations in the characteristic root behavior affect the handling qualities was studied by considering a generic second order system. Through the nature of the GMS solutions, it was determined that as long as the path of the characteristic roots do not go beyond the rectangle defined by its initial and final points, the handling quality behavior falls in between those of the constant systems with roots fixed at the initial and final points. Also, it was found that the faster the roots of a system roots move, the handling quality behavior approaches that of the constant system with fixed roots at the final point. become more Conversely, the slower the characteristic roots travel along a path, the behavior of the system approaches that of the constant system defined by the initial point. As long as the path of roots does not extend beyond the rectangle defined by the initial and final root positions, the handling quality behavior of the system falls in between those of the constant system defined by these points.

8.2 Suggestions for Further Work

The following is suggested for further work regarding the GHAME vehicle and GMS theory:

- The reentry dynamics of the GHAME vehicle be studied for a trajectory which is designed for an aircraft closer to configuration of the GHAME vehicle.
- GMS control theory be utilized to stabilize the lateral-directional reentry dynamics and improve the handling qualities of the GHAME vehicle.

- Human factors issues be considered in determining the optimal manner of presenting a flight crew with the stability information in Chapter 2.
- Further theoretical investigation of the GMS method be conducted to better determine when only the 'fast' solution is adequate for accurate approximation of solutions to linear differential equations.
- The implications of characteristic root behavior on the response of a system be studied further. This may lead to the use of GMS theory in the design process of systems which exhibit non-autonomous behavior.

Appendix A

Stability Derivative Estimation

A.1 Longitudinal Stability Derivatives

The following equation are used to estimate the longitudinal stability derivatives of the GHAME vehicle along the Shuttle reentry trajectory.[9, 10, 11]

$$D_\alpha \approx \frac{2g}{\pi e A} C_{L_\alpha} \tag{A.1}$$

$$D_V \approx \frac{2g}{V C_L}\left(C_D + \frac{M_{no}}{2}\frac{\partial C_D}{\partial M_{no}}\right) \tag{A.2}$$

$$L_\alpha / V_0 \approx \frac{\rho V S}{2m} C_{L_\alpha} \tag{A.3}$$

$$L_V / V_0 \approx \frac{2g}{V^2 C_L}\left(C_L + \frac{M_{no}}{2}\frac{\partial C_L}{\partial M_{no}}\right) \tag{A.4}$$

$$M_\alpha \approx \frac{gc}{C_L k_y^2} C_{m_\alpha} \tag{A.5}$$

$$M_V \approx \frac{2gc}{V C_L k_y^2}\left(C_m + \frac{M_{no}}{2}\frac{\partial C_m}{\partial M_{no}}\right) \tag{A.6}$$

$$M_{\dot{\theta}} \approx \frac{gc^2}{2VC_L k_y^2} C_{m_{\dot{\theta}}} \tag{A.7}$$

A.2 Lateral-Directional Stability Derivatives

The following equations are employed to approximate the GHAME vehicle lateral-directional stability derivatives along the Shuttle reentry trajectory.[9, 10, 11]

$$Y_v \approx \frac{g}{VC_L} C_{y_\beta} \tag{A.8}$$

$$L_v \approx \frac{gb}{VC_L k_x^2} C_{l_\beta} \tag{A.9}$$

$$L_r \approx \frac{gb^2}{2VC_L k_x^2} C_{l_r} \tag{A.10}$$

$$L_p \approx \frac{gb^2}{2VC_L k_x^2} C_{l_p} \tag{A.11}$$

$$N_v \approx \frac{gb}{VC_L k_z^2} C_{N_\beta} \tag{A.12}$$

$$N_r \approx \frac{gb^2}{2VC_L k_z^2} C_{N_r} \tag{A.13}$$

$$N_p \approx \frac{gb^2}{2vC_L k_z^2} C_{N_p} \tag{A.14}$$

Appendix B

Fourth Order Lateral-Directional Sensitivity Differentiation

The differentiation is carried out for N_v in this section, however, the general process is the same for the other stability derivatives. We start with the equation

$$s^4 + \omega_3 s^3 + \omega_2 s^2 + \omega_1 s + \omega_0 = 0 \tag{B.1}$$

where the coefficients are as defined in Eqs6.12 through 6.15. This equation which defines the roots describing the lateral-directional motion is rewritten as[12]

$$x^3 + px^2 + qx + r = 0 \tag{B.2}$$

where

$$p = -\omega_2 \tag{B.3}$$

$$q = \omega_3\omega_2 - 4\omega_0 \tag{B.4}$$

$$r = 4\omega_2\omega_0 - \omega_3^2\omega_0 - \omega_1^2 \tag{B.5}$$

Now, let

$$a = \frac{1}{3}(3q - p^2) \tag{B.6}$$

$$b = \frac{1}{27}(2p^3 - 9pq + 27r) \tag{B.7}$$

$$A = \left[-\frac{b}{2} + \left(\frac{b^2}{4} + \frac{a^3}{27}\right)^{\frac{1}{2}}\right]^{\frac{1}{3}} \tag{B.8}$$

$$B = -\left[\frac{b}{2} + \left(\frac{b^2}{4} + \frac{a^3}{27}\right)^{\frac{1}{2}}\right]^{\frac{1}{3}} \tag{B.9}$$

then one root of Eq.B.2 is given by

$$x = A + B - p/3 \tag{B.10}$$

Now let,

$$R = \left(\frac{\omega_3^2}{4} - \omega_2 + x\right)^{\frac{1}{2}} \tag{B.11}$$

$$D = \left(\frac{3}{4}\omega_3^2 - R^2 - 2\omega_2 + \frac{4\omega_3\omega_2 - 8\omega_1 - \omega_3^3}{4R}\right)^{\frac{1}{2}} \tag{B.12}$$

$$E = \left(-\frac{3}{4}\omega_3^2 + R^2 + 2\omega_2 + \frac{4\omega_3\omega_2 - \omega 1 - \omega_3^3}{4R}\right)^{\frac{1}{2}} \tag{B.13}$$

Then, the roots representing the three lateral-directional modes of motion are given by

$$k_{rc} = -\frac{\omega_3}{4} + \frac{R}{2} + \frac{D}{2} \tag{B.14}$$

$$k_{sp} = -\frac{\omega_3}{4} + \frac{R}{2} - \frac{D}{2} \tag{B.15}$$

$$k_{drr} = -\frac{\omega_3}{4} - \frac{R}{2} \tag{B.16}$$

$$k_{dri} = \frac{E}{2} \tag{B.17}$$

We will now concentrate on finding $\frac{\partial k_{rc}}{\partial N_v}$, but again the same procedure can be followed for the other roots. We can write that

$$\frac{\partial k_{rc}}{\partial N_v} = \frac{\partial k_{rc}}{\partial \omega_0}\frac{\partial \omega_0}{\partial N_v} + \frac{\partial k_{rc}}{\partial \omega_1}\frac{\partial \omega_1}{\partial N_v} + \frac{\partial k_{rc}}{\partial \omega_2}\frac{\partial \omega_2}{\partial N_v} + \frac{\partial k_{rc}}{\partial \omega_3}\frac{\partial \omega_3}{\partial N_v} \tag{B.18}$$

Differentiating Eqs.6.12 through 6.15 with respect to N_w, we get

$$\frac{\partial \omega_3}{\partial N_v} = 0 \tag{B.19}$$

$$\frac{\partial \omega_2}{\partial N_v} = v \tag{B.20}$$

$$\frac{\partial \omega_1}{\partial N_v} = -vL_p \tag{B.21}$$

$$\frac{\partial \omega_0}{\partial N_v} = -gL_r \tag{B.22}$$

These four equations are in terms of parameters which are known for the shuttle trajectory and can be directly substituted into Eq.B.18. We must now determine the partial derivative of k_{rc} with respect to the ω's. Differentiating Eq.B.14, we get

$$\frac{\partial k_{rc}}{\partial \omega_n} = \frac{1}{2}\frac{\partial R}{\partial \omega_n} - \frac{1}{2}\frac{\partial D}{\partial \omega_n} \qquad n = 0,1,2 \tag{B.23}$$

$$\frac{\partial k_{rc}}{\partial \omega_3} = \frac{1}{2}\frac{\partial R}{\partial \omega_3} - \frac{1}{2}\frac{\partial D}{\partial \omega_3} - \frac{1}{4} \tag{B.24}$$

In order to evaluate the above two expressions, we are now left to determine the partial derivatives of D and R with respect to the ω's. Differentiating Eq.B.11 leaves

$$\frac{\partial R}{\partial \omega_n} = \frac{1}{2}R^{-1}\left(\frac{\partial x}{\partial \omega_n}\right) \qquad n = 0,1 \tag{B.25}$$

$$\frac{\partial R}{\partial \omega_2} = \frac{1}{2}R^{-1}\left(-1 + \frac{\partial x}{\partial \omega_2}\right) \tag{B.26}$$

$$\frac{\partial R}{\partial \omega_3} = \frac{1}{2}R^{-1}\left(\frac{1}{2}\omega_3 + \frac{\partial x}{\partial \omega_3}\right) \tag{B.27}$$

Also differentiating Eq.B.12, we get

$$\frac{\partial D}{\partial \omega_0} = \frac{1}{2}D^{-1}\left[-2R - \frac{1}{4R^2}(4\omega_3\omega_2 - 8\omega_1 - \omega_3^3)\right]\frac{\partial R}{\partial \omega_0} \tag{B.28}$$

$$\frac{\partial D}{\partial \omega_1} = \frac{1}{2}D^{-1}\left[-2R\frac{\partial R}{\partial \omega_1} - \frac{2}{R} - \frac{1}{4R^2}(4\omega_3\omega_2 - 8\omega_1 - \omega_3^3)\frac{\partial R}{\partial \omega_1}\right] \tag{B.29}$$

$$\frac{\partial D}{\partial \omega_2} = \frac{1}{2} D^{-1} \left[-2R \frac{\partial R}{\partial \omega_2} + \frac{\omega_3}{R} - \frac{1}{4R^2}(4\omega_3\omega_2 - 8\omega_1 - \omega_3^3) \frac{\partial R}{\partial \omega_2} - 2 \right] \tag{B.30}$$

$$\begin{aligned} \frac{\partial D}{\partial \omega_3} &= \frac{1}{2} D^{-1} \left[-2R \frac{\partial R}{\partial \omega_3} + \frac{1}{4R}(4\omega_2 - 3\omega_3^2) - \right. \\ &\left. \frac{1}{4R^2}(4\omega_3\omega_2 - 8\omega_1 - \omega_3^3) \frac{\partial R}{\partial \omega_3} + \frac{3}{2}\omega_3 \right] \end{aligned} \tag{B.31}$$

Eqs.B.25 through B.31 are substituted into Eqs.B.23 and B.24 which are in turn substituted into Eq.B.18. The expression for $\frac{\partial k_{rc}}{\partial N_s}$ is now in terms of trajectory parameters which are all known except for the partial derivatives of x with respect to the ω's. We differentiate Eq.B.10 which results in

$$\frac{\partial x}{\partial \omega_n} = \frac{\partial A}{\partial \omega_n} + \frac{\partial B}{\partial \omega_n} - \frac{1}{3}\frac{\partial p}{\partial \omega_n} \qquad n = 0, 1, 2, 3 \tag{B.32}$$

In order to determine the above expression, we finally differentiate Eqs.B.3 through B.9 with respect to the ω's. This results in the following.

$$\frac{\partial p}{\partial \omega_n} = 0 \qquad n = 0, 1, 3 \tag{B.33}$$

$$\frac{\partial p}{\partial \omega_2} = -1 \tag{B.34}$$

$$\frac{\partial q}{\partial \omega_0} = -4 \tag{B.35}$$

$$\frac{\partial q}{\partial \omega_1} = \omega_3 \tag{B.36}$$

$$\frac{\partial q}{\partial \omega_2} = 0 \tag{B.37}$$

$$\frac{\partial q}{\partial \omega_3} = \omega_1 \tag{B.38}$$

$$\frac{\partial r}{\partial \omega_0} = -\omega_3^2 + 4\omega_2 \tag{B.39}$$

$$\frac{\partial r}{\partial \omega 1} = -2\omega_0 \tag{B.40}$$

$$\frac{\partial r}{\partial \omega_2} = 4\omega_0 \tag{B.41}$$

$$\frac{\partial r}{\partial \omega_3} = -2\omega_3\omega_0 \tag{B.42}$$

$$\frac{\partial a}{\partial \omega_n} = \frac{\partial q}{\partial \omega_n} - \frac{2}{3}p\frac{\partial p}{\partial \omega_n} \qquad n = 0,1,2,3 \tag{B.43}$$

$$\frac{\partial b}{\partial \omega_n} = \left(\frac{2}{9}p^2 - \frac{1}{3}q\right)\frac{\partial p}{\partial \omega_n} - \frac{1}{3}p\frac{\partial q}{\partial \omega_n} + \frac{\partial r}{\partial \omega_n} \qquad n = 0,1,2,3 \tag{B.44}$$

$$\begin{aligned}\frac{\partial A}{\partial \omega_n} &= \frac{1}{54}A^{-2}\left(\frac{b^2}{4} + \frac{a^3}{27}\right)^{-\frac{1}{2}} a^2\frac{\partial a}{\partial \omega_n} + \\ &\frac{1}{3}A^{-2}\left[-\frac{1}{2} + \frac{1}{4}b\left(\frac{b^2}{4} + \frac{a^3}{27}\right)^{-\frac{1}{2}}\right]\frac{\partial b}{\partial \omega_n} \qquad n = 0,1,2,3\end{aligned} \tag{B.45}$$

$$\begin{aligned}\frac{\partial B}{\partial \omega_n} &= \frac{1}{54}B^{-2}\left(\frac{b^2}{4} + \frac{a^3}{27}\right)^{-\frac{1}{2}} a^2\frac{\partial a}{\partial \omega_n} + \\ &\frac{1}{3}B^{-2}\left[\frac{1}{2} + \frac{1}{4}b\left(\frac{b^2}{4} + \frac{a^3}{27}\right)^{-\frac{1}{2}}\right]\frac{\partial b}{\partial \omega_n} \qquad n = 0,1,2,3\end{aligned} \tag{B.46}$$

We substitute the above equations into Eq.B.32 then subsequently substitute the resulting expression into Eq.B.18. This finally results in an expression of $\frac{\partial k_{rc}}{\partial N_v}$ in terms of the ω's which are known along the trajectory. Eq.B.18 is calculated in this way and then substituted into the final sensitivity equation shown in Eq.6.

Bibliography

[1] Bowers, Albion and Iliff, Kenneth ,"A Generic Hypersonic Aerodynamic Model Example(GHAME) for Computer Simulation", Dryden Flight Research Facility, August 5, 1988

[2] Deyst, J., Kriegsman, B., and Marcus, F., "Entry- Trajectory Design to Minimize Thermal-Protection-System Weight", Charles Stark Draper Laboratory, November, 1971

[3] Ramnath, R. V. and Sinha, P., "Dynamics of the Space Shuttle during Entry into Earth's Atmosphere", AIAA Journal, Vol. 13, No. 3, March, 1975

[4] Vinh, N. X. and Laitone, E. V., "Longitudinal Dymnamic Stability of a Shutttle Vehicle", Journal of Aeronautial Sciences, Vol.XIX, No. 5, March, 1972

[5] Allen, H. J., "Motion of a Ballistic Missle Angularly Misaligned with the Flight Path Upon Entering the Atmosphere and its Effect Upon Aerodynamic Heating, Aerodynamic Loads, and Miss Distance", TN 4048, October, 1957, NACA

[6] Etkin, B., "Longitudinal Dynamics of Lifting Vehicle in Orbital Flight", Journal of Aeronautical Sciences, Vol. 28, October, 1961

[7] Ramnath, R. V. and Sandri, G., 'A Generalized Multiple Scales Approach to a Class of Linear Differential Equations", Journal of Mathematical Analysis and Application", Vol. 28, 1969

[8] Ramnath, R. V., "A Multiple Time Scales Approach to a Class of Linear Systems", Rept. AFFDL-TR-68-60, October, 1968

[9] Ramnath, R.V. , Flight Dynamics and Control class notes, Fall, 1990

[10] Etkin, B., Dynamics of Atmospheric Flight, Wiley, New York, 1972

[11] Etkin, B., Dynamics of Flight: Stability and Control, Wiley, New York, 1982

[12] Beyer, W., CRC Standard Mathematical Tables, CRC Press, Boca Raton, Florida, 1979

[13] "Military Specification: Flying Qualities of Piloted Airplanes", MIL-F-87585C, November 5, 1980

[14] Cooper, G. and Harper, R, Jr., "The Use of Pilot Ratings in Evaluation of Aircraft Handling Qualities", NASA TN D-5153, April, 1969

[15] Ramnath, R.V., "Presentation to NASA Dryden Flight Research Facility", 1989,1990, and April, 1991

[16] Ramnath, R.V. and Radovsky, S., "Sensitivity Analysis of Variable Systems", Proc. JACC, Denver, 1978